

KfK 4670
CNEA NT-16/89
August 1990

Chemical Behavior of (Ag, In, Cd) Absorber Rods in Severe LWR Accidents

P. Hofmann, M. Markiewicz
Institut für Material- und Festkörperforschung
Projekt Nukleare Sicherheitsforschung

Kernforschungszentrum Karlsruhe

**Kernforschungszentrum Karlsruhe
Institut für Material- und Festkörperforschung
Projekt Nukleare Sicherheitsforschung**

KfK 4670

CNEA NT- 16/89

**Chemical behavior of (Ag,In,Cd) absorber rods
in severe LWR accidents**

P. Hofmann, M. Markiewicz*

***Comisión Nacional de Energia Atómica
Av. de Libertador 8250, 1429 Buenos Aires
Argentina**

Kernforschungszentrum Karlsruhe GmbH, Karlsruhe

Als Manuskript gedruckt
Für diesen Bericht behalten wir uns alle Rechte vor

Kernforschungszentrum Karlsruhe GmbH
Postfach 3640, 7500 Karlsruhe 1

ISSN 0303-4003

Abstract

The chemical behavior of the various pressurized water reactor (PWR) absorber rod components has been studied at temperatures up to 1200 °C. Higher temperatures could not be applied since a fast and complete liquefaction of the (Ag,In,Cd) absorber alloy, stainless steel cladding and Zircaloy guide tube materials occurred as a result of eutectic chemical interactions. Thin oxide layers on the Zircaloy surface can delay the chemical interactions with the (Ag,In,Cd) alloy or stainless steel but they cannot prevent them because these layers will disappear after some time. In this work the reaction kinetics has been determined for the systems (Ag,In,Cd) alloy/Zircaloy-4 and Zircaloy-4/stainless steel 1.4919 (AISI 316). The interactions can be described by parabolic rate laws; the Arrhenius equations for the various interactions are given.

Chemisches Verhalten von (Ag,In,Cd) Absorberstäben bei schweren LWR-Störfällen

Zusammenfassung

Es wurde das chemische Reaktionsverhalten der verschiedenen DWR-Absorberstabkomponenten bis 1200 °C untersucht. Höhere Temperaturen konnten nicht angewandt werden, da es oberhalb etwa 1250 °C zu einer schnellen und vollständigen Verflüssigung der (Ag,In,Cd)-Absorberlegierung, der rostfreien Stahlhülle und des Zircaloy-Führungsrohrmaterials infolge eutektischer Reaktionen kommt. Dünne Oxidschichten auf der Zircaloy-Oberfläche können die chemischen Wechselwirkungen mit der (Ag,In,Cd)-Legierung oder dem Stahl verzögern aber nicht verhindern, da die Oxidschichten nach einiger Zeit verschwinden. In dieser Arbeit wurde die Reaktionskinetik für die Materialpaarungen (Ag,In,Cd) alloy/Zircaloy-4 und Zircaloy-4/rostfreier Stahl 1.4919 (AISI 316) ermittelt. Die Wechselwirkungen können durch parabolische Zeitgesetze beschrieben werden; die Arrhenius-Gleichungen für die verschiedenen Wechselwirkungen sind angegeben.

Contents

1.	Introduction	1
2.	Experimental Details	3
3.	Results	4
3.1	Chemical interactions between molten (Ag,In,Cd) alloy and stainless steel	4
3.2	Chemical interactions between molten (Ag,In,Cd) alloy and Zircaloy-4	4
3.2.1	Chemical behavior	4
3.2.2	Reaction kinetics	6
3.2.3	Influence of an oxide layer on the (Ag,In,Cd)/Zry interactions	6
3.3	Chemical interactions between stainless steel and Zircaloy-4	7
3.3.1	Chemical behavior	7
3.3.2	Reaction kinetics	8
3.3.3	Influence of an oxide layer on the stainless steel/Zircaloy-4 interactions	9
4.	Discussion	10
5.	Summary and Conclusions	13
6.	Acknowledgements	14
7.	References	14
	List of Tables	16
	List of Figures	17

1. Introduction

In beyond-design-basis accidents, called severe reactor accidents, the fuel rod cladding may exceed the temperature limit of 1200 °C, which is the maximum tolerable temperature for a large break loss-of-coolant accident (LOCA). Although the fuel rod behavior at temperatures above 1200 °C is reasonably understood [1,2], the (Ag,In,Cd) absorber rod behavior requires further investigations. Due to the low melting temperature of the (Ag,In,Cd) absorber material at about 800 °C, the liquid control rod alloy may affect the course of fuel element and core degradation in a severe LWR (Light Water Reactor) accident.

Most pressurized water reactor (PWR) control rods are composed of a (Ag,In,Cd) neutron absorber alloy with stainless steel (AISI 304 or 316) cladding. The initial composition of the alloy is approximately 80 wt.% silver, 15 wt.% indium, and 5 wt.% cadmium. The standard PWR contains about 2800 kg of the (Ag,In,Cd) alloy in the core (about 2.2 % of the core materials in the TMI-2 reactor).

The geometry of a PWR control rod is very similar to that of a fuel rod (Fig. 1). The control rod consists of (Ag,In,Cd) absorber material with stainless steel cladding. The gap between the (Ag,In,Cd) alloy and the cladding is filled with helium. The stainless steel rod is inserted into a Zircaloy guide tube with enough space between the two to allow the flow of coolant water.

Experiments were performed at several laboratories to investigate the behavior of (Ag,In,Cd) control rods during severe reactor accidents [3,4,5,6]. The essential results are summarized in the publication by D.A. Petti [5], who made the following observations:

The (Ag,In,Cd) alloy melts at about 800 °C, but will not affect core degradation as long as the molten material is contained within the stainless steel cladding. As the temperature increases, some of the control rod constituents will vaporize within the cladding until failure occurs, either from internal pressurization or from melting of the cladding. At low pressures of the primary system and when no Zircaloy is present, the control rod fails between 1350 and 1450 °C. Failure of the control rods with the Zircaloy guide tubes occurs at about 1200 °C as a result of thermal expansion, physical contact, and eutectic chemical interactions between the stainless steel cladding and the Zircaloy guide tube. The high internal pressure in the control rod will result in a violent ejection of vapour, aerosol and molten material when the cladding fails. The ejected material results in the formation

of low-temperature melting alloys consisting of the (Ag,In) constituents and the surrounding Zircaloy. Due to the high vapour pressure of Cd it vaporizes. Liquid control rod material continues to vaporize if it remains at high temperatures. The control rod material which will flow out of the hot regions of the core freezes and may inhibit steam and/or water flow. At high system pressure, overpressurization of the rod does not occur. Instead, upon failure, the alloy flows to cooler regions of the reactor core. In all cases the resulting reaction products melt at low temperatures and enhance by this the degradation of the reactor core [5].

At temperatures above 1000 °C, the rapid oxidation of the Zircaloy guide tube and fuel rod cladding by steam results in the formation of thin ZrO₂ oxide layers. The oxide layers can prevent or delay the chemical interactions between the Zircaloy guide tube and the stainless steel cladding of the control rods or (Ag,In,Cd) absorber alloy if the cladding fails. For this reason, the influence exerted by about 10 μm thick ZrO₂ layers covering the Zircaloy surface on the interaction behavior has been studied.

Of particular interest is the knowledge of the reaction kinetics and the determination of the critical temperature at which the components will be liquefied as a result of these chemical interactions and relocate.

In this work the following reaction couples have been examined at temperatures greater than or equal to 800 °C.

- (Ag,In,Cd) alloy/stainless steel AISI 316,
- (Ag,In,Cd) alloy/Zircaloy-4, and
- Zircaloy-4/stainless steel AISI 316.

The Zircaloy-4 was used in both the as-received and slightly oxidized condition, that is, with an oxide layer of about 10 μm thickness on its surface. The maximum temperature which could be examined was limited by the disintegration (complete liquefaction) of the specimens during heatup.

2. Experimental Details

The isothermal annealing experiments were performed with Zircaloy-4 (Zry) capsules in which short cylindrical rods of (Ag,In,Cd) alloy or 1.4919 (AISI 316) stainless steel (ss) were pressed and gas-tight closed by a conical Zry plug. Figure 2 shows the components of a compatibility specimen before being loaded.

The annealing experiments were performed in a tube furnace under flowing argon. The specimens were heated up to about 900 °C and then placed into the pre-heated furnace which had the desired annealing temperature. The annealing time started when the temperature of the specimen was 20 K below the annealing temperature. Cooldown of the specimens occurred outside the furnace at room temperature. For the Zry/(Ag,In,Cd) alloy and Zry/ss reaction couples, the investigated temperatures ranged from 1000 to 1200 °C and the maximum applied annealing time was 30 minutes. The highest temperature examined (1200 °C) was limited by the failure of the specimens due to the onset of liquid phase formation followed by a fast and complete liquefaction of the Zry crucible at slightly higher temperatures.

After annealing, the specimens were mechanically cut and then metallographically prepared for examinations of the reaction zones with an optical microscope. A part of the specimens was etched to recognize better the various phases. The reaction zone thicknesses were measured at four different locations of the interface. For the evaluation of the kinetic data the maximum reaction zone thickness was used. In addition, some Scanning Electron Microscopy (SEM)/Energy Dispersive X-Ray (EDX) or SEM/Wave Length Dispersive X-ray (WDX) and Auger Electron Spectroscopy (AES) examinations were performed to obtain information on the chemical compositions of the reaction products and diffusion zones.

For the pre-oxidized Zircaloy specimens, the crucibles were oxidized in air for 9 minutes at 870 °C to obtain a ZrO₂ layer of about 10 μm thickness. The actual oxide layer thickness varied between 9 and 12 μm. The subsequent compatibility experiments were performed in argon.

To avoid damage to the thin oxide layer on the inner crucible wall, the stainless steel and (Ag,In,Cd) alloy rods were cooled in liquid nitrogen before being loaded into the pre-oxidized Zircaloy crucibles.

3. Results

The different chemical interactions of the control rod components can be quantitatively described by Arrhenius equations which may be used in a code to predict the material behavior at high temperatures. However, in some cases models must be developed and benchmarked using the same experimental results.

3.1 Chemical interactions between molten (Ag,In,Cd) alloy and stainless steel

According to the binary phase diagrams (Figure 3) [7] Ag does not interact chemically with Fe or Ni, even not in the molten state, apart from very small solubilities. However, some limited interactions do take place in the Ag-Cr system. At about 1450 °C, approximately 15 at.% Cr can be dissolved in liquid Ag, but no Ag can be dissolved in Cr (Figure 4). Two immiscible melts form at higher temperatures. For this reason, it was not surprising to find that only negligible chemical interactions took place between the (Ag,In,Cd) alloy and stainless steel. The molten absorber alloy causes some enhanced formation of precipitates along the grain boundaries (where Cr is present in an enriched form as carbides) similar to the observations described by Bowsher et al. in [4]. Transverse macro- and micrographs of a (Ag,In,Cd)/ss specimen after annealing at 1400 °C for 20 minutes are shown in Figure 5. Practically no chemical interactions took place and no reaction zone was detected. Only the grain boundaries showed the enhanced formation of carbide precipitates. Although Ag diffusion into the ss along the grain boundaries was described in the literature [4], it did not result in embrittlement of the ss. Failure of the reaction specimens due to physical failure of the crucible occurred when the melting point of ss was approached.

3.2 Chemical interactions between molten (Ag,In,Cd) alloy and Zircaloy-4

After mechanical failure of the ss absorber rod cladding due to overpressurization or melting of the ss or due to eutectic interactions between ss cladding and the Zry guide tube, the molten (Ag,In,Cd) absorber alloy will be ejected and allowed to interact chemically with the Zircaloy of the guide tube and/or fuel rod cladding.

3.2.1 Chemical behavior

The molten (Ag,In,Cd) alloy chemically dissolves the Zry. There is no reaction zone in the Zry. Therefore, only the increase in diameter (or decrease in wall thickness) of the Zry crucible can be measured as a function of temperature and time. The

chemical composition of the absorber melt changes continuously and various phases form during solidification. According to the binary phase diagram (Figure 6, [7]) Ag can dissolve up to 80 at.% (77 wt.%) Zr at about 1200 °C. The resulting melt will be either a homogeneous or heterogeneous (Ag,Zr) melt, depending on the chemical composition. The cooldown process results in the formation of AgZr and/or AgZr₂, beside solid Ag or Zr. Ag and Zr have little or no solubility for each other at low temperatures (Fig. 6).

The phase relations in the In-Zr and Cd-Zr systems are only partially known [7]. In and Cd are both soluble in solid Zr, but there seems to exist an extended solution of Zr in liquid In and liquid Cd at higher temperatures.

Cross-sections of the (Ag,In,Cd) alloy/Zry reaction specimens annealed at 1000, 1100, 1150 and 1200 °C for various times are shown in Figure 7. The influence exerted by a 10 µm thick ZrO₂ layer on the chemical interaction is also shown for comparison; for the same temperature/time combinations, the oxide layer delays the interactions. One can recognize the strong increase in diameter of the (Ag,In,Cd)/Zry interface. The 2.25 mm thick wall of the Zry crucible was completely melted or dissolved within less than 15 minutes at 1150 °C and in less than 4 minutes at 1200 °C. Figure 8 shows the remaining wall thickness of the Zry crucibles at 1000, 1100 and 1150 °C after an interaction time of 5 minutes. One can recognize the smooth liquid/solid interface with no visible reaction zone in the remaining Zry crucible wall because the Zr has been dissolved in the liquid (Ag,In,Cd) alloy. The resulting (Ag,In,Cd,Zr) alloy decomposes in various phases on cooldown. Since equilibrium conditions will not always be reached as a result of the fast cooldown, the phase diagram information can be used to a limited extent only.

The cross-sections and typical microstructures of the resulting (Ag,In,Cd,Zr) interaction alloy for various temperatures and times are shown in Figures 9 through 18. During cooldown the metallic (Ag,In,Cd,Zr) melt, which forms at temperature, decomposes into various phases of complicated chemical composition. The integral chemical composition of two specimens, which were annealed at 1000 and 1200 °C, and examined by SEM/EDX, is about 68 wt.% Ag, 23 wt.% Zr, 5 wt.% In, and 4 wt.% Cd. The decomposed phases correspond to pure Ag and the compound AgZr as shown in Figure 6. In addition, a ternary compound could be detected (45 wt.% In, 42 % Zr, 13 % Ag) at both annealing temperatures. A second ternary compound (65 wt.% Ag, 25 % Zr, 10 % In) was formed after annealing at 1200 °C, but not at 1000 °C.

3.2.2 Reaction kinetics

In order to determine the (Ag,In,Cd)/Zry reaction kinetics, the maximum increase of the crucible inner diameter or maximum decrease of the Zry wall thickness was measured as function of temperature and time and used as a fictive maximum reaction zone thickness. The results are listed in Table 1 and plotted against time and the square root of time in Figures 19, 20, respectively. The dissolution of Zry occurs by diffusion of Ag, In and Cd into the Zry changing the initial composition. With increasing concentration of the absorber alloy elements in the Zry the solid/liquid two phase region will be reached and liquefaction takes place. The lines in Figure 20 were determined by linear regression, using the method of least squares. The agreement between the experimental data points and the regression line is very good for 1000 and 1100 °C, but larger scatter occurs at higher temperatures (Fig. 20). The reaction zone growth rates for the (Ag,In,Cd)/Zry system are listed in Table 2 and plotted as a function of the reciprocal temperature in Figure 21. The reaction zone growth rate equation for temperatures between 1000 and 1200 °C is:

$$x^2/t \text{ (cm}^2\text{/s)} = 1.355 \cdot 10^8 \cdot \exp(-344874/RT)$$
$$R = 8.314 \text{ J/mol}\cdot\text{K}$$

This equation for the reaction zone can be extrapolated to lower temperatures, but not to higher temperatures since a fast and complete liquefaction of the specimens occurred above 1200 °C. The obtained rates are very high compared for example to the oxidation of Zry; the activation energy is a factor of about two higher, indicating a stronger temperature-dependent diffusion controlled process.

3.2.3 Influence of an oxide layer on the (Ag,In,Cd)/Zry interactions

A comparison of the macroscopic behavior of the compatibility specimens without and with a 10 µm thick ZrO₂ layer is made in Figure 7. The oxide layer on the inner crucible wall delays and reduces the chemical interaction between the (Ag,In,Cd) alloy and the pre-oxidized Zry, but cannot prevent it. The (Ag,In,Cd) alloy does not interact with ZrO₂. The maximum reaction zone thicknesses in Zircaloy are listed in Table 3 and plotted versus the square root of time in Figure 2. Differences in the interaction behavior of oxidized and as-received Zry can be

seen when Figure 20 is compared to Figure 22. At temperatures below 1150 °C the interaction begins after a temperature-dependent incubation period, t_0 . The incubation period, t_0 , is necessary to dissolve the ceramic ZrO_2 layer and form a metallic α -Zr(O) layer which allows the interactions with the (Ag,In,Cd) absorber alloy to take place. The reaction zone growth rates are listed in Table 4 and are plotted as a function of the reciprocal temperature in Figure 23. The growth rate equations and the t_0 values were determined from x^2 versus t correlations of the experimental data. The differences in the reaction behavior between the pre-oxidized Zry (10 μm thick ZrO_2 layer) and the as-received Zry (no oxide layer) specimens are, that at lower temperatures, the oxidized specimens require an incubation period and, at all temperatures examined, the reaction rates are slower in the pre-oxidized specimens than in the as-received Zry specimens. The oxygen dissolved in the Zry delays the dissolution of Zr in the absorber melt. The reason may be that the oxygen dissolved in the Zry crystal lattice exerts an influence on the diffusion of Ag into the Zry. At such a small initial oxide-layer thickness of 10 μm the liquefaction temperature of the specimen of about 1250 °C will not essentially be affected. However, for much thicker initial ZrO_2 layers, this temperature will be shifted to higher values [9].

3.3 Chemical interactions between stainless steel and Zircaloy-4

This material combination corresponds to the interaction between the ss 1.4919 (AISI 316) absorber rod cladding and the Zry guide tube. As a result of the chemical interaction, the ss cladding may fail at low temperatures and release the molten (Ag,In,Cd) absorber alloy.

3.3.1 Chemical behavior

The Fe-Zr, Ni-Zr, and Cr-Zr phase diagrams indicate that eutectic interactions occur in each system (Figures 24, 25) [7,8]. The lowest eutectic temperature exists in the Fe-Zr system at about 950 °C on the Zr rich side. The diffusion of approximately 5 wt.% Fe into the Zr results in the formation of a liquid phase even at this low temperature (Fig. 25). The eutectic temperature on the Fe rich side is at about 1300 °C. The Ni-Zr system has four eutectic temperatures which vary between 960 and 1170 °C, while the eutectic temperatures in the binary Cr-Zr system are 1332 and 1592 °C.

The cross-sections of the Zry/ss reaction specimens after annealing at 1000, 1100, 1150 and 1200 °C for various duration of reaction times are shown in [Figure 26](#). The cross sections of both pre-oxidized Zry/ss reaction specimens (initial ZrO₂ layer thickness: 10 μm) are presented for comparison. In order to recognize better the metallic reaction zone which forms as a result of the chemical interactions the specimens were etched forming a dark looking phase (Fig. 26). The eutectic interactions, which occur between 1000 °C and higher, result in the formation of liquid reaction products and voids form as some of the molten material relocates.

Although the specimens were annealed in an upright position, the reaction zones of the as-received Zry are not symmetrical around the circumference. Apparently, very small forces are sufficient to induce asymmetric reaction zones in the Zry wall. First interactions could be noticed at 1000 °C after annealing times longer than 5 minutes. At 1200 °C, the Zry crucible wall of 2.25 mm thickness was already completely dissolved after 2 minutes. In all cases, the reaction in the Zry was much stronger than in the stainless steel. This may be explained by phase diagram considerations (Fig. 24, 25). Only small amounts (≥ 5 wt.%) of Fe, Cr or Ni are necessary to dissolve (liquefy) large quantities of Zr. Also, since the lowest eutectic temperatures in the Fe-Zr, Cr-Zr, and Ni-Zr systems are on the Zr rich side, Zr can be liquefied at much lower temperatures than Fe, Cr, or Ni. Liquefaction starts as soon as the solid/liquid two phase field has been reached.

The cross sections of Zry/ss specimens and typical microstructures produced by the chemical interactions are shown in [Figures 27 through 38](#). The metallic (Zr,Fe,Cr,Ni) melts decompose into various phases on cooldown. The integral chemical composition of the solidified melt (about 83 wt.% Zr, 12 % Fe, 3 % Ni, 2 % Cr) is very similar to the chemical composition of the eutectic point on the Zr rich side of the Fe-Zr system (Fig. 24) [8]. The three individual phases which form during cooldown have the following composition:

- a) approximately 50 wt.% Zr, 27 % Fe, 23 % Cr
- b) approximately 78 wt. % Zr, 17 % Fe, 5 % Ni and traces of Cr
- c) approximately 96 wt.% Zr, 3 % Sn and some Fe and Cr.

Phase b) may correspond to FeZr₂ in the binary Fe-Zr phase diagram (Fig. 24), while phase c) is essentially Zr with small amounts of other elements. Apparently, the expected FeZr₃ equilibrium phase does not form as a result of rapid cooling.

3.3.2 Reaction kinetics

The maximum reaction zone thicknesses in the Zry crucible and ss rod are listed in Tables 5 and 6. The reaction zones in Zry and ss are plotted versus the square root of time in Figures 39 and 40, respectively. The isothermal growth of the reaction zones (dissolution of Zr and ss) obey parabolic rate laws, indicating a diffusion-controlled process. Fe and/or Ni diffuse into the Zry and initiate the Zry liquefaction as soon as the solid/liquid phase field has been reached. To show the large differences in the amount of dissolved Zry and ss, the reaction zone thicknesses in Zry and ss are plotted in dependence on temperature for an annealing time of 5 minutes in Figure 41. Only small amounts of ss are necessary to dissolve large amounts of Zry. Above about 1250 °C a complete liquefaction of the specimens occurs.

The reaction zone growth rates for the Zry/ss interactions are listed in Table 7 and plotted as a function of the reciprocal temperature in Figure 42. The growth rate equations determined for the temperature range of 1000 to 1200 °C are:

For Zircaloy-4:

$$x^2/t \text{ (cm}^2/\text{s)} = 2.78 \cdot 10^{19} \cdot \exp(-642864/RT)$$

For stainless steel:

$$x^2/t \text{ (cm}^2/\text{s)} = 1.08 \cdot 10^{19} \cdot \exp(-688790/RT)$$

$$R = 8.314 \text{ J/mol}\cdot\text{K}$$

These equations can be extrapolated to lower temperatures, but not to higher temperatures since a fast and complete liquefaction of the materials takes place at about 1250 °C. One can recognize the difference of the reaction zone growth rates for Zry and ss. At temperatures above 1150 °C the liquefaction of the Zry by ss is even faster than by the (Ag,In,Cd) alloy (Fig. 42). The reason is the higher activation energy indicating a stronger temperature-dependence of these interactions.

3.3.3 Influence of an oxide layer on the stainless steel/Zircaloy-4 interactions

The macroscopic behavior of pre-oxidized Zry/ss interaction specimens has been compared to as-received Zry/ss specimens in Figure 26. Similar to the (Ag,In,Cd)/Zry system, the 10 μm thick ZrO_2 layer on the inner Zry crucible wall delays and reduces the chemical interactions between Zry and ss. Stainless steel does not interact with ZrO_2 , but the oxide layer will be dissolved by the Zry during a time-dependent incubation period, t_0 . The Zry/ss interaction will begin as soon as the oxide layer has disappeared and does not protect anymore the metallic Zry substrate.

The measured reaction zone thicknesses in Zry and ss for the pre-oxidized Zry/ss reaction specimens are listed in Table 8 and plotted versus the square root of time in Figures 43 and 44. The strong impact of the oxide layer on the chemical interactions between Zry and ss is shown in Figure 43. No chemical interactions take place at 1000 °C up to the examined reaction time of 30 minutes since the time is too short for the dissolution of the ZrO_2 layer. Further experimental studies with pre-oxidized Zry specimens (20 to 100 μm thick ZrO_2 layers) at higher temperatures have shown that the liquefaction of the specimens will be shifted to higher temperatures, but cannot be prevented [9].

The reaction zone growth rates in Zry and ss are listed in Table 8 and plotted versus the reciprocal temperature in Figure 46 along with the as-received Zry/ss interaction results. The growth rate equations and the t_0 values were determined from x^2 versus t correlations of the experimental data.

4. Discussion

Because of the low-temperature melting point (range) of the (Ag,In,Cd) absorber alloy of about 800 °C, in all (Ag,In,Cd) alloy/Zry compatibility experiments a liquid phase is present from the beginning. The Zr is dissolved by the melt and the wall thickness of the Zry crucible will decrease continuously during the annealing process. At temperatures above 1200 °C, the dissolution rate is so fast that the specimens fail already during heatup.

In the Zry/ss system, a considerable amount of liquid phase is formed around 1000 °C, and the amount of liquefied material increases with increasing tempera-

ture and time. In this reaction system, the 2.25 mm thick Zry crucible fails during heatup above 1200 °C and the molten alloy is released.

These results are in agreement with results of integral tests where fuel rod bundles containing (Ag,In,Cd) absorber rods were heated to temperatures of about 2000 °C [2,10,11]. The onset of liquid-phase formation and the complete liquefaction of the absorber rod components at temperatures above 1200 °C was detected by video systems. The low-temperature failure of the absorber rods initiated core melt progression. The resulting melt attacked the fuel rods chemically dissolving the Zry cladding and a part of the UO₂ fuel. By this process, "molten" fuel relocation and early fission product release can take place even well below the melting point of Zry cladding (\approx 1760 °C). The melts relocate towards cooler regions of the core where it may form coolant channel blockages on solidification.

The main purpose of this work has been to determine the reaction kinetics between the various (Ag,In,Cd) absorber rod components. Although some interaction experiments were described in the literature [3,4,5,6], no Arrhenius equations had been previously developed from the data. In all cases, the maximum reaction zone thickness was used for the evaluation of the kinetic data to obtain conservative results.

Thin oxide layers (about 10 μ m) on the Zry surface can delay the chemical interactions with the (Ag,In,Cd) alloy or the ss, but cannot prevent them. The ZrO₂ interacts with metallic Zr under the formation of oxygen-stabilized α -Zr(O). The interaction of Zry with the absorber alloy or ss will begin as soon as the oxide layer has disappeared, that means after an incubation period, t_0 , has been passed. In general the reaction zone growth rates for pre-oxidized Zry are slower than those of as-received Zry (Fig. 46). The oxygen dissolved in the Zr lattice exerts an influence on the diffusion and/or dissolution processes; the reaction rates are slower. Experiments with thicker oxide layers (20, 45, 100 μ m) indicate that the incubation period, t_0 , increases with increasing ZrO₂ thickness, and that complete meltdown of the absorber rod components will be shifted to higher temperatures (up to 1400 °C) for thicker oxide layers [9].

The ZrO₂ layers on metallic Zry disappear only if no further oxygen in the environment is available or has no access to the Zry to continue the oxidation. In all other cases the reaction of Zry with oxygen or steam is thermodynamically more favorable than the reactions with (Ag, In, Cd) and ss, respectively. But, as the integral PWR bundle meltdown experiments [2,11,12] show, a steam environment cannot prevent the chemical interactions between Zry and (Ag, In, Cd) and ss since local-

ized steam-starvation conditions may exist. In these experiments, the bundle components were used in the as-received condition. The chemical/physical behavior of heavily pre-oxidized bundle components has not yet been studied in integral experiments. A different meltdown behavior has to be expected since thick oxide layers ($\geq 20 \mu\text{m}$) on Zry protect the metallic substrate against interactions even by molten (Ag, In, Cd) alloy and/or ss. The relocation of molten absorber material and ss should occur faster as the wettability of the ZrO_2 surface by metallic melts is extremely poor. Blockage formation within the core region is therefore more difficult under these conditions.

During a severe reactor accident not only Zry but also ss will be oxidized by steam at comparable rates [12]. If, the resulting oxide layers are in solid contact with each other, eutectic interactions will take place with liquid phase formation between 1200 and 1400 °C [13]. Therefore, the oxide layers offer only limited protection from the chemical interactions. In all cases, liquefaction of the non-oxidized and oxidized components will occur below their melting points.

The metallographic and chemical/analytical examinations of the specimens revealed a large number of various phases at room temperature. Since only binary phase diagrams are available, the observed phases cannot all be described by phase diagram considerations. In addition, some of the phases will not be in equilibrium condition since cooldown of the specimens occurred rather fast. The integral chemical compositions of the solidified melts indicate for the Zry/ss system that only small amounts of ss are needed to dissolve large quantities of Zry (Fig. 25). The integral compositions are nearly identical for all interaction temperatures examined.

The kinetic evaluation of these interaction experiments is problematic since a liquid phase forms as reaction product. The liquid causes relative movements between the Zry crucible and the ss rod during annealing of the diffusion couple. Depending on the annealing conditions of the specimens (upright, horizontal) the ss rod can penetrate into the Zry crucible wall by liquefying it with different velocities. As a result, the interaction zones in the Zry crucible or the amount of Zry dissolved are not uniform along their axis and circumference. This can be clearly recognized in [Figure 47](#) showing specimens which were annealed in upright and horizontal position at 1100 °C for 15 minutes. In a few cases the inserted ss rod turned even around for about 90° at higher temperatures ([Figure 48](#)). The penetration of the ss rod into the Zry is strongest at locations where the liquid film is thinnest. For the kinetic evaluation of the Zry/ss reaction experiments the

maximum attack of the Zry was therefore considered. The different extents of Zry liquefaction by the ss is shown in Figure 49 in dependence on the annealing conditions. The ss rod behaves similar as the Zry, but, at lower temperatures, the differences with respect to the reaction zone growth rates between the two examined annealing conditions become larger.

5. Summary and Conclusions

- The (Ag,In,Cd) absorber alloy starts to melt at about 800 °C, but this will not affect core degradation as long as the molten material is contained within the stainless steel (AISI 316) cladding. The chemical interaction between the absorber alloy and stainless steel is negligible.
- Failure of the stainless steel absorber rod cladding takes place as a result of either internal pressurization (high Cd vapour pressure) or eutectic interactions with the Zircaloy guide tube (bowing of the rods at high temperatures). The released (Ag,In,Cd) melt can then interact with the Zircaloy guide tube.
- The Zircaloy will be chemically dissolved by the absorber alloy. The dissolution of the Zircaloy can be described by a parabolic rate law. The dissolution rate is very fast; at 1200 °C, it takes only about 50 s to dissolve 1 mm Zircaloy and about 4 minutes to destroy the entire 2.25 mm thick Zircaloy crucible wall.
- As soon as solid state contact occurs between the stainless steel cladding and the Zircaloy guide tube, eutectic interactions take place which can be described by parabolic rate laws. Liquid phases form at around 1000 °C, and a fast and complete liquefaction of both components takes place above 1250 °C. Only small amounts of stainless steel are necessary to dissolve great amounts of Zircaloy, and it takes only a little more than 2 minutes to destroy the 2.25 mm thick Zircaloy crucible wall at 1200 °C.
- Thin ZrO₂ layers ($\approx 10 \mu\text{m}$) on the Zircaloy surface delay the chemical interactions of Zircaloy with the (Ag,In,Cd) alloy or the stainless steel, but cannot prevent them. The ZrO₂ layer must be dissolved by the Zry before chemical interactions can take place. The required incubation period depends on temperature and time. Dissolved oxygen in the Zircaloy, forming

oxygen-stabilized α -Zr(O), reduces the reaction rates and shifts the liquefaction temperature to slightly higher levels.

- With respect to the chemical behavior of (Ag,In,Cd) absorber rods during severe reactor accidents, meltdown and relocation must be assumed to occur at temperatures around 1250 °C. The resulting melt destroys the Zircaloy cladding of the fuel rods and dissolves a part of the UO₂, contributing substantially to fuel element degradation. Since UO₂ fuel can be liquefied at temperatures as low as 1250 °C, this process has a strong impact on the release of volatile fission products.
- The premature low-temperature failure of the PWR absorber rods and the localized relocation of (Ag,In,Cd) alloy within the reactor core may cause criticality problems during flooding of the destroyed core.

6. Acknowledgements

We would like to thank Prof. Dr. W. Dienst (KfK) and Mrs. K. McNeil (EG + G Idaho, Inc.) for their thorough technical and editorial reviews of the manuscript.

7. References

- [1] P. Hofmann, H.J. Neitzel, E.A. Garcia; Chemical interactions of Zircaloy-4 tubing with UO₂ fuel and oxygen at temperatures between 900 and 2000 °C, KfK 4422 (1988)
- [2] S. Hagen, P. Hofmann; Physical and chemical behavior of LWR fuel elements up to very high temperatures, KfK 4104 (1987)
- [3] D.A. Powers; Behavior of control rods during core degradation, NUREG/CR-4401, SAND85-0469 (1985)
- [4] B.R. Bowsher, R.A. Jenkins, A.L. Nichols, N.A. Rowe, J.A.H. Simpson; Silver-Indium-Cadmium control rod behavior during a severe reactor accident, AEEWR-R 1991 (1986)
- [5] David A. Petti; Silver-Indium-Cadmium control rod behavior and aerosol formation in severe reactor accidents, NUREG/CR-4876, EG + E-2501 (1987)
- [6] F. Nagase, H. Uetsuka; Some topics from the basic experiments on high-temperature core materials behavior at JAERI; JAERI, Tokai Research Establishment, Japan, to be published.

- [7] T.B. Massalski; Binary alloy phase diagrams, Vol. 1,2, American Society for Metals, Ohio (1986)
- [8] D. Arias, J.P. Abriata; The Fe-Zr system, Bulletin of Alloy Phase Diagrams, Vol. 9 No. 5 (1988) 597-604
- [9] P. Hofmann, M. Markiewicz; Influence of ZrO₂ layers on the chemical interactions between Zircaloy-4 cladding and Inconel 718 spacer grids, KfK 4729 (1990)
- [10] S. Hagen, P. Hofmann, G. Schanz, L. Sepold; CORA Experiments on the behavior of LWR fuel rod bundles under SFD conditions, Kerntechnik 53, No. 1 (1988) 15
- [11] S. Hagen, P. Hofmann, G. Schanz, L. Sepold; Out-of-pile-experiments on LWR severe fuel damage behavior (Tests CORA-5 and CORA-12), KfK 4419 (1990)
- [12] P. Hofmann, S. Hagen, G. Schanz, A. Skokan; Reactor core materials interactions at very high temperatures, Nuclear Technology 87 (1989) 147-182
- [13] M.E. Reser (Editor), Phase Diagrams for Ceramists, The American Ceramic Society (1975)

List of Tables

- Table 1:** Measured maximum reaction zone thickness in Zircaloy for the diffusion couple Zircaloy-4/(Ag,In,Cd) alloy as a function of temperature and time.
- Table 2:** Reaction zone growth rate in Zircaloy for the diffusion couple Zircaloy-4/(Ag,In,Cd) alloy.
- Table 3:** Measured maximum reaction zone thickness in Zircaloy for the diffusion couple pre-oxidized Zircaloy-4/(Ag,In,Cd) alloy; initial ZrO₂ oxide layer thickness: 10 μm.
- Table 4:** Reaction zone growth rate in Zircaloy for the diffusion couple pre-oxidized Zircaloy-4/(Ag,In,Cd) alloy; initial ZrO₂ oxide layer thickness: 10 μm.
- Table 5:** Measured maximum reaction zone thickness in Zircaloy for the diffusion couple Zircaloy-4/stainless steel 1.4919 (AISI 316) as a function of temperature and time.
- Table 6:** Measured maximal reaction zone thickness in stainless steel for the diffusion couple Zircaloy-4/stainless steel 1.4919 (AISI 316) as a function of temperature and time.
- Table 7:** Reaction zone growth rates in Zircaloy and stainless steel for the diffusion couple Zircaloy-4/stainless steel 1.4919 (AISI 316).
- Table 8:** Measured maximum reaction zone thickness in Zircaloy and stainless steel for the diffusion couple pre-oxidized Zircaloy-4/stainless steel 1.4919 (AISI 316); initial ZrO₂ oxide layer thickness: 10 μm.
- Table 9:** Reaction zone growth rates in Zircaloy and stainless steel for the diffusion couple pre-oxidized Zircaloy-4/stainless steel 1.4919 (AISI 316); initial ZrO₂ oxide layer thickness: 10 μm.

List of Figures

- Fig. 1:** Schematic of the PWR (Ag,In,Cd) absorber rod arrangement within the fuel element.
- Fig. 2:** Setup of the reaction couples.
- Fig. 3:** Binary alloy phase diagrams of the systems Ag-Fe and Ag-Ni [7].
- Fig. 4:** Binary alloy phase diagram of the system Ag-Cr [7].
- Fig. 5:** (Ag,In,Cd) alloy/stainless steel 1.4919 (AISI 316) reaction couple after annealing at 1400 °C for 20 minutes.
- Fig. 6:** Binary alloy phase diagram of the system Ag-Zr [7].
- Fig. 7:** Chemical interaction between (Ag,In,Cd) alloy and Zircaloy-4 at different temperatures; influence of a thin ZrO₂ layer on the reaction behavior (right row of pictures).
- Fig. 8:** Zircaloy-4 wall thickness decrease due to chemical interactions with the (Ag,In,Cd) alloy at different temperatures after annealing for 5 minutes.
- Fig. 9:** Chemical interactions between (Ag,In,Cd) alloy and Zircaloy-4; 1000 °C/ 5 min.
- Fig. 10:** Chemical interactions between (Ag,In,Cd) alloy and Zircaloy-4; 1000 °C/ 15 min.
- Fig. 11:** Chemical interactions between (Ag,In,Cd) alloy and Zircaloy-4; 1000 °C/ 30 min.
- Fig. 12:** Chemical interactions between (Ag,In,Cd) alloy and Zircaloy-4; 1100 °C/ 5 min.
- Fig. 13:** Chemical interactions between (Ag,In,Cd) alloy and Zircaloy-4; 1100 °C/ 10 min.
- Fig. 14:** Chemical interactions between (Ag,In,Cd) alloy and Zircaloy-4; 1100 °C/ 15 min.
- Fig. 15:** Chemical interactions between (Ag,In,Cd) alloy and Zircaloy-4; 1150 °C/ 2 min.
- Fig. 16:** Chemical interactions between (Ag,In,Cd) alloy and Zircaloy-4; 1150 °C/ 5 min.
- Fig. 17:** Chemical interactions between (Ag,In,Cd) alloy and Zircaloy-4; 1150 °C/ 15 min.
- Fig. 18:** Chemical interactions between (Ag,In,Cd) alloy and Zircaloy-4; 1200 °C/ 1 min.
- Fig. 19:** Maximum reaction zone thicknesses in the system (Ag,In,Cd) alloy/ Zircaloy-4 as a function of time between 1000 and 1200 °C (table 1).

- Fig. 20:** Maximum reaction zone thicknesses in the system (Ag,In,Cd) alloy/Zircaloy-4 as a function of the square root of time between 1000 and 1200 °C (table 1).
- Fig. 21:** Reaction zone growth rates for the reaction system (Ag,In,Cd) alloy/Zircaloy-4 (table 2).
- Fig. 22:** Maximum reaction zone thicknesses in the system (Ag,In,Cd) alloy/pre-oxidized Zircaloy-4 versus the square root of time; initial ZrO₂ layer thickness: 10 μm. At temperatures below 1150 °C the interactions start after the incubation time t_0 (table 3).
- Fig. 23:** Reaction zone growth rates for the reaction system (Ag,In,Cd) alloy/pre-oxidized Zircaloy-4; initial ZrO₂ layer thickness: 10 μm (table 4).
- Fig. 24:** Binary alloy phase diagram of the system Fe-Zr [7,8].
- Fig. 25:** Binary alloy phase diagrams of the systems Ni-Zr and Cr-Zr [7].
- Fig. 26:** Chemical interactions between Zircaloy-4 and stainless steel 1.4919 (AISI 316) at different temperatures; influence of a thin ZrO₂ layer on the reaction behavior (right row of pictures).
- Fig. 27:** Chemical interactions between Zircaloy-4 and stainless steel 1.4919 (AISI 316); 1000 °C/5 min.
- Fig. 28:** Chemical interactions between Zircaloy-4 and stainless steel 1.4919 (AISI 316); 1000 °C/15 min.
- Fig. 29:** Chemical interactions between Zircaloy-4 and stainless steel 1.4919 (AISI 316); 1100 °C/2 min.
- Fig. 30:** Chemical interactions between Zircaloy-4 and stainless steel 1.4919 (AISI 316); 1100 °C/ 5 min.
- Fig. 31:** Chemical interactions between Zircaloy-4 and stainless steel 1.4919 (AISI 316); 1100 °C/15 min.
- Fig. 32:** Chemical interactions between Zircaloy-4 and stainless steel 1.4919 (AISI 316); 1100 °C/30 min.
- Fig. 33:** Chemical interactions between Zircaloy-4 and stainless steel 1.4919 (AISI 316); 1150 °C/1 min.
- Fig. 34:** Chemical interactions between Zircaloy-4 and stainless steel 1.4919 (AISI 316); 1150 °C/2 min.
- Fig. 35:** Chemical interactions between Zircaloy-4 and stainless steel 1.4919 (AISI 316); 1150 °C/5 min.
- Fig. 36:** Chemical interactions between Zircaloy-4 and stainless steel 1.4919 (AISI 316) ; 1200 °C/1 min.
- Fig. 37:** Chemical interactions between Zircaloy-4 and stainless steel 1.4919 (AISI 316); 1200 °C/2 min.

- Fig. 38:** Chemical interactions between Zircaloy-4 and stainless steel 1.4919 (AISI 316); 1200 °C/4.5 min.
- Fig. 39:** Maximum reaction zone thicknesses in Zircaloy for the system Zircaloy-4/stainless steel 1.4919 (AISI 316) versus the square root of time between 1000 and 1200 °C (table 5).
- Fig. 40:** Maximum reaction zone thicknesses in stainless steel for the system Zircaloy-4/stainless steel 1.4919 (AISI 316) versus the square root of time between 1000 and 1200 °C (table 6).
- Fig. 41:** Comparison of the reaction zone thicknesses in Zircaloy and stainless steel for the system Zircaloy-4/stainless steel 1.4919 (AISI 316) versus temperature; annealing time: 5 min.
- Fig. 42:** Reaction zone growth rates for the reaction system Zircaloy-4/stainless steel 1.4919 (AISI 316) (table 7).
- Fig. 43:** Maximum reaction zone thicknesses in Zircaloy for the system pre-oxidized Zircaloy-4/stainless steel 1.4919 (AISI 316) versus the square root of time; initial ZrO₂ layer thickness: 10 μm. The interactions start first after the incubation time t_0 has been passed (table 8).
- Fig. 44:** Maximum reaction zone thicknesses in stainless steel for the system pre-oxidized Zircaloy-4/stainless steel 1.4919 (AISI 316) versus the square root of time; initial ZrO₂ layer thickness: 10 μm. The interactions start first after the incubation time t_0 has been passed (table 8).
- Fig. 45:** Comparison of the reaction zone thicknesses in Zircaloy and stainless steel for as-received and pre-oxidized Zircaloy-4 (initial ZrO₂ layer thickness: 10 μm) versus temperature; annealing time 5 min.
- Fig. 46:** Reaction zone growth rates for the reaction system pre-oxidized Zircaloy-4/stainless steel 1.4919 (AISI 316). Comparison with as-received Zircaloy specimens (table 9).
- Fig. 47:** Extent of chemical interactions between Zircaloy and stainless steel in dependence on annealing conditions (upright or horizontal).
- Fig. 48:** Turning of the stainless steel rod within the Zircaloy crucible as a results of liquid phase formation. The relocated melt form a large void.
- Fig. 49:** Reaction zone growth rates for the reaction system Zircaloy/stainless steel 1.4919 (AISI 316) for two modes of annealing conditions (upright or horizontal).

Table 1: Measured maximum reaction zone thickness in Zircaloy for the diffusion couple Zircaloy-4/(Ag,In,Cd) alloy as a function of temperature and time (figures 19 and 20).

Specimen	Temperature	Time	Reaction zone thickness
	°C	min	µm
164	1000	5	315
165	"	15	525
166	"	30	660
169	1100	5	830
168	"	10	1260
167	"	15	1550
174	1150	2	730
171	"	5	1850
175	"	5	1070
172	"	15	molten
176	1200	1	840
173	"	3.5	2250
191	"	4	2250

Table 2: Reaction zone growth rate in Zircaloy for the diffusion couple Zircaloy-4/(Ag,In,Cd) alloy (fig. 21).

Temperature		Reaction zone growth rate, x^2/t cm^2/s
$^{\circ}\text{C}$	1/K	
1000	$7.855 \cdot 10^{-4}$	$2.565 \cdot 10^{-6}$
1100	$7.283 \cdot 10^{-4}$	$2.636 \cdot 10^{-5}$
1150	$7.027 \cdot 10^{-4}$	$7.377 \cdot 10^{-5}$
1200	$6.789 \cdot 10^{-4}$	$2.204 \cdot 10^{-4}$

Growth rate equation:

$$x^2/t \text{ (cm}^2/\text{s)} = 3.55 \cdot 10^8 \cdot \exp(-344874/RT)$$

$$R = 8.314 \text{ J/mol}\cdot\text{K}$$

Table 3: Measured maximum reaction zone thickness in Zircaloy for the diffusion couple pre-oxidized Zircaloy-4/(Ag,In,Cd) alloy; initial ZrO₂ oxide layer thickness: 10 μm (fig. 22).

Specimen	Temperature	Time	Reaction zone thickness
	°C	min	μm
178	1000	5	65
167	"	15	203
163	"	30	340
177	1100	2	73
173	"	5	430
169	"	10	453
161	"	10	320
170	"	15	650
166	"	15	570
175	1150	2	398
168	"	3.5	494
176	"	5	578
162	"	5	625
179	"	10	653
174	"	10	668
180	"	15	885
165	1200	1	377
164	"	2	626
172	"	3,5	663

Table 4: Reaction zone growth rate in Zircaloy for the diffusion couple pre-oxidized Zircaloy-4/(Ag,In,Cd) alloy; initial ZrO₂ oxide layer thickness: 10 μm (fig. 23).

Temperature		Reaction zone growth rate, x ² /t
°C	1/K	cm ² /s
1000	7.855·10 ⁻⁴	7.5·10 ⁻⁷
1100	7.283·10 ⁻⁴	4.1·10 ⁻⁶
1150	7.027·10 ⁻⁴	8.6·10 ⁻⁶
1200	6.789·10 ⁻⁴	2.4·10 ⁻⁵

Growth rate equation:

$$x^2/(t - t_0) \text{ (cm}^2/\text{s)} = 4.67 \cdot 10^4 \cdot \exp(-263685/RT)$$

$$R = 8.314 \text{ J/mol}\cdot\text{K}$$

t₀ values (10 μm ZrO₂ layer), s

1000 °C: 280

1100 °C: 66

1150 °C: 0

1200 °C: 0

Table 5: Measured maximum reaction zone thickness in Zircaloy for the diffusion couple Zircaloy-4/stainless steel 1.4919 (AISI 316) as a function of temperature and time (fig. 39).

Specimen	Temperature	Time	Reaction zone thickness
	°C	min	µm
177	1000	5	0
178	"	15	80
179	"	15	80
198	"	30	150
197	"	30	120
192	1100	2	370
189	"	5	670
196	"	10	840
180	"	15	1200
182	"	30	1610
193	1150	1	550
184	"	2	960
183	"	5	1530
194	1200	1	1390
187	"	1	1150
188	"	2	1740
185	"	3	2250

Table 6: Measured maximal reaction zone thickness in stainless steel for the diffusion couple Zircaloy-4/stainless steel 1.4919 (AISI 316) as a function of temperature and time (fig. 40).

Specimen	Temperature	Time	Reaction zone thickness
	°C	min	µm
177	1000	5	0
178	"	15	0
179	"	15	0
198	"	30	15
197	"	30	6
192	1100	2	35
181	"	5	15
189	"	5	65
196	"	10	105
180	"	15	65
193	1150	1	30
184	"	2	60
183	"	5	110
194	1200	1	145
188	"	2	190
199	"	4.5	375

Table 7: Reaction zone growth rates in Zircaloy and stainless steel for the diffusion couple Zircaloy-4/stainless steel 1.4919 (AISI 316) (fig. 42).

Temperature		Reaction zone growth rate, x^2/t cm^2/s	
$^{\circ}C$	1/K	Zircaloy-4	stainless steel
1000	$7.855 \cdot 10^{-4}$	$9.48 \cdot 10^{-8}$	$5.74 \cdot 10^{-10}$
1100	$7.283 \cdot 10^{-4}$	$1.44 \cdot 10^{-5}$	$8.72 \cdot 10^{-8}$
1150	$7.027 \cdot 10^{-4}$	$7.69 \cdot 10^{-5}$	$3.81 \cdot 10^{-7}$
1200	$6.789 \cdot 10^{-4}$	$3.33 \cdot 10^{-4}$	$4.79 \cdot 10^{-6}$

Growth rate equation:

For Zircaloy-4:

$$x^2/t (cm^2/s) = 2.78 \cdot 10^{19} \cdot \exp(-642864/RT)$$

For stainless steel:

$$x^2/t (cm^2/s) = 1.08 \cdot 10^{19} \cdot \exp(-688790/RT)$$

$$R = 8.314 \text{ J/mol}\cdot\text{K}$$

Table 8: Measured maximum reaction zone thickness in Zircaloy and stainless steel for the diffusion couple pre-oxidized Zircaloy-4/stainless steel 1.4919 (AISI 316); initial ZrO₂ oxide layer thickness: 10 μm (figs. 43 and 44).

Specimen	Temperature °C	Time min	Reaction zone thickness μm	
			Zircaloy-4	1.4919 ss
29	1000	15	0	0
22	"	30	0	0
37	"	30	0	0
38	"	60	0	0
25	1100	3	0	0
33	"	10	198	54
21	"	15	287	66
27	"	30	513	119
34	1150	2	0	0
26	"	5	263	57
30	"	5	192	45
35	"	10	440	95
23	"	15	683	124
36	1200	1	0	0
32	"	2	160	40
31	"	3	393	73
24	"	5	490	112
28	"	10	793	151

Table 9: Reaction zone growth rates in Zircaloy and stainless steel for the diffusion couple pre-oxidized Zircaloy-4/stainless steel 1.4919 (AISI 316); initial ZrO₂ oxide layer thickness: 10 μm (fig. 46).

Temperature		Reaction zone growth rate, x ² /t cm ² /s	
°C	1/K	Zircaloy-4	stainless steel
1000	7.855·10 ⁻⁴	—	—
1100	7.283·10 ⁻⁴	1.9·10 ⁻⁶	9.7·10 ⁻⁸
1150	7.027·10 ⁻⁴	6.7·10 ⁻⁶	2.1·10 ⁻⁷
1200	6.789·10 ⁻⁴	1.2·10 ⁻⁵	4.3·10 ⁻⁷

Growth rate equation:

For Zircaloy-4:

$$x^2/(t - t_0) \text{ (cm}^2/\text{s)} = 1.43 \cdot 10^6 \cdot \exp(-311100/RT)$$

For stainless steel:

$$x^2/(t - t_0) \text{ (cm}^2/\text{s)} = 3.4 \cdot 10^2 \cdot \exp(-250817/RT)$$

$$R = 8.314 \text{ J/mol}\cdot\text{K}$$

t₀ values (10 μm ZrO₂ layer), s

	Zry	ss
1000 °C	—	—
1100 °C	426	371
1150 °C	239	176
1200 °C	83	56

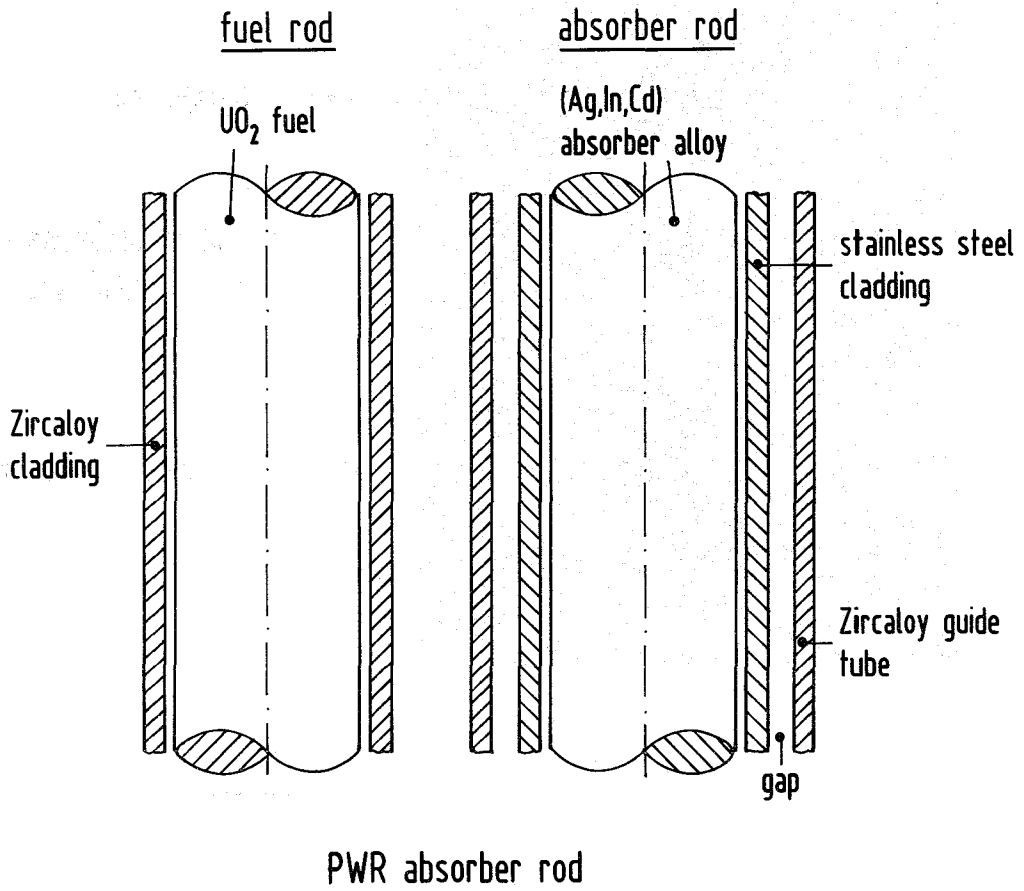


Fig. 1: Schematic of the PWR (Ag,In,Cd) absorber rod arrangement within the fuel element.

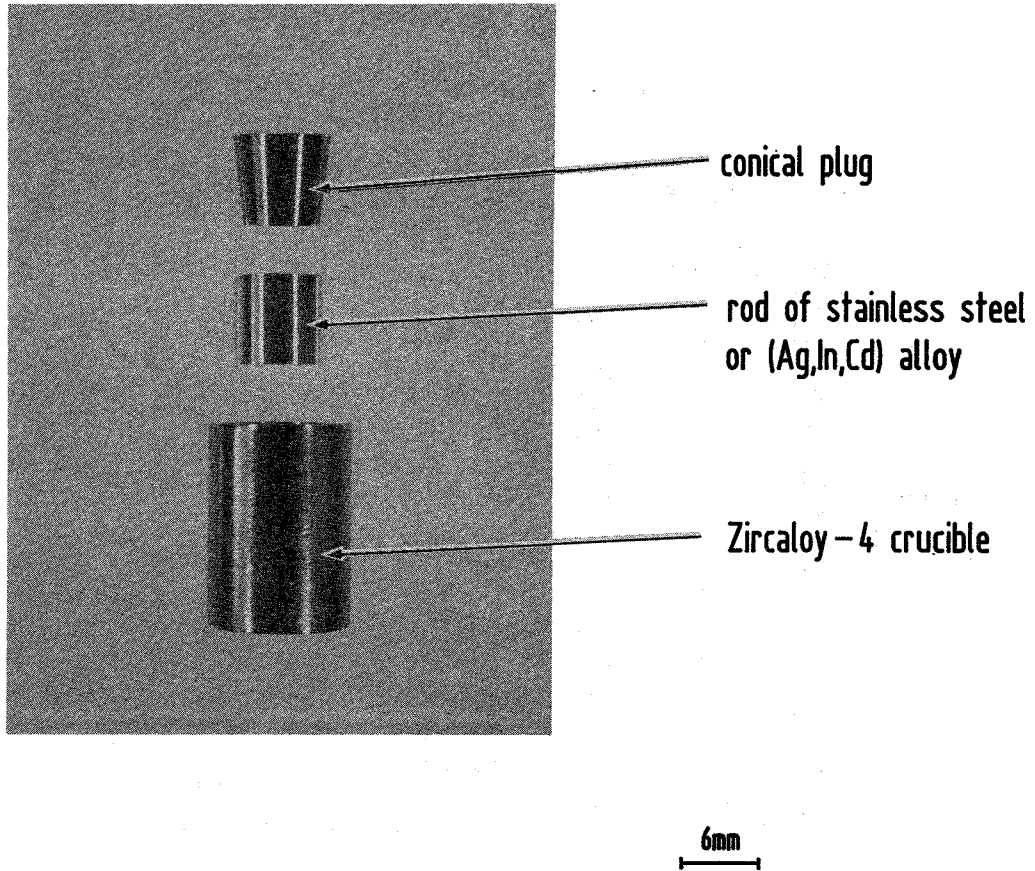


Fig. 2: Setup of the reaction couples.

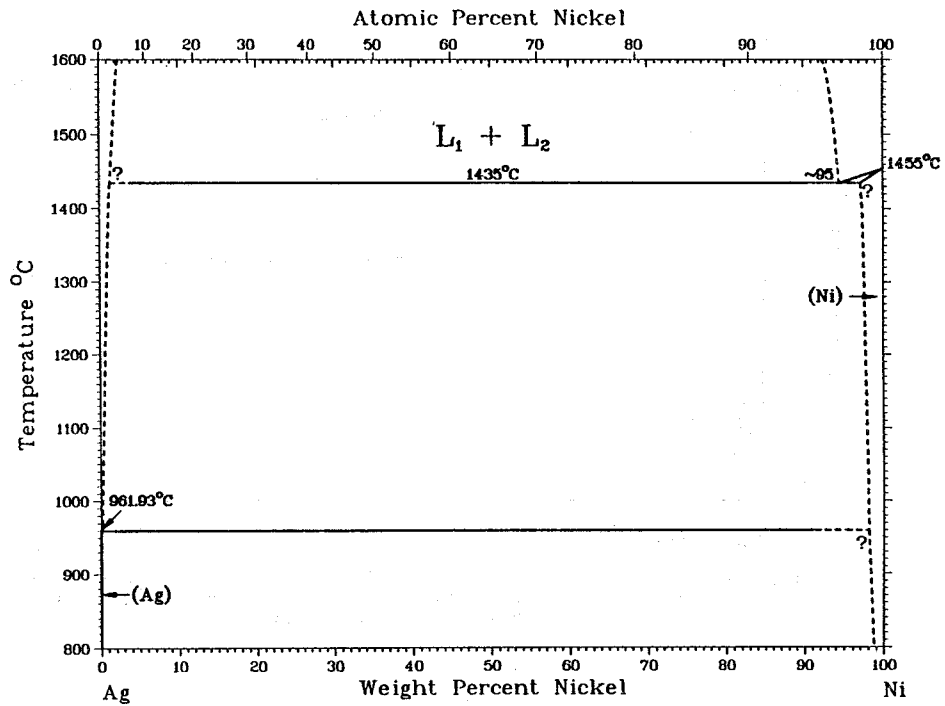
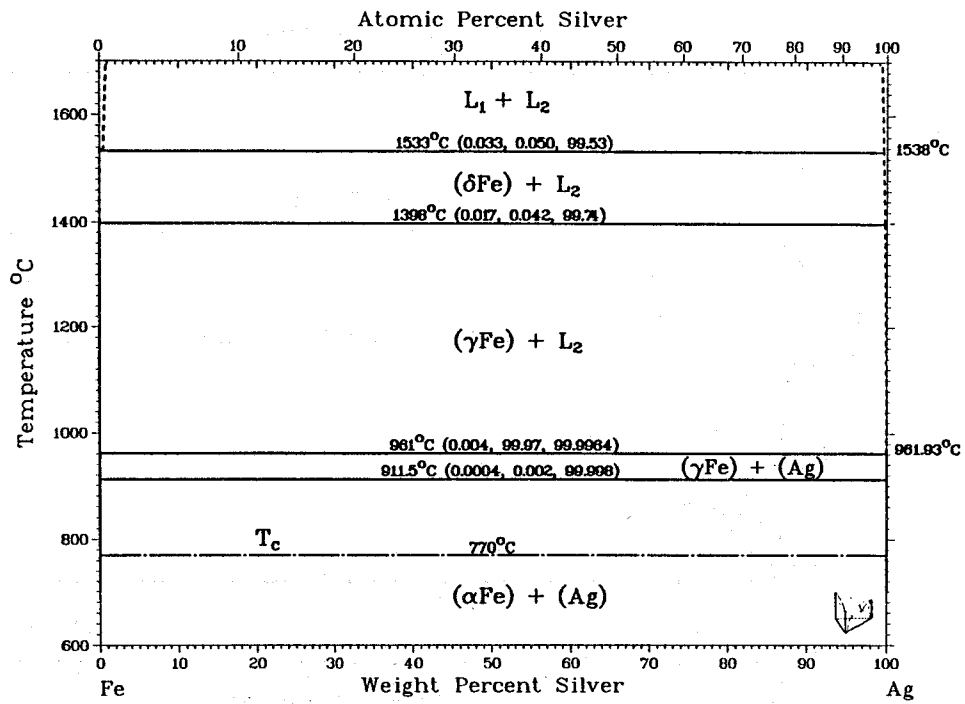


Fig. 3: Binary alloy phase diagrams of the systems Ag-Fe and Ag-Ni [7].

Ag-Cr Phase Diagram

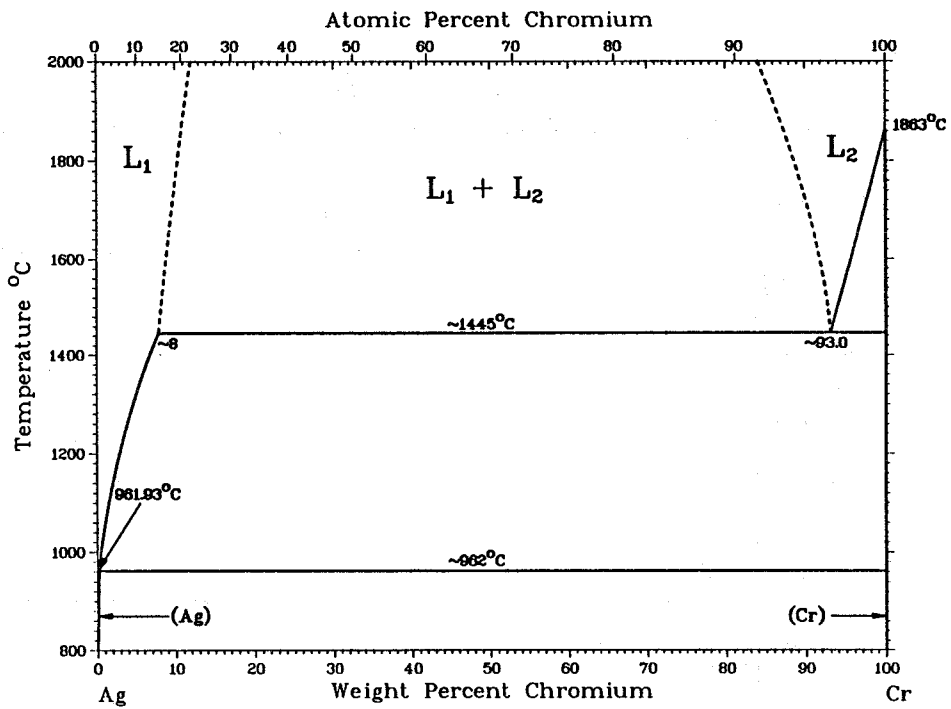
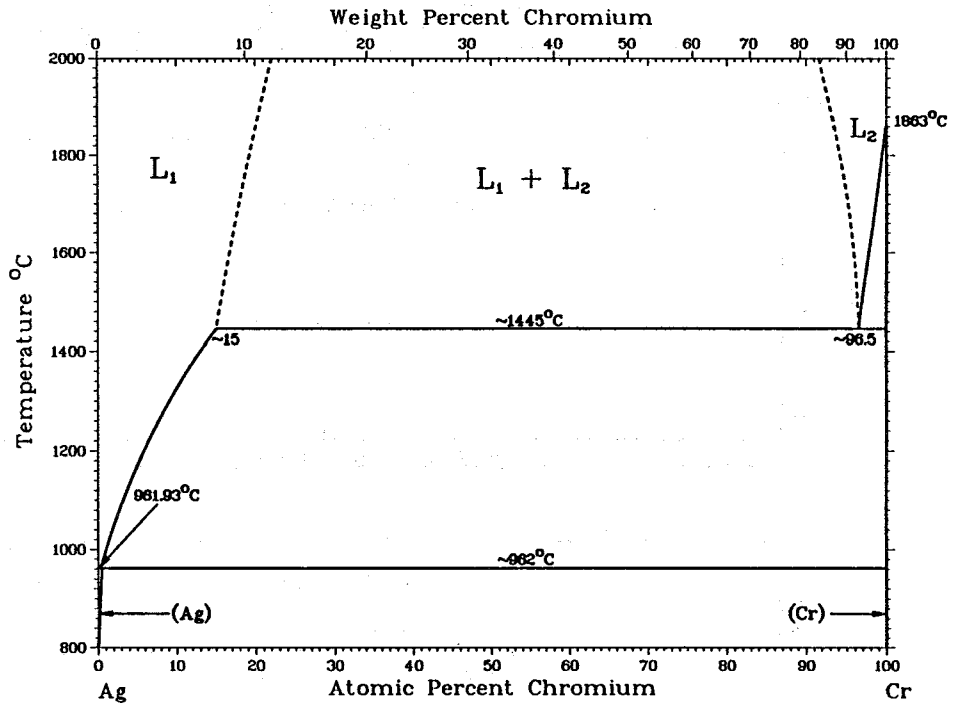


Fig. 4: Binary alloy phase diagram of the system Ag-Cr [7].

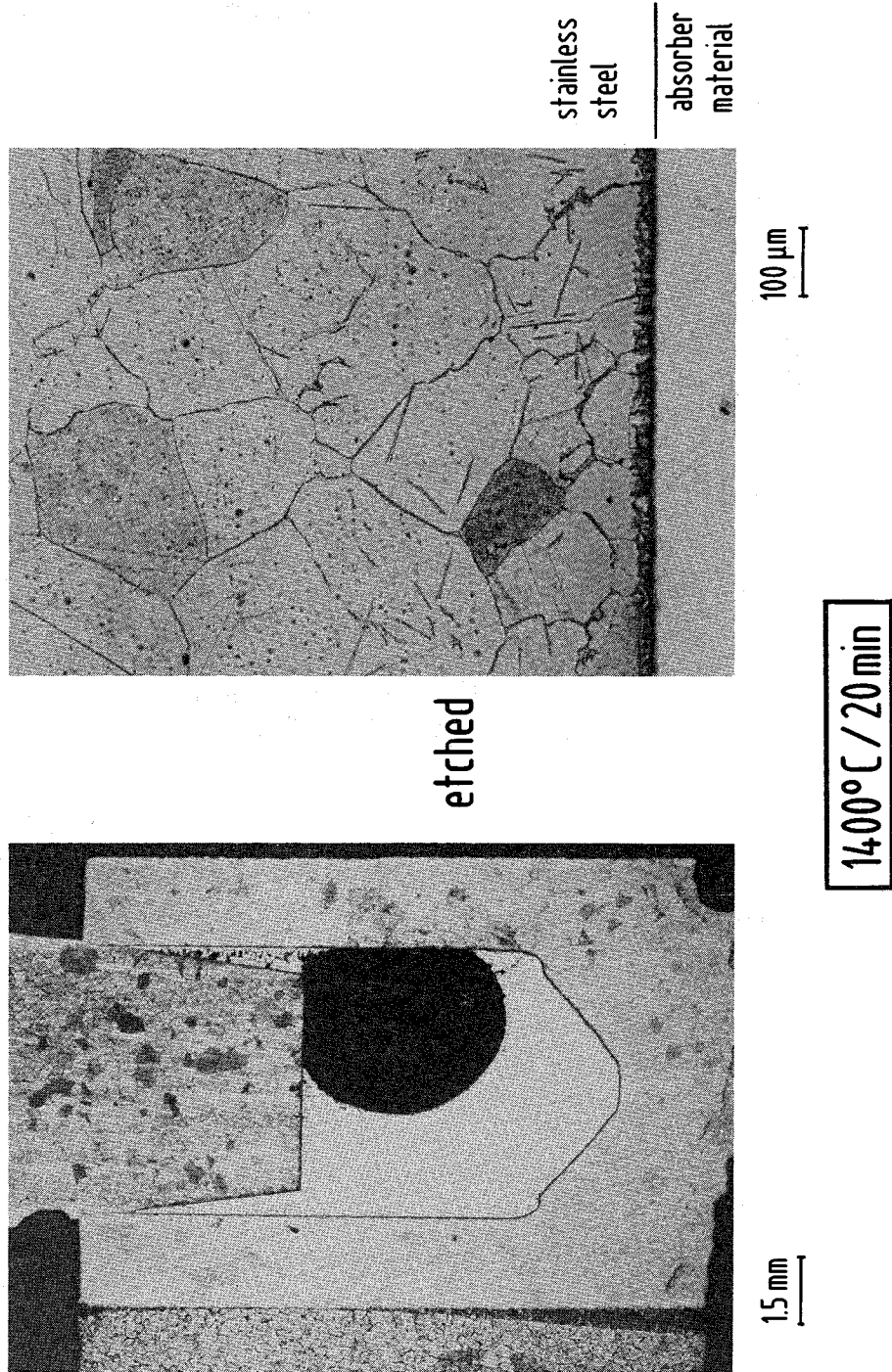


Fig. 5: (Ag,In,Cd) alloy/stainless steel 1.4919 (AISI 316) reaction couple after annealing at 1400 °C for 20 minutes.

Ag-Zr Phase Diagram

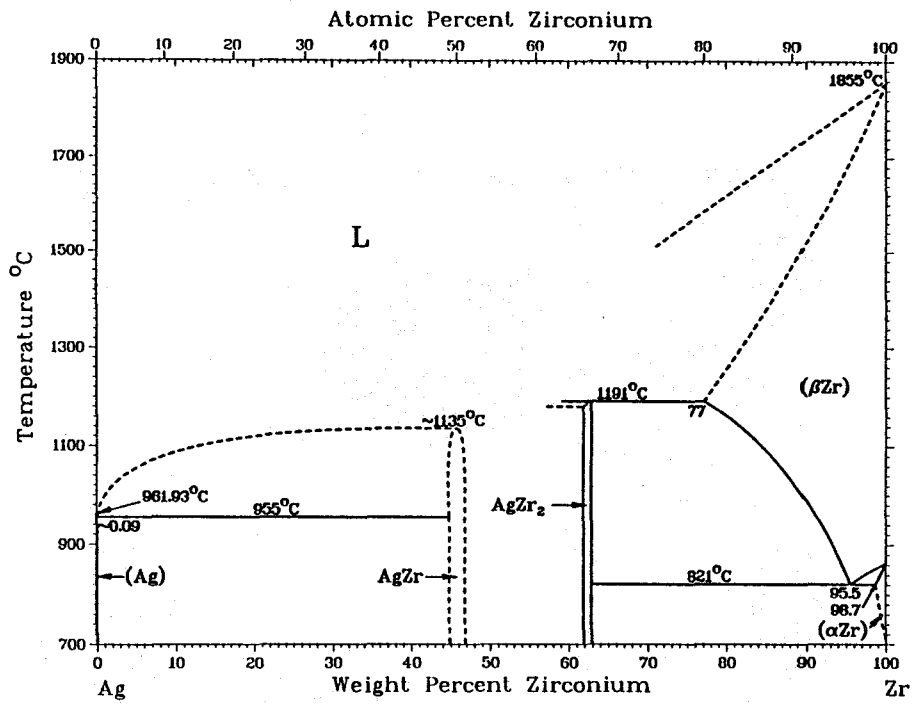
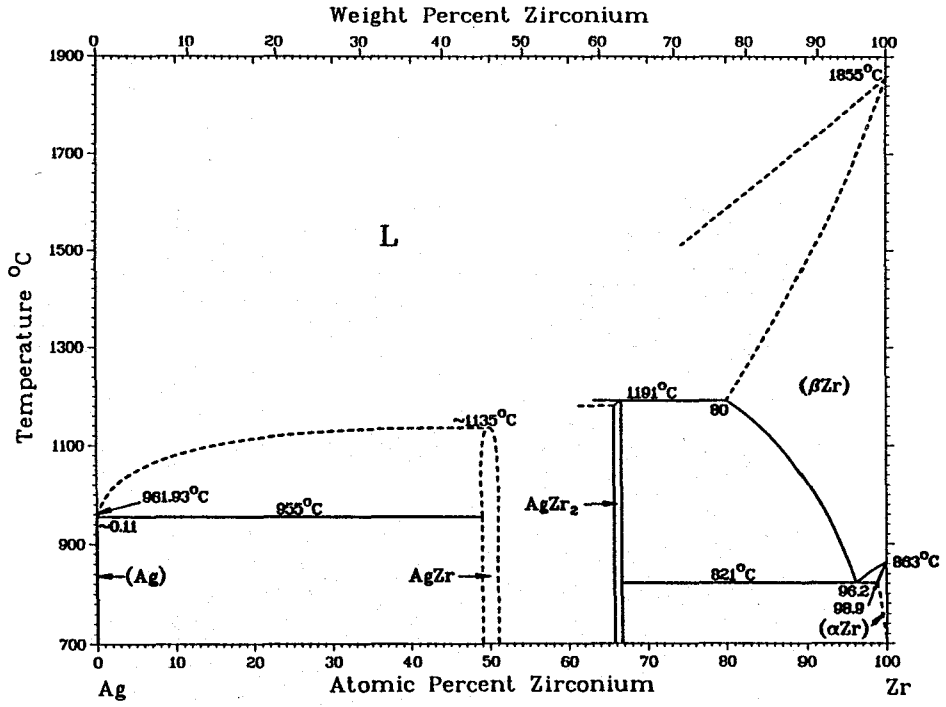


Fig. 6: Binary alloy phase diagram of the system Ag-Zr [7].

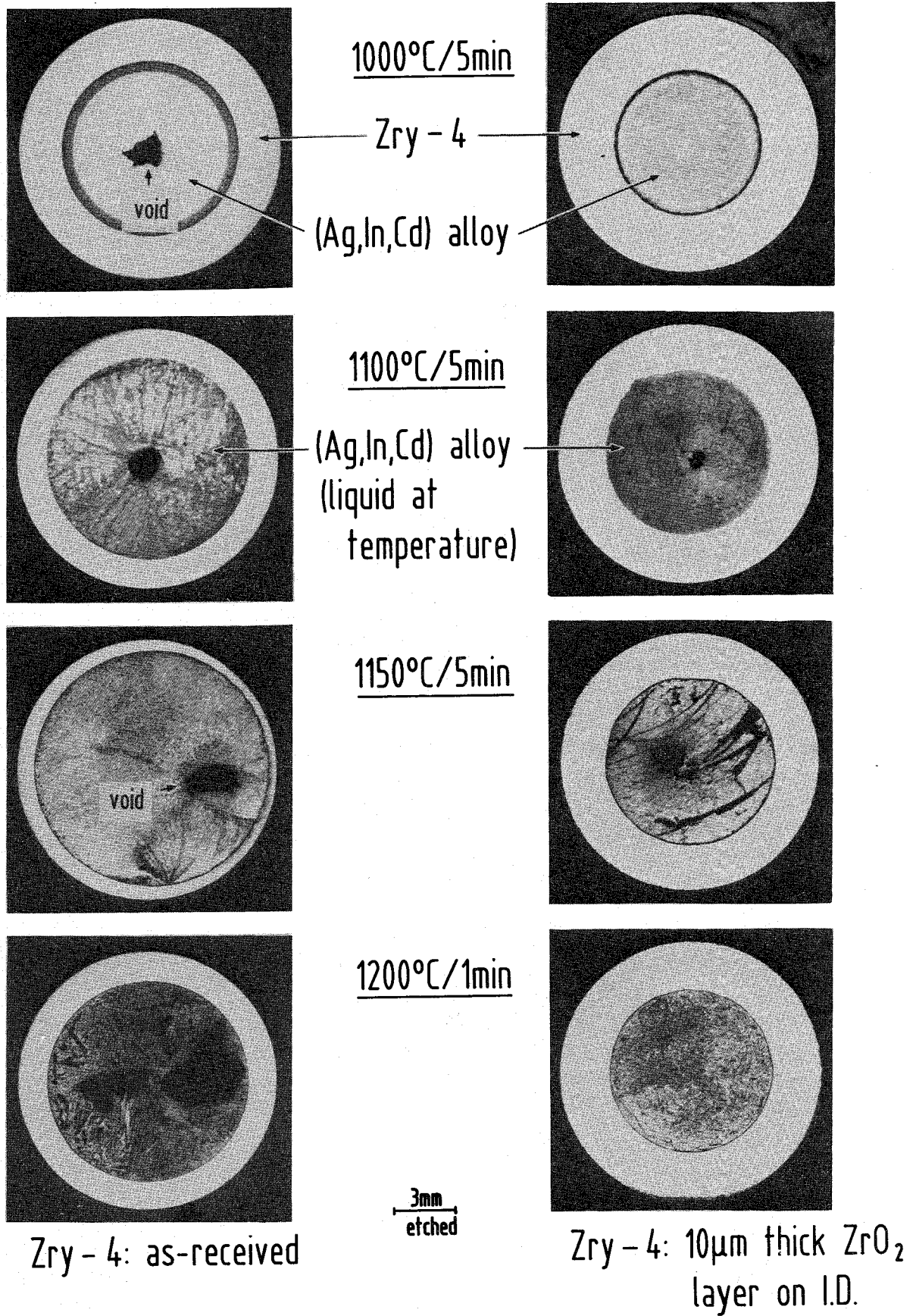


Fig. 7: Chemical interaction between (Ag,In,Cd) alloy and Zircaloy-4 at different temperatures; influence of a thin ZrO₂ layer on the reaction behavior (right row of pictures).

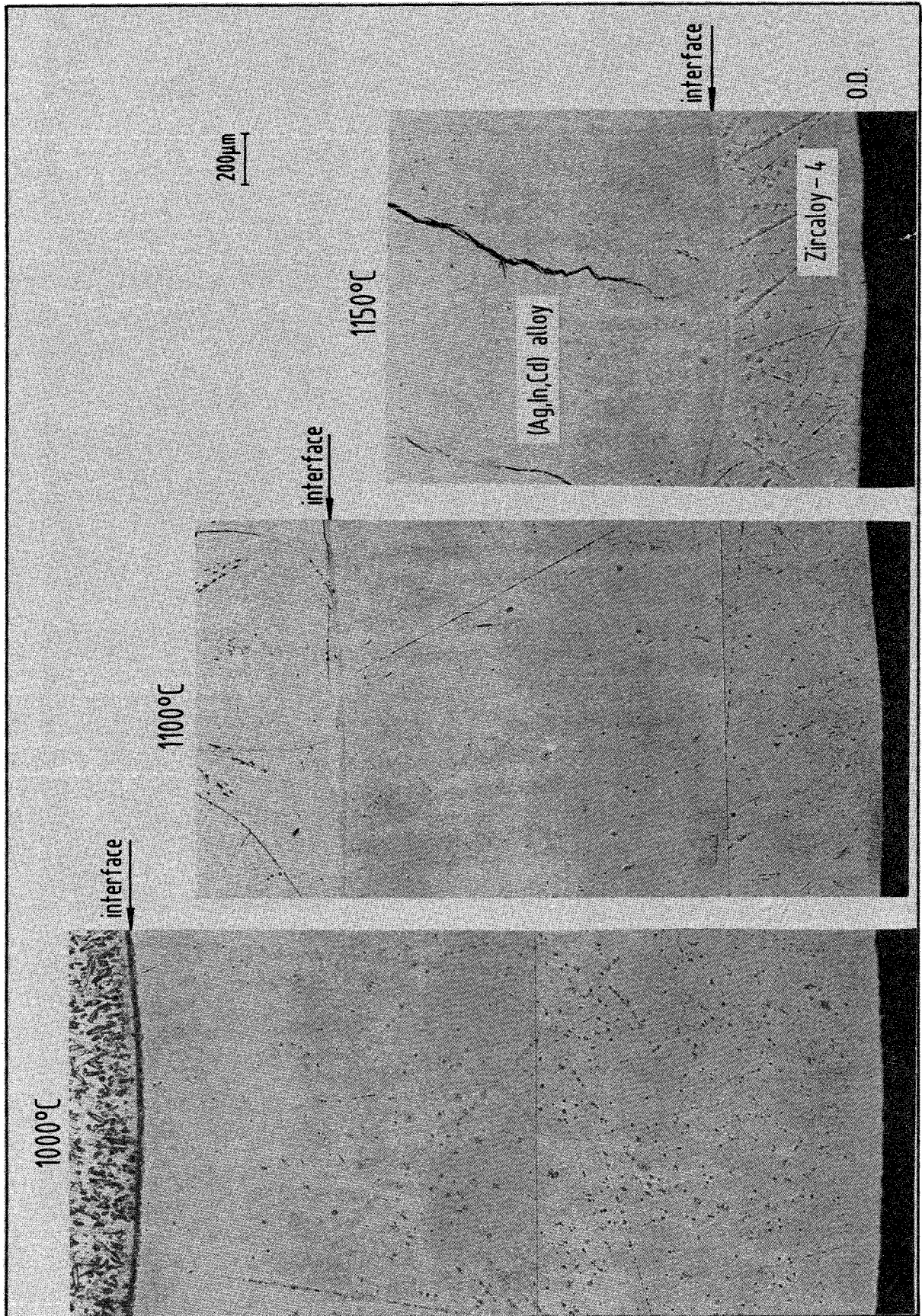


Fig. 8: Zircaloy-4 wall thickness decrease due to chemical interactions with the (Ag,In,Cd) alloy at different temperatures after annealing for 5 minutes.

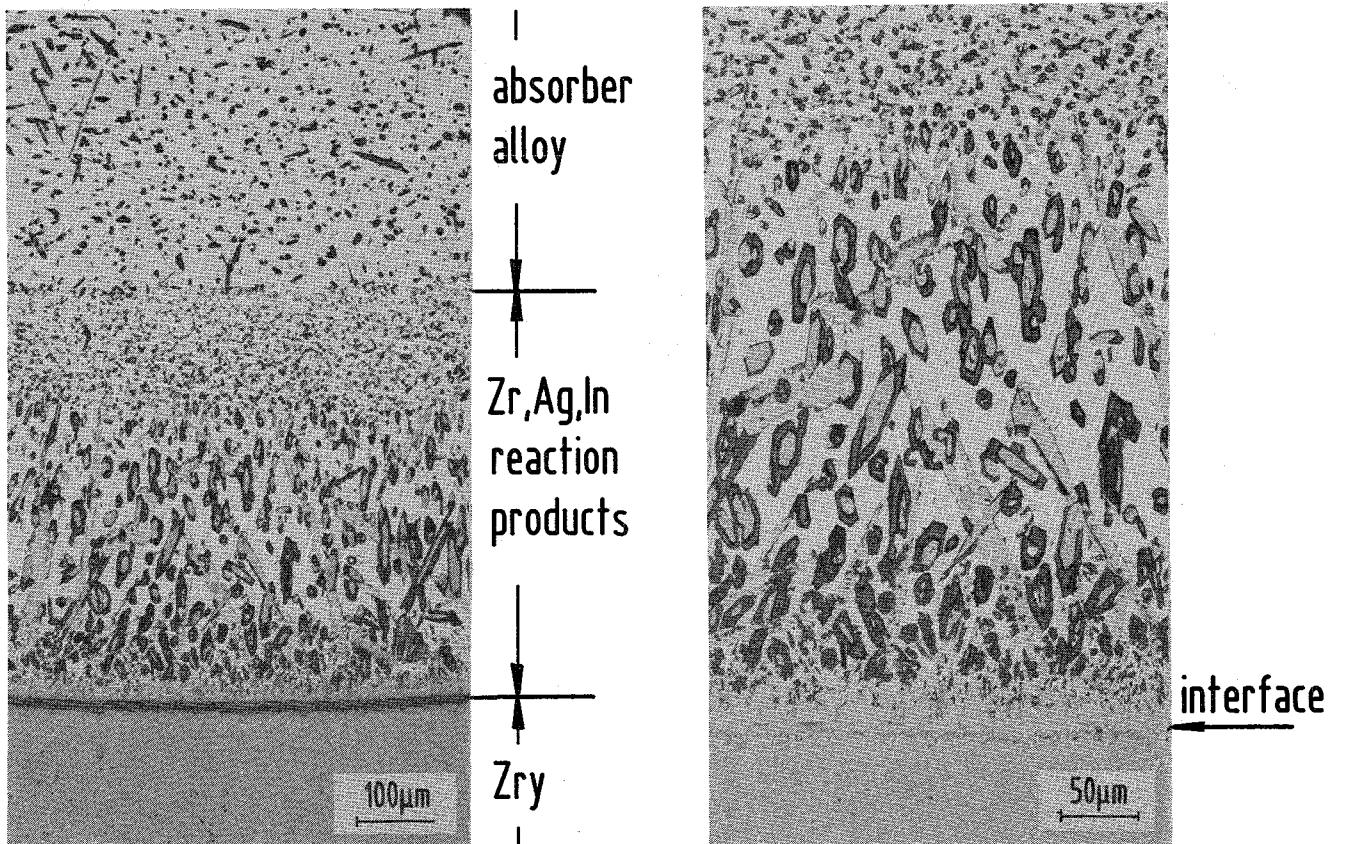
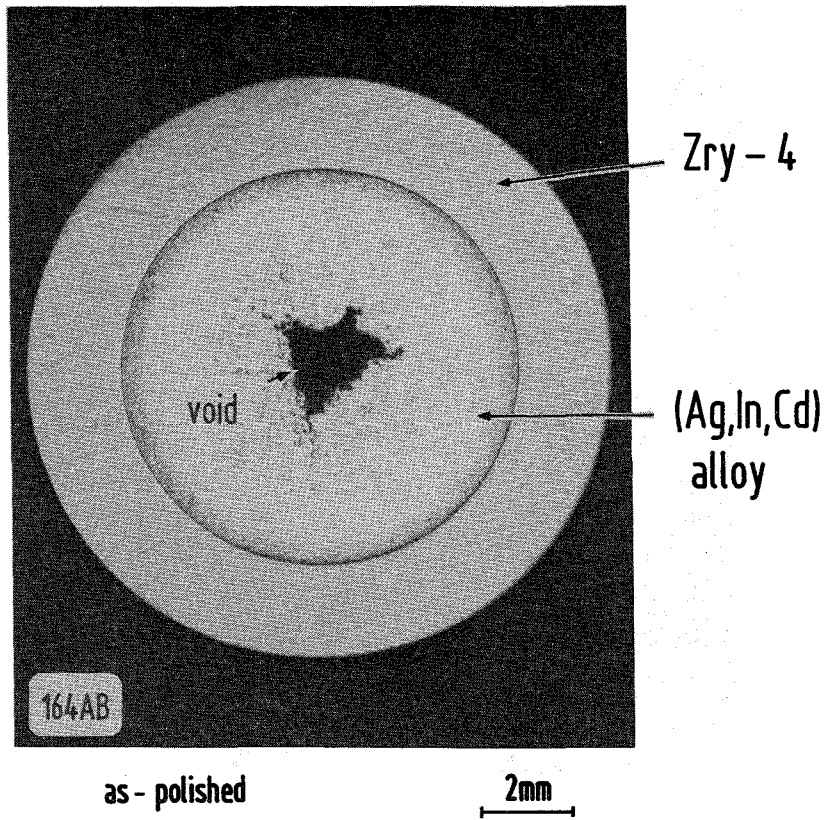


Fig. 9: Chemical interactions between (Ag,In,Cd) alloy and Zircaloy-4; 1000 °C/ 5 min.

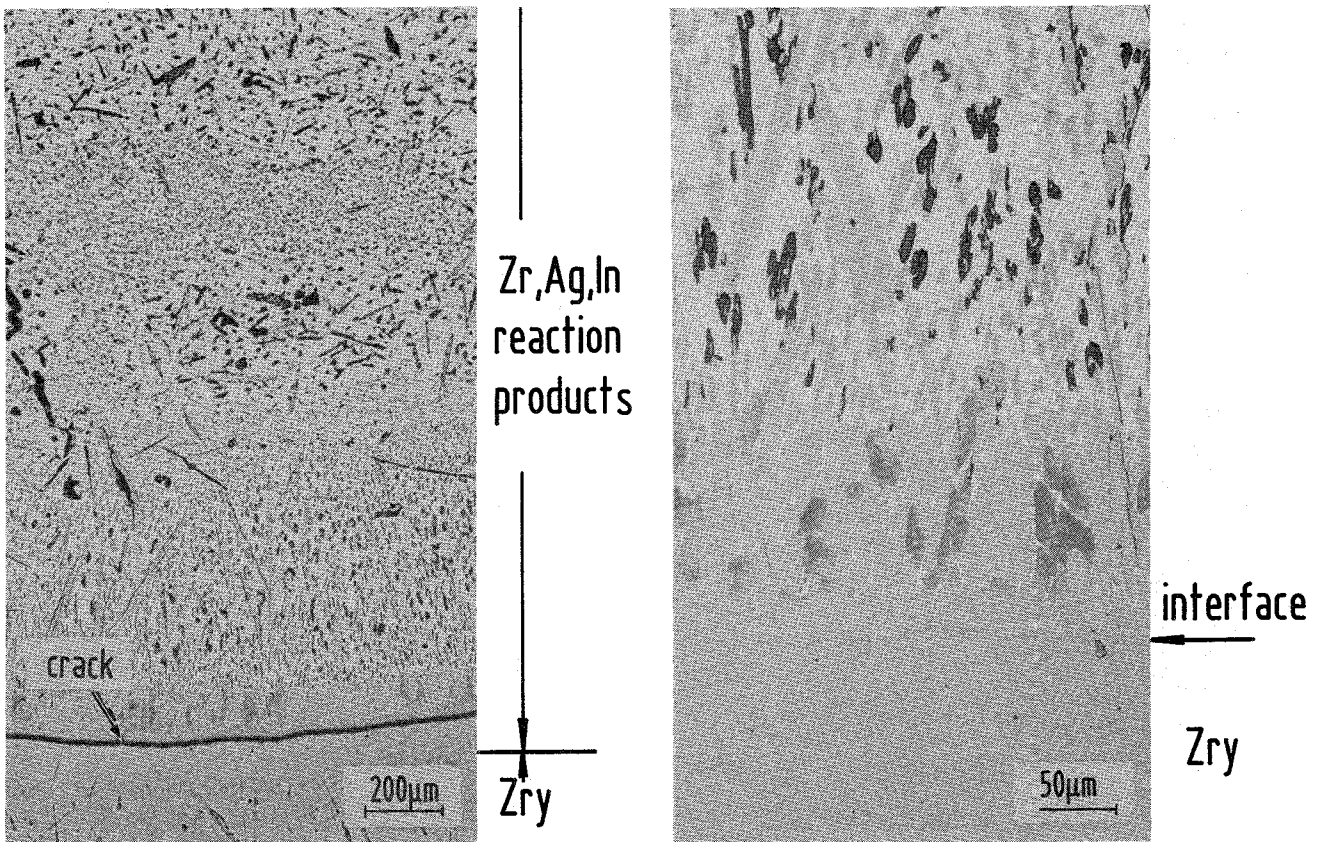
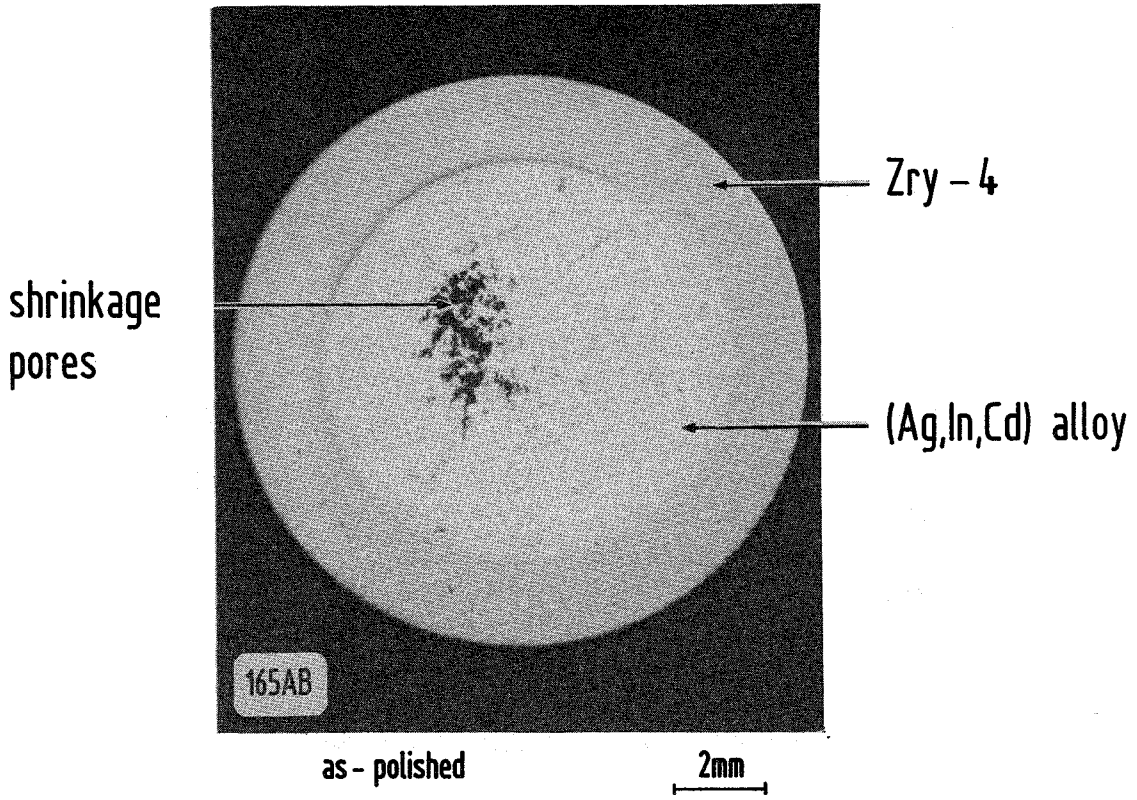


Fig. 10: Chemical interactions between (Ag,In,Cd) alloy and Zircaloy-4; 1000 °C/ 15 min.

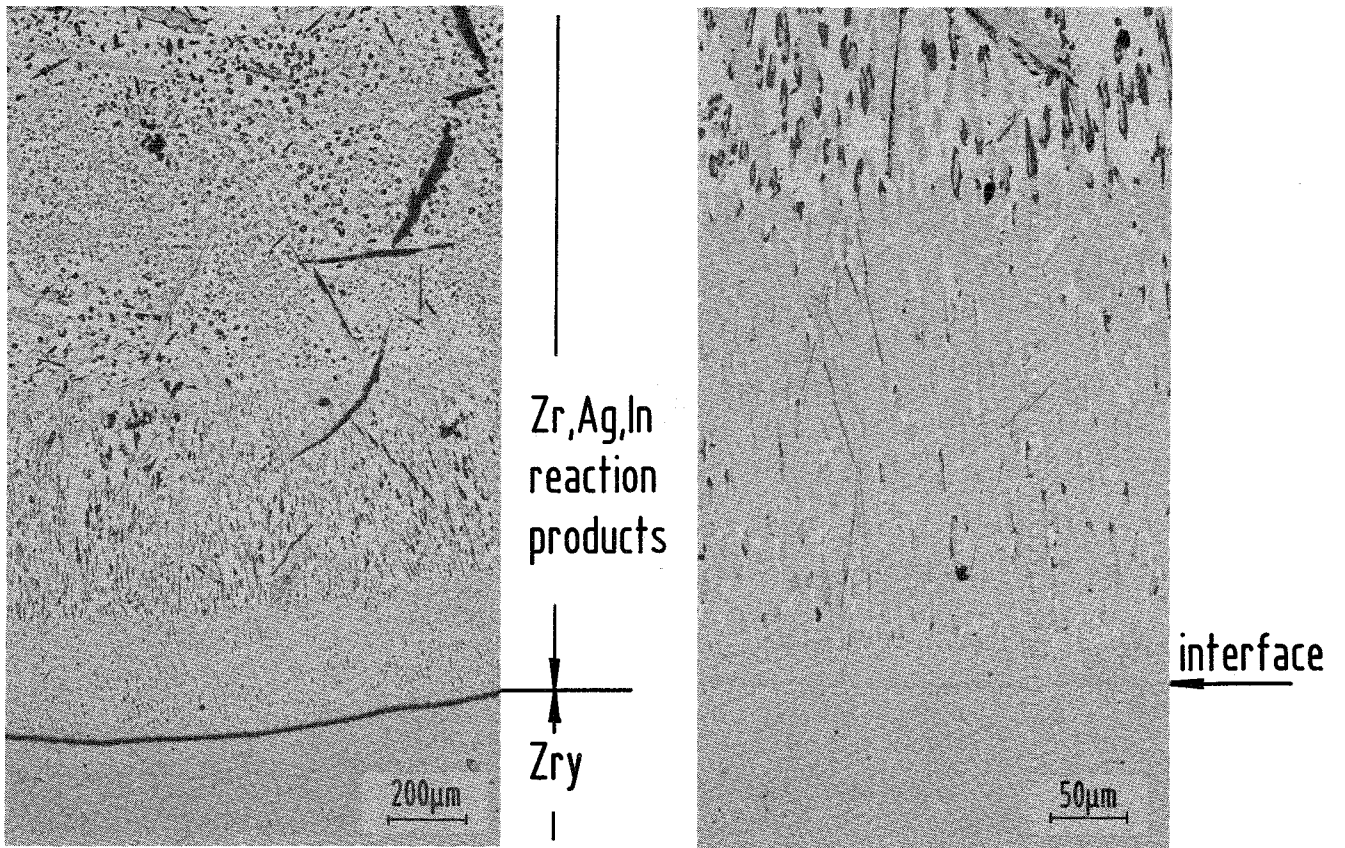
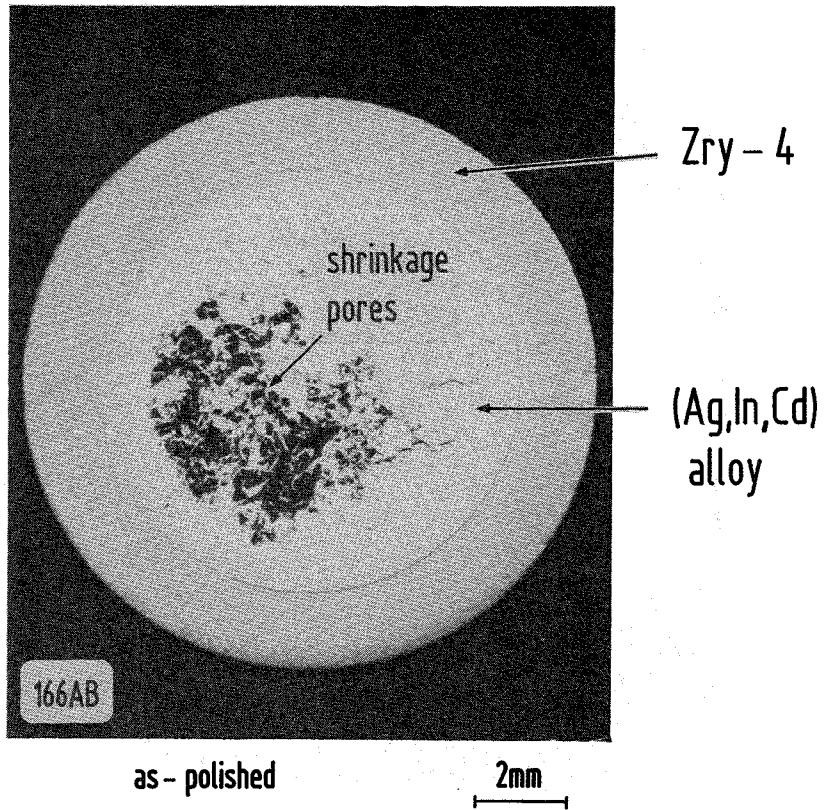


Fig. 11: Chemical interactions between (Ag,In,Cd) alloy and Zircaloy-4; 1000 °C/ 30 min.

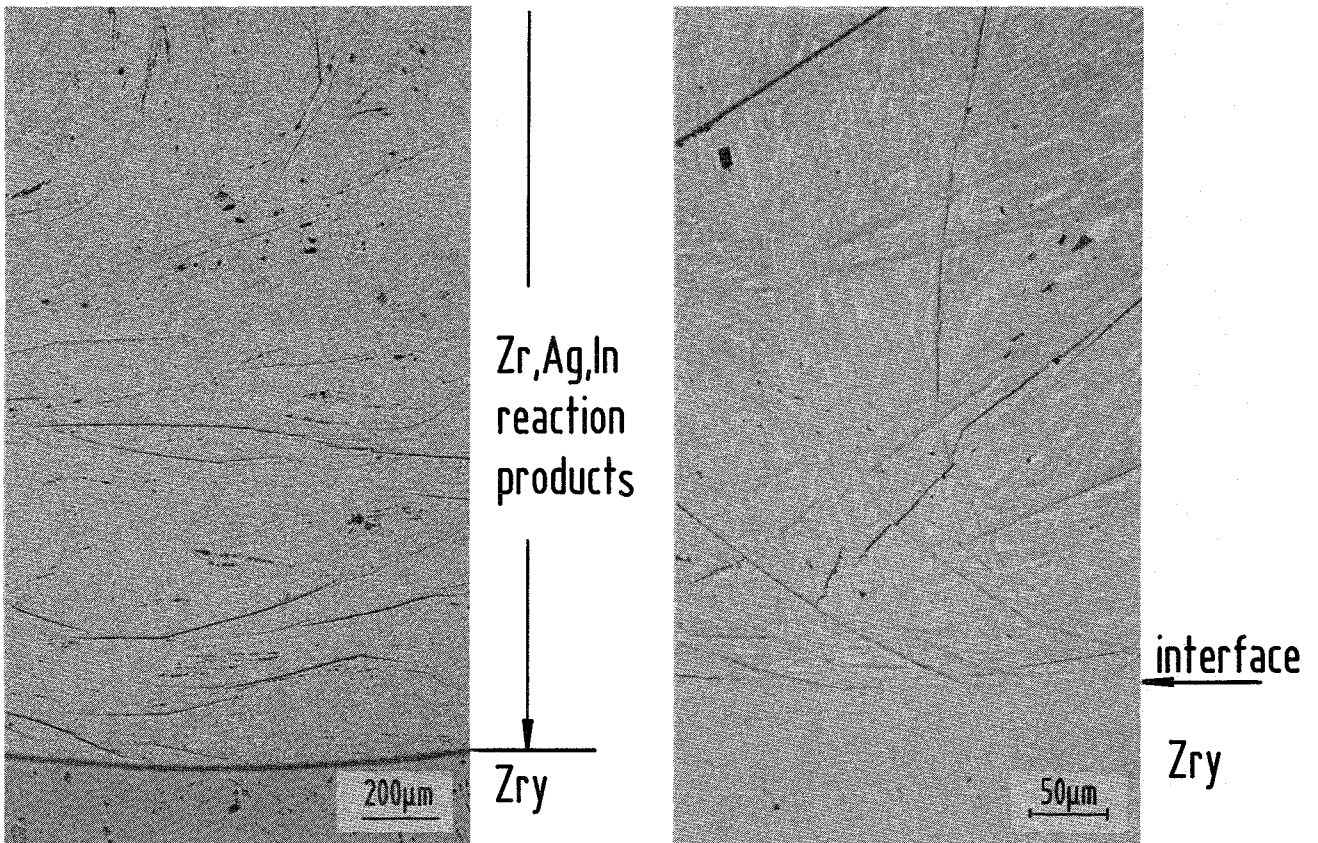
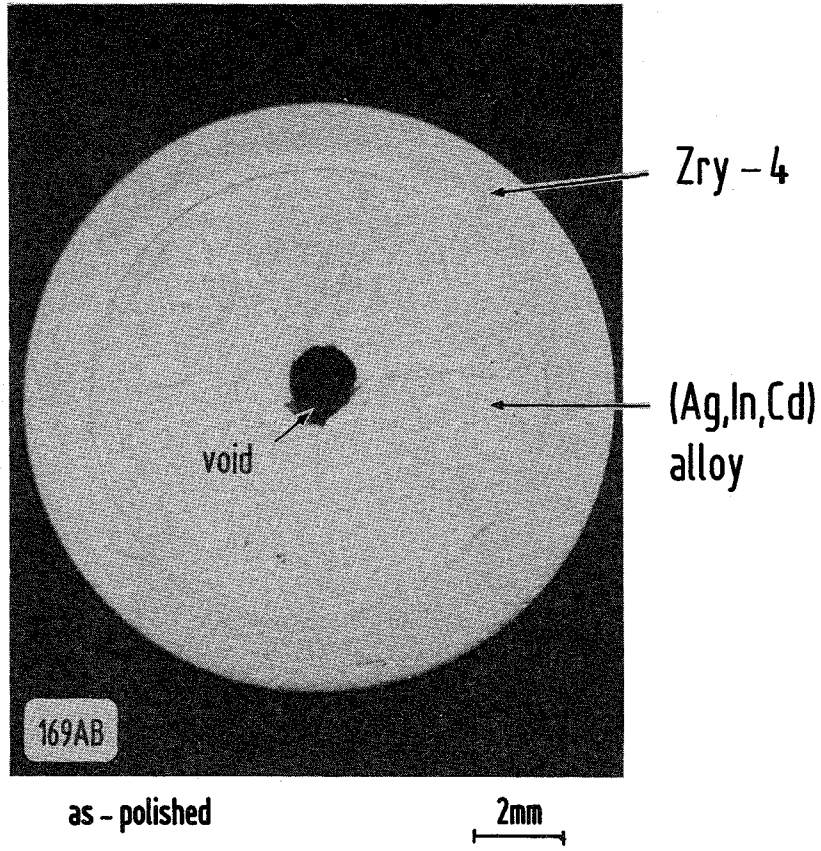


Fig. 12: Chemical interactions between (Ag,In,Cd) alloy and Zircaloy-4; 1100 °C/ 5 min.

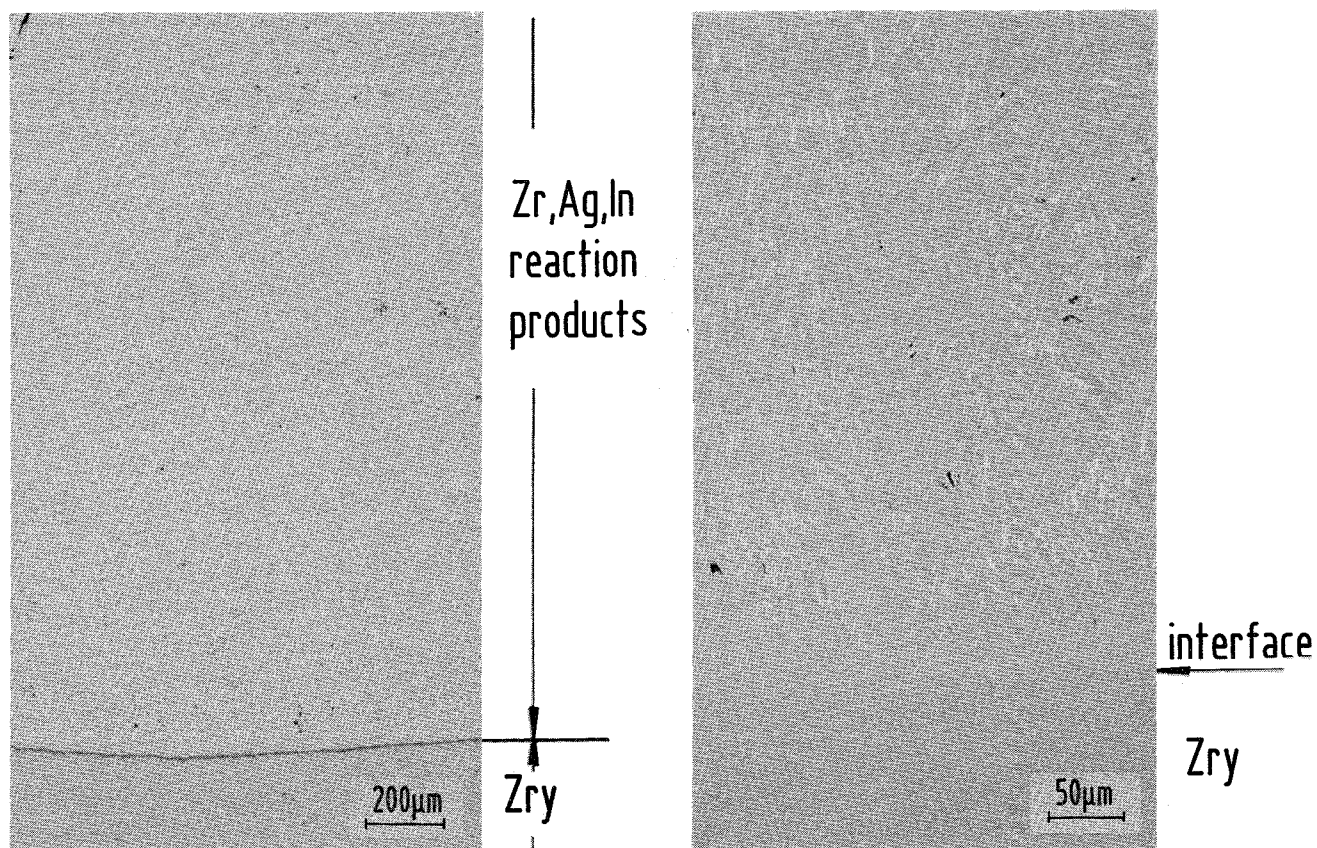
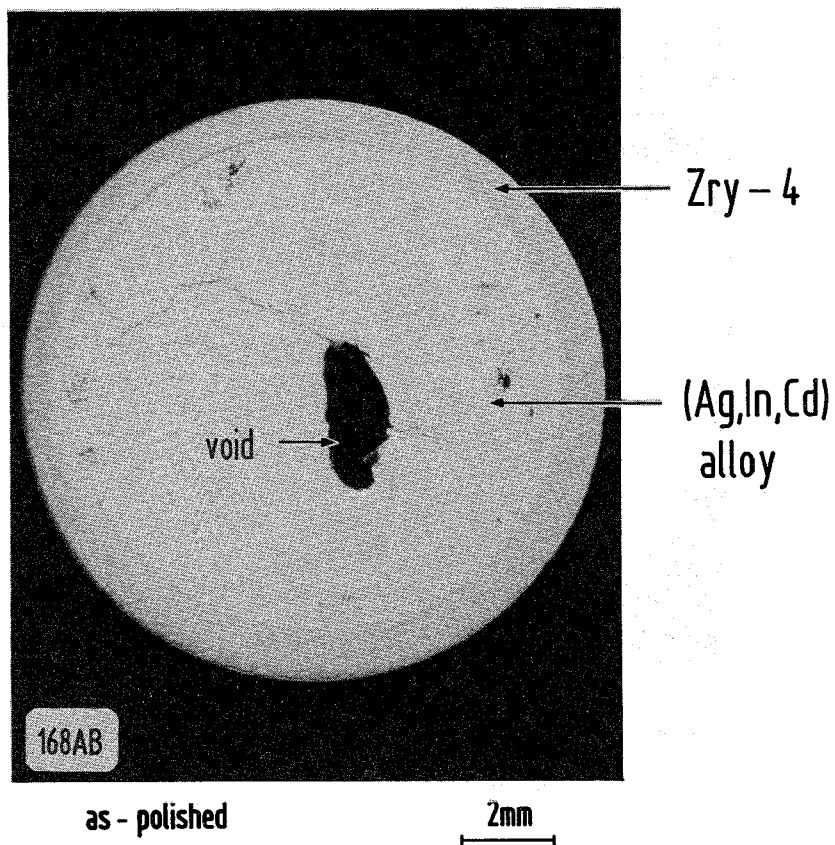


Fig. 13: Chemical interactions between (Ag,In,Cd) alloy and Zircaloy-4; 1100 °C/ 10 min.

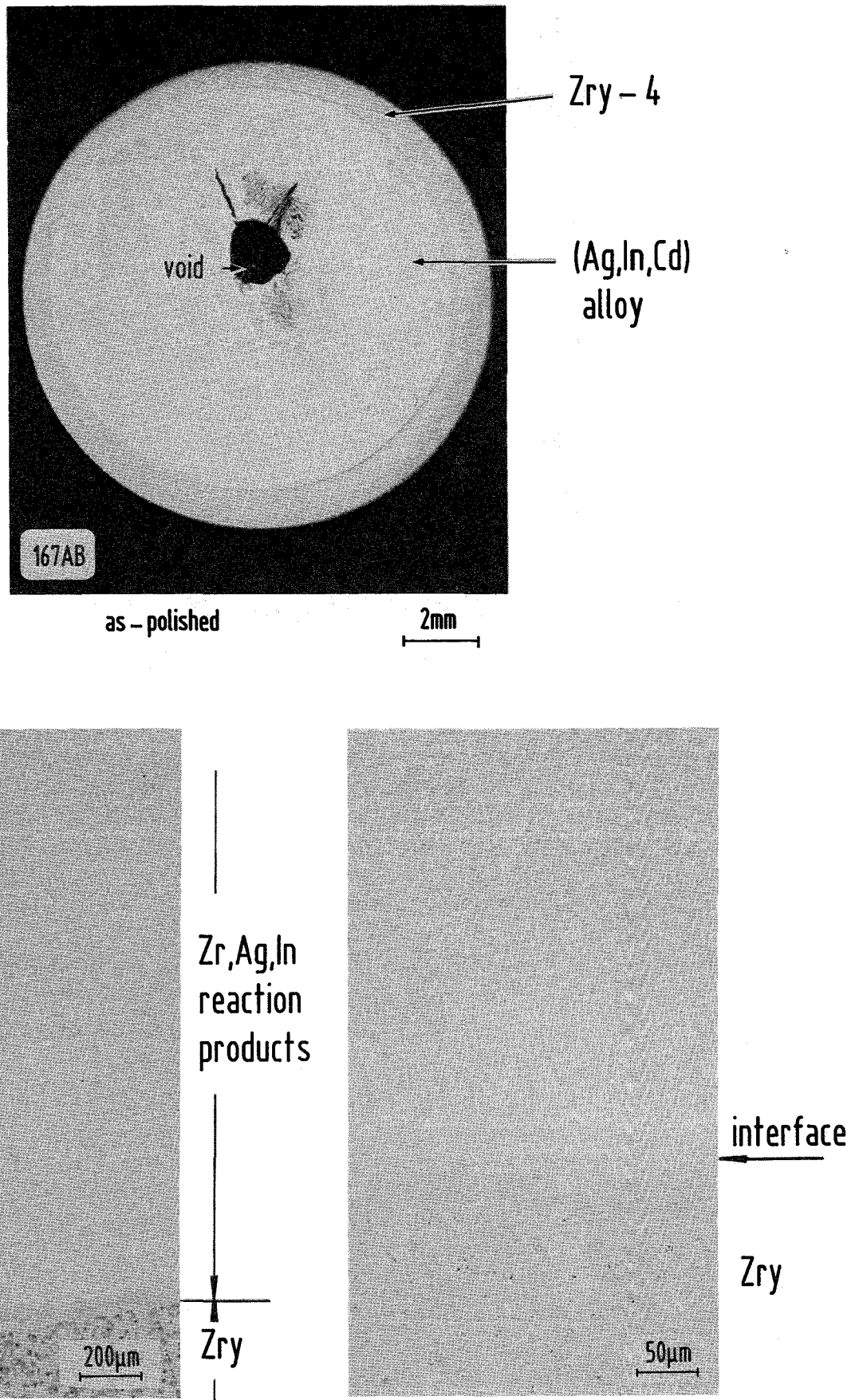


Fig. 14: Chemical interactions between (Ag,In,Cd) alloy and Zircaloy-4; 1100 °C/ 15 min.

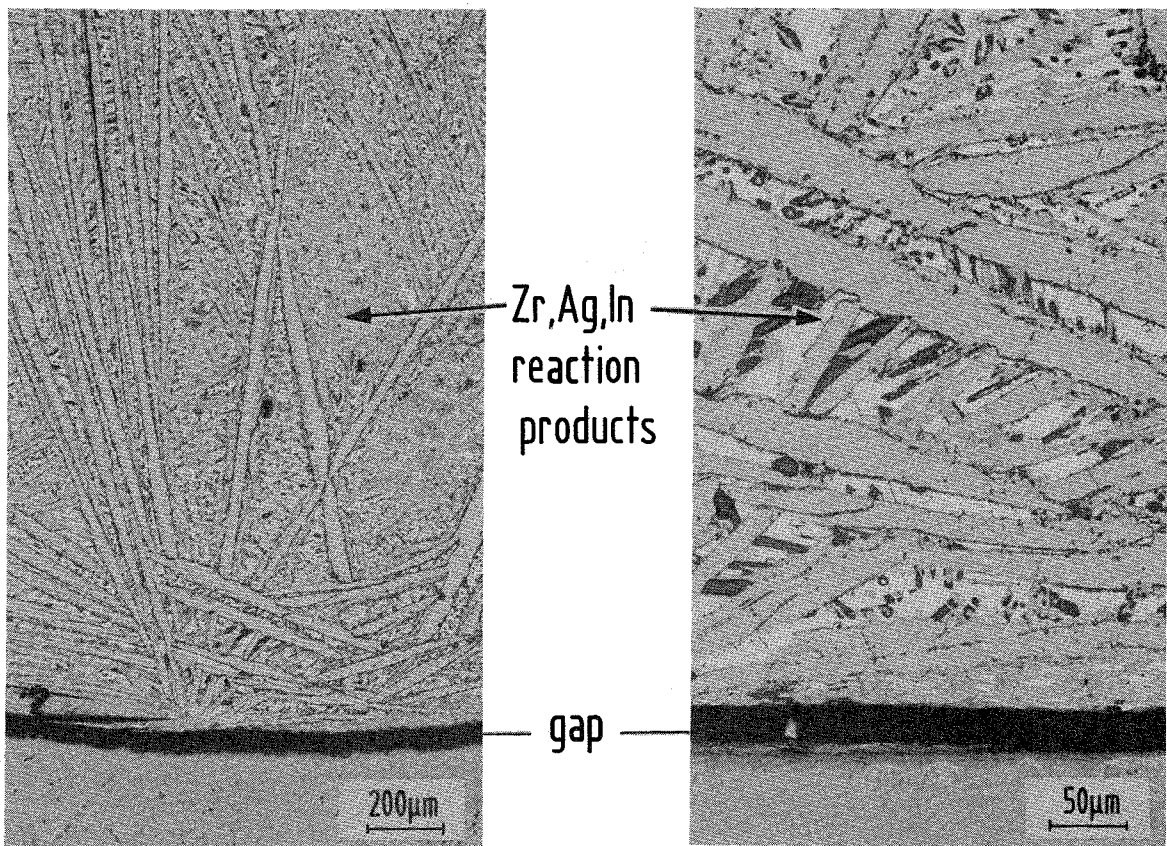
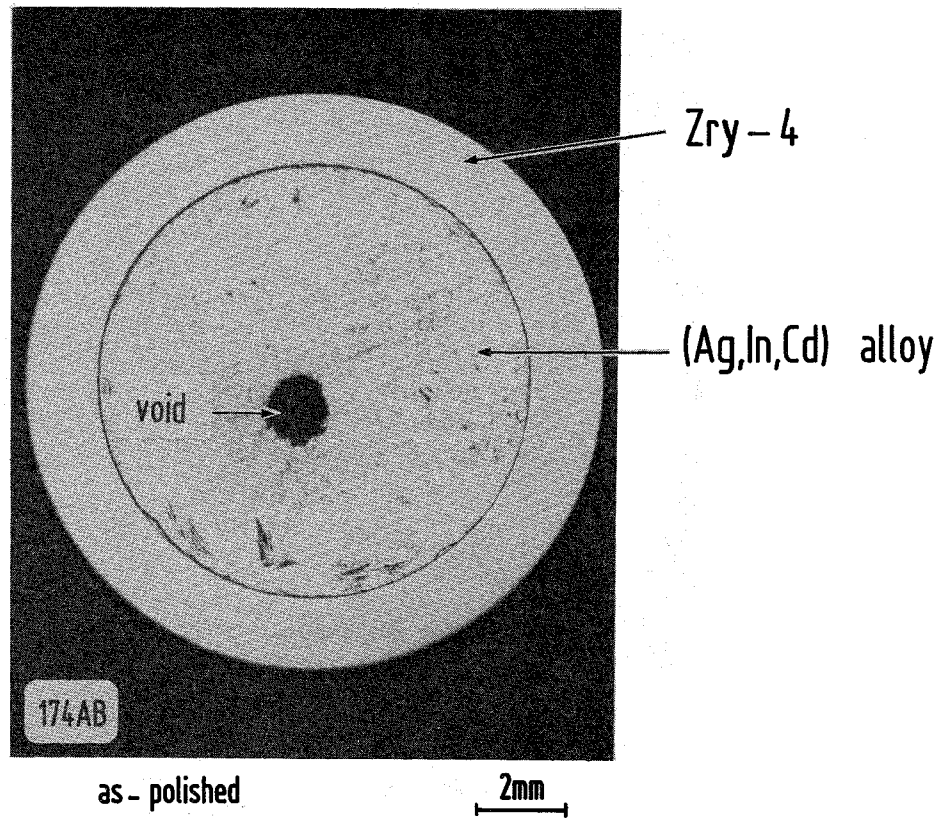


Fig. 15: Chemical interactions between (Ag,In,Cd) alloy and Zircaloy-4; 1150 °C/ 2 min.

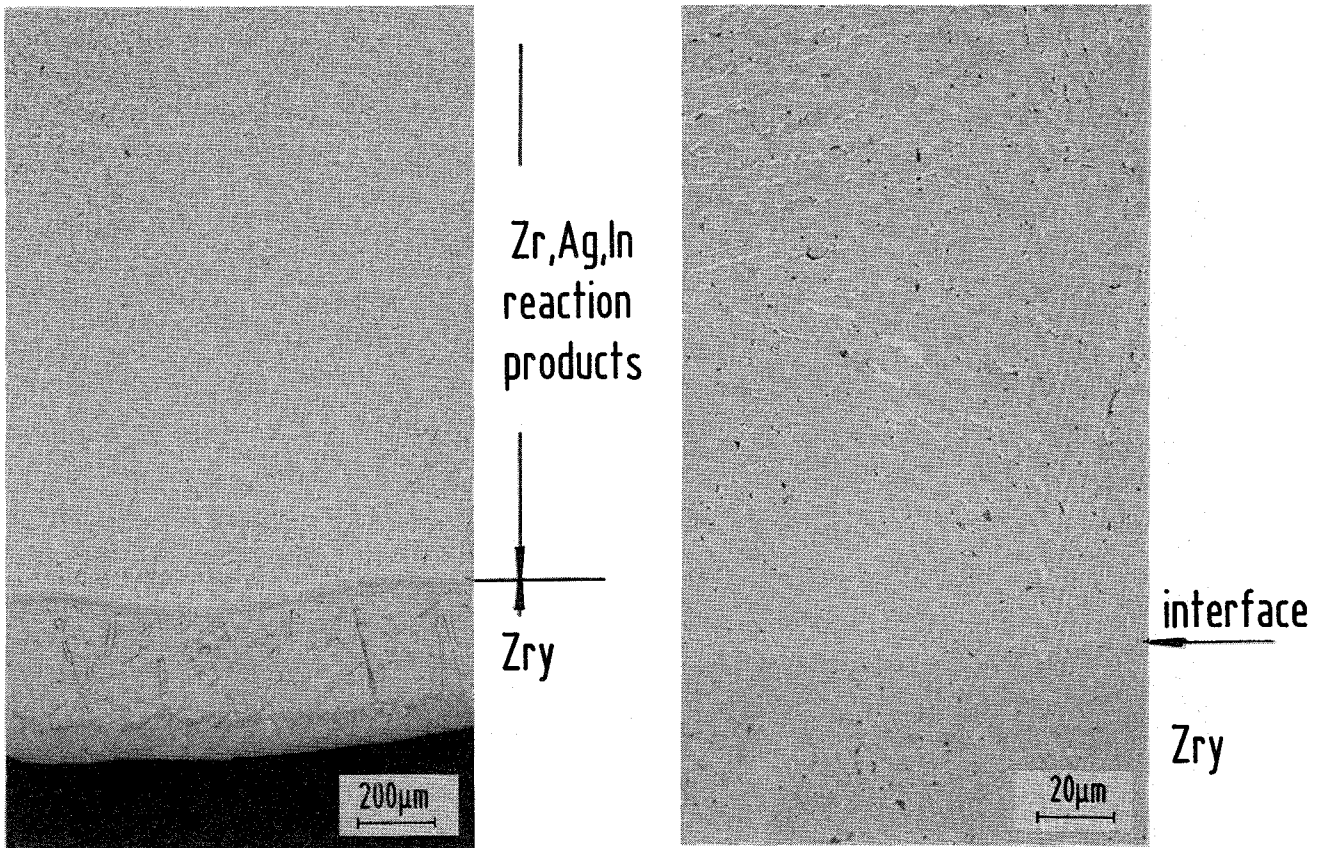
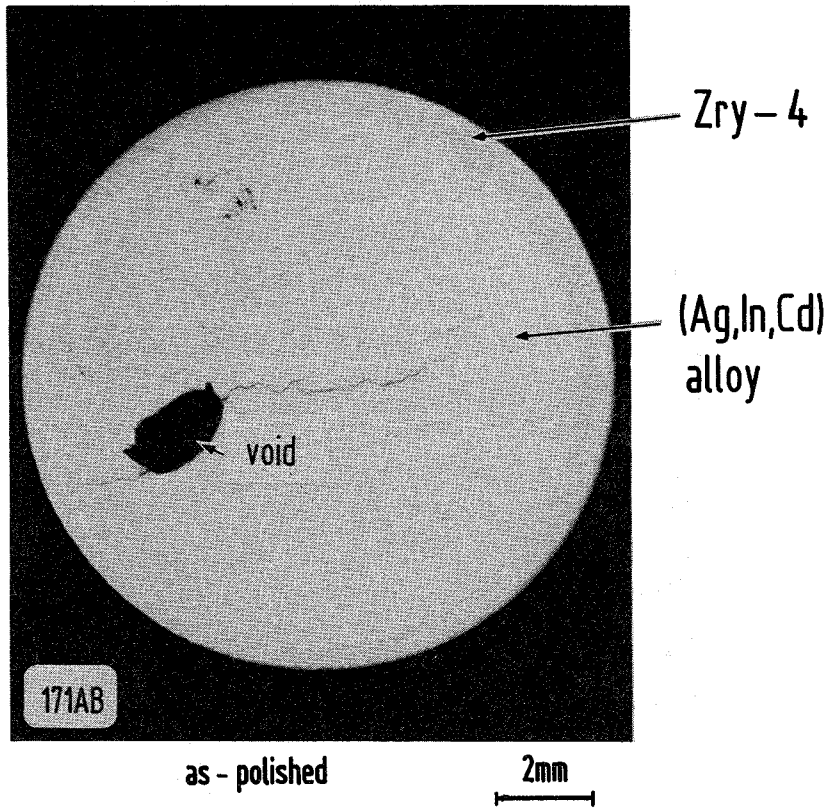


Fig. 16: Chemical interactions between (Ag,In,Cd) alloy and Zircaloy-4; 1150 °C/ 5 min.

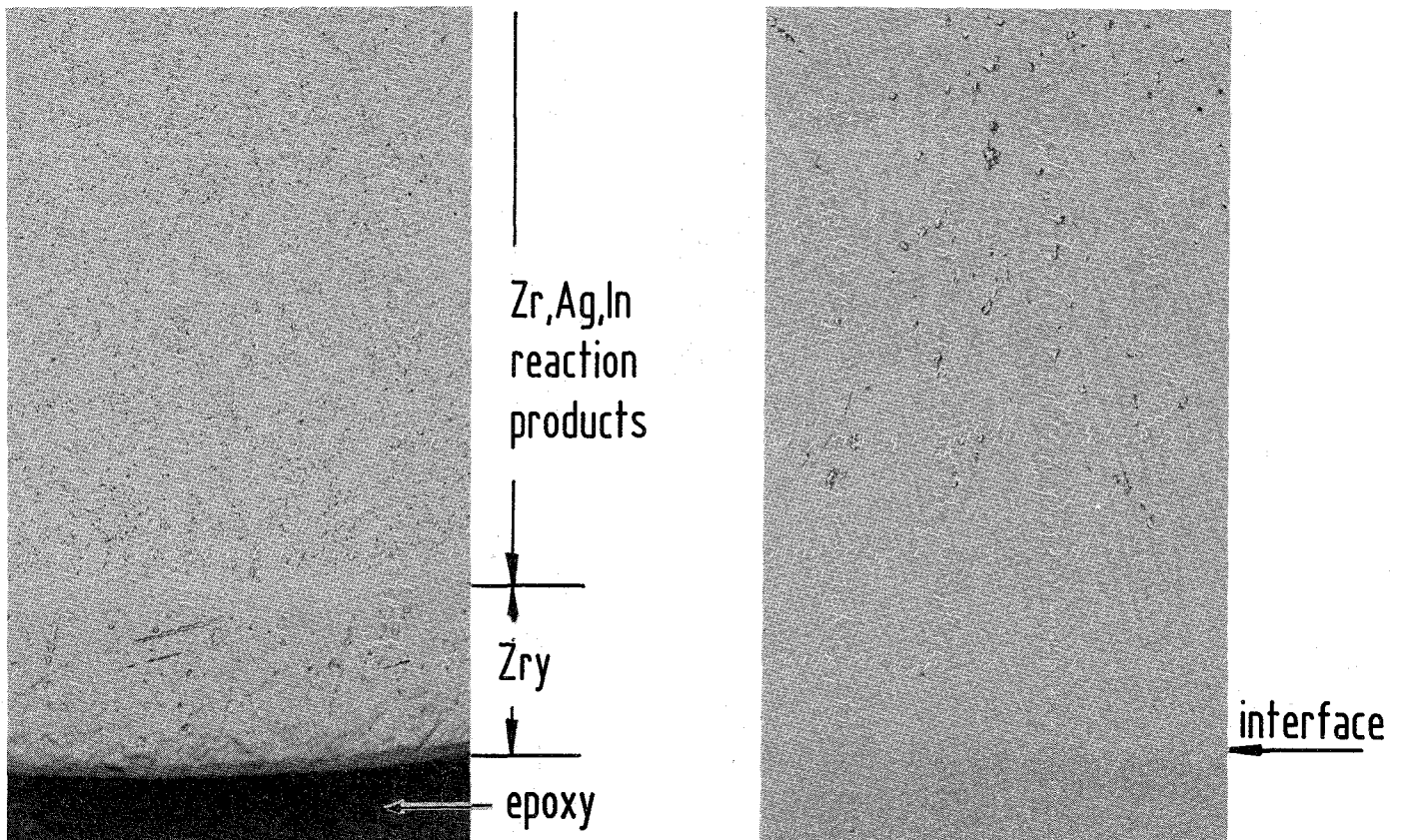
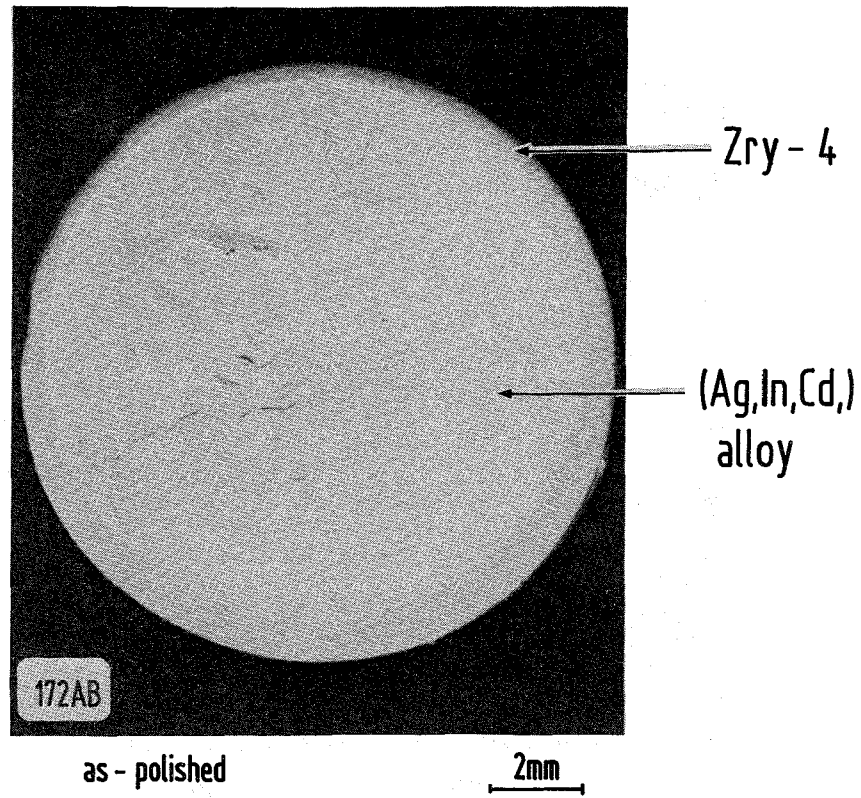


Fig. 17: Chemical interactions between (Ag,In,Cd) alloy and Zircaloy-4; 1150 °C/ 15 min.

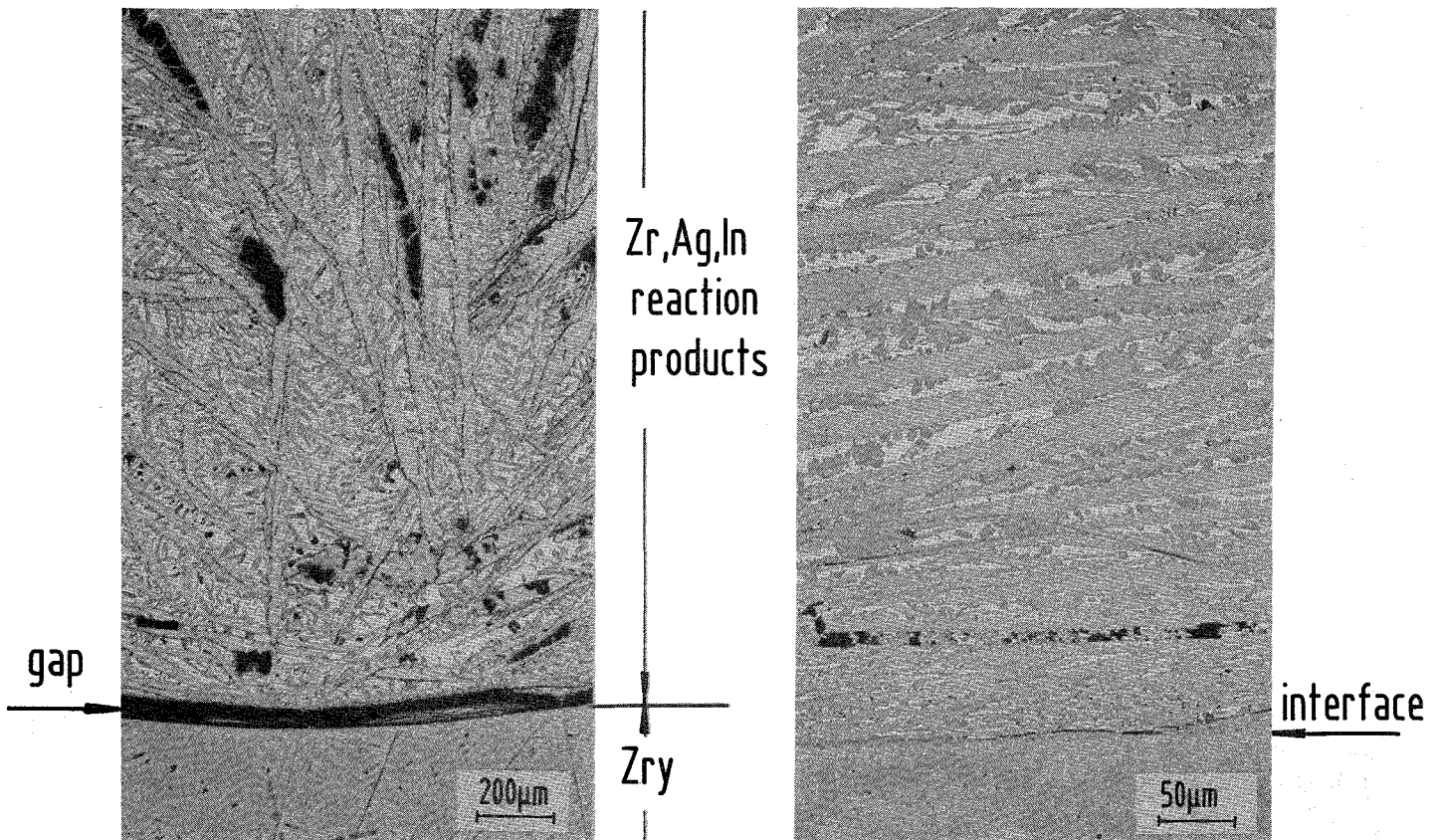
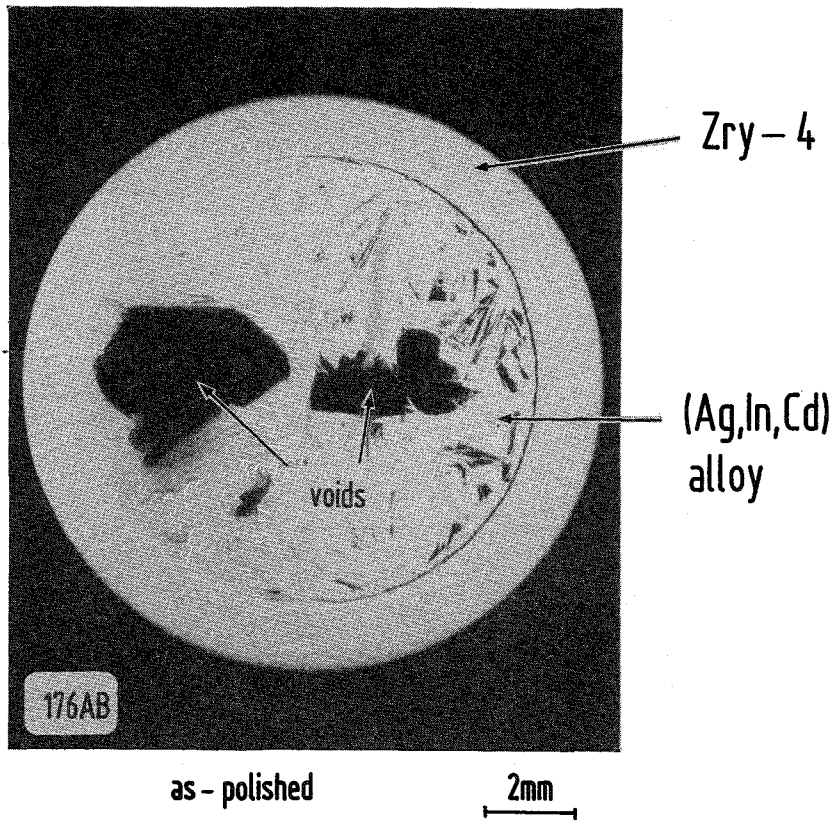
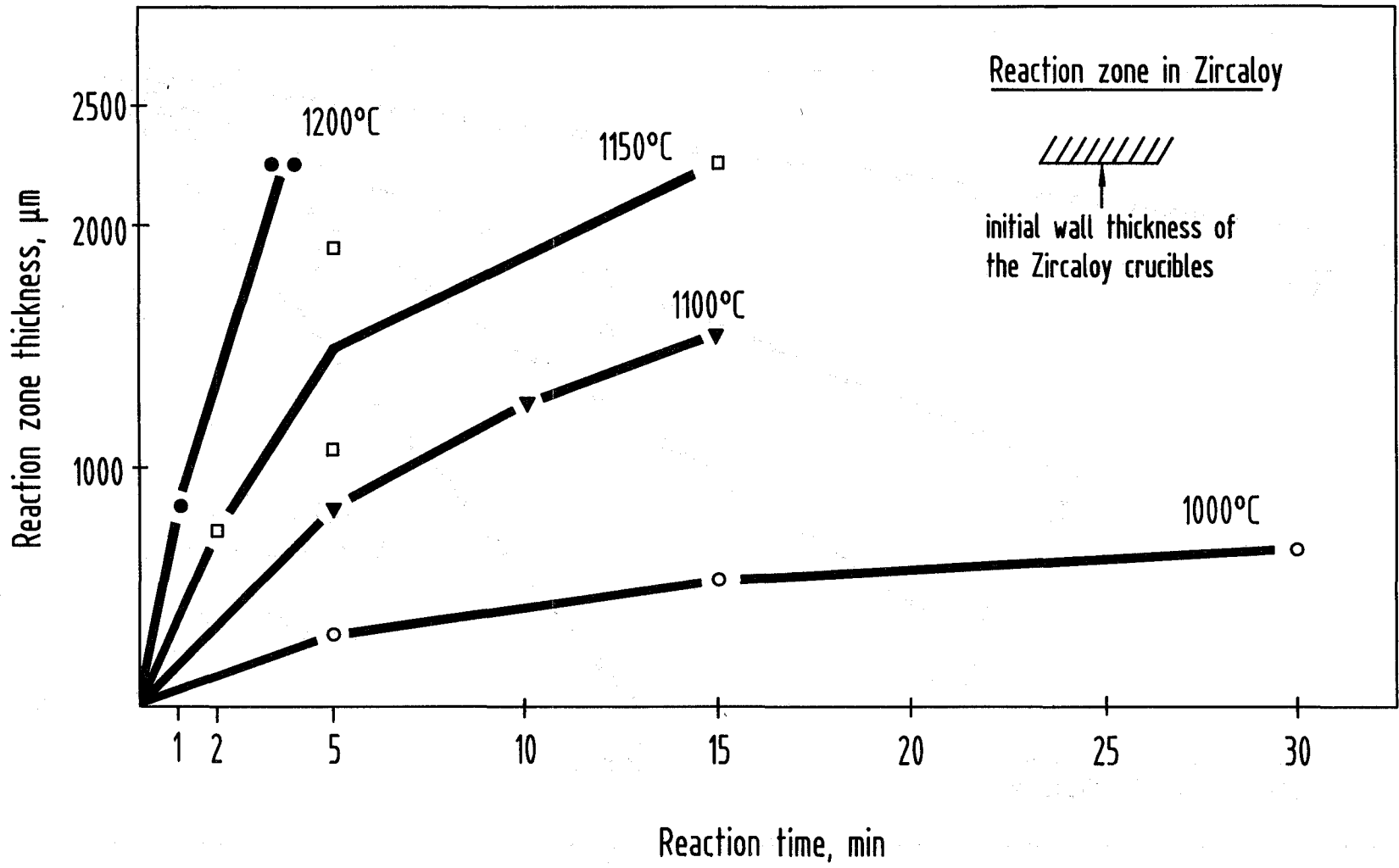


Fig. 18: Chemical interactions between (Ag,In,Cd) alloy and Zircaloy-4; 1200 °C/ 1 min.

Fig. 19: Maximum reaction zone thicknesses in the system (Ag,In,Cd) alloy/ Zircaloy-4 as a function of time between 1000 and 1200 °C (table 1).



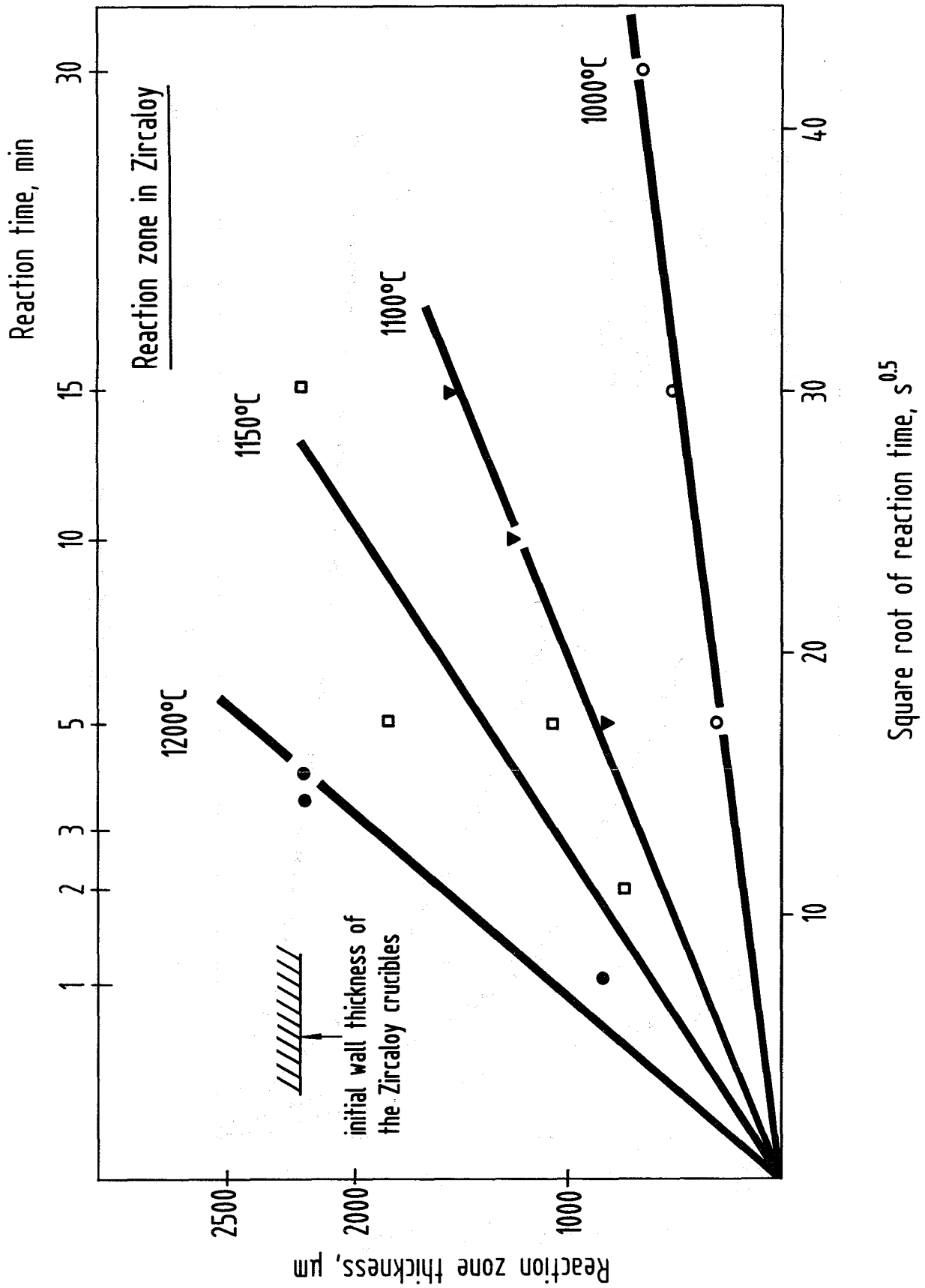


Fig. 20: Maximum reaction zone thicknesses in the system (Ag,In,Cd) alloy/ Zircaloy-4 as a function of the square root of time between 1000 and 1200 °C (table 1).

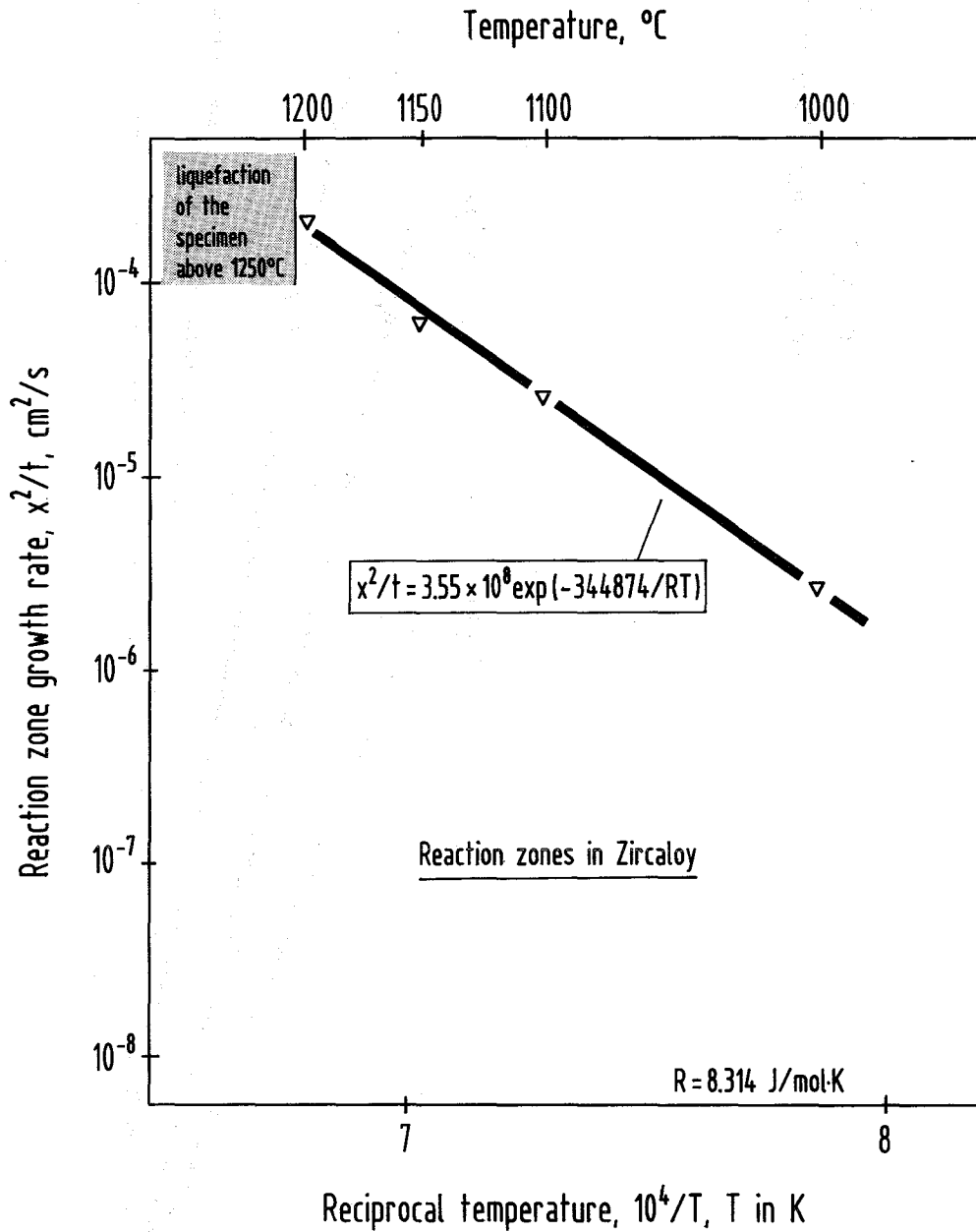


Fig. 21: Reaction zone growth rates for the reaction system (Ag,In,Cd) alloy/Zircaloy-4 (table 2).

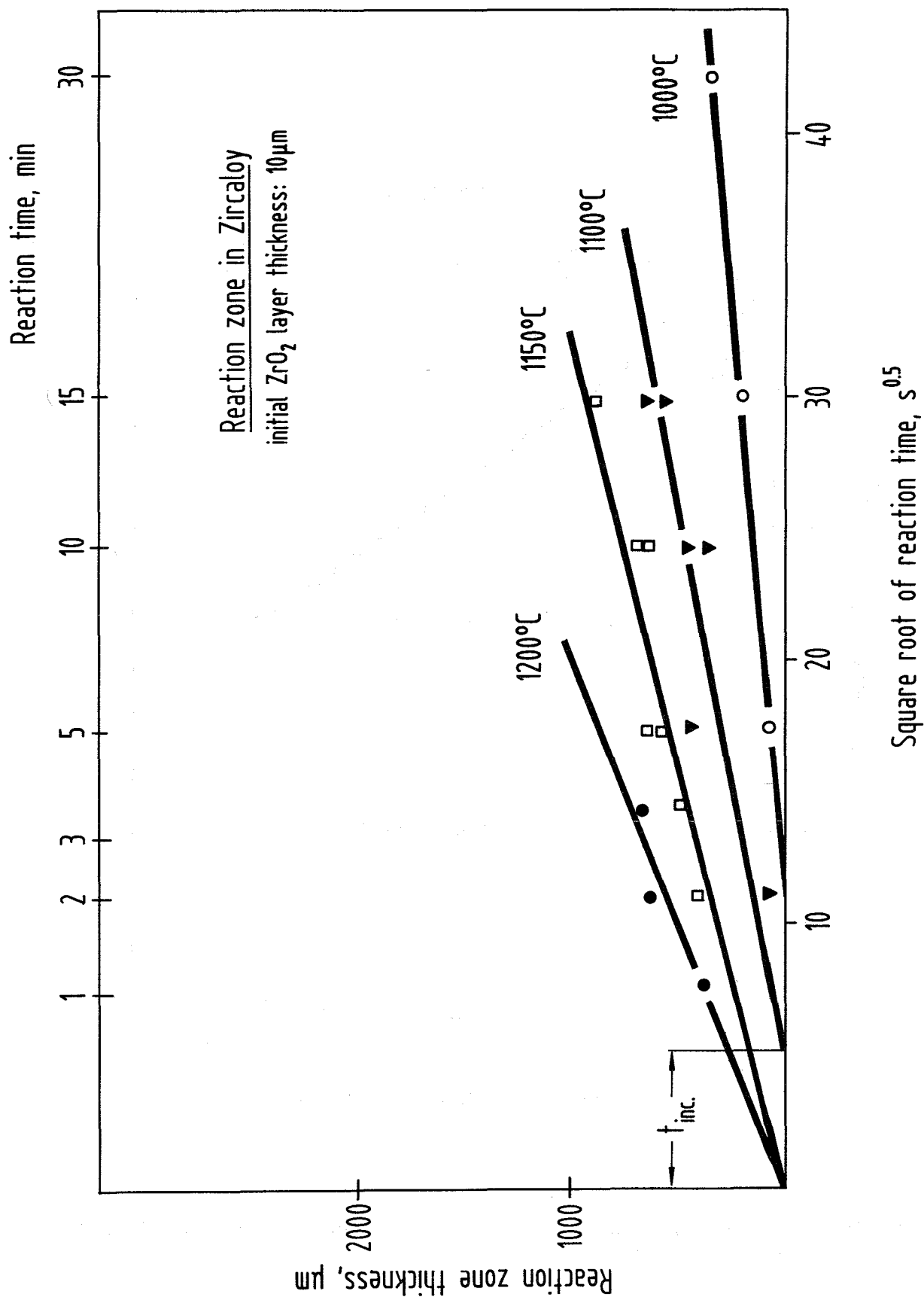


Fig. 22: Maximum reaction zone thicknesses in the system (Ag,In,Cd) alloy/pre-oxidized Zircaloy-4 versus the square root of time; initial ZrO_2 layer thickness: $10\mu m$. At temperatures below $1150\text{ }^\circ C$ the interactions start after the incubation time t_0 (table 3).

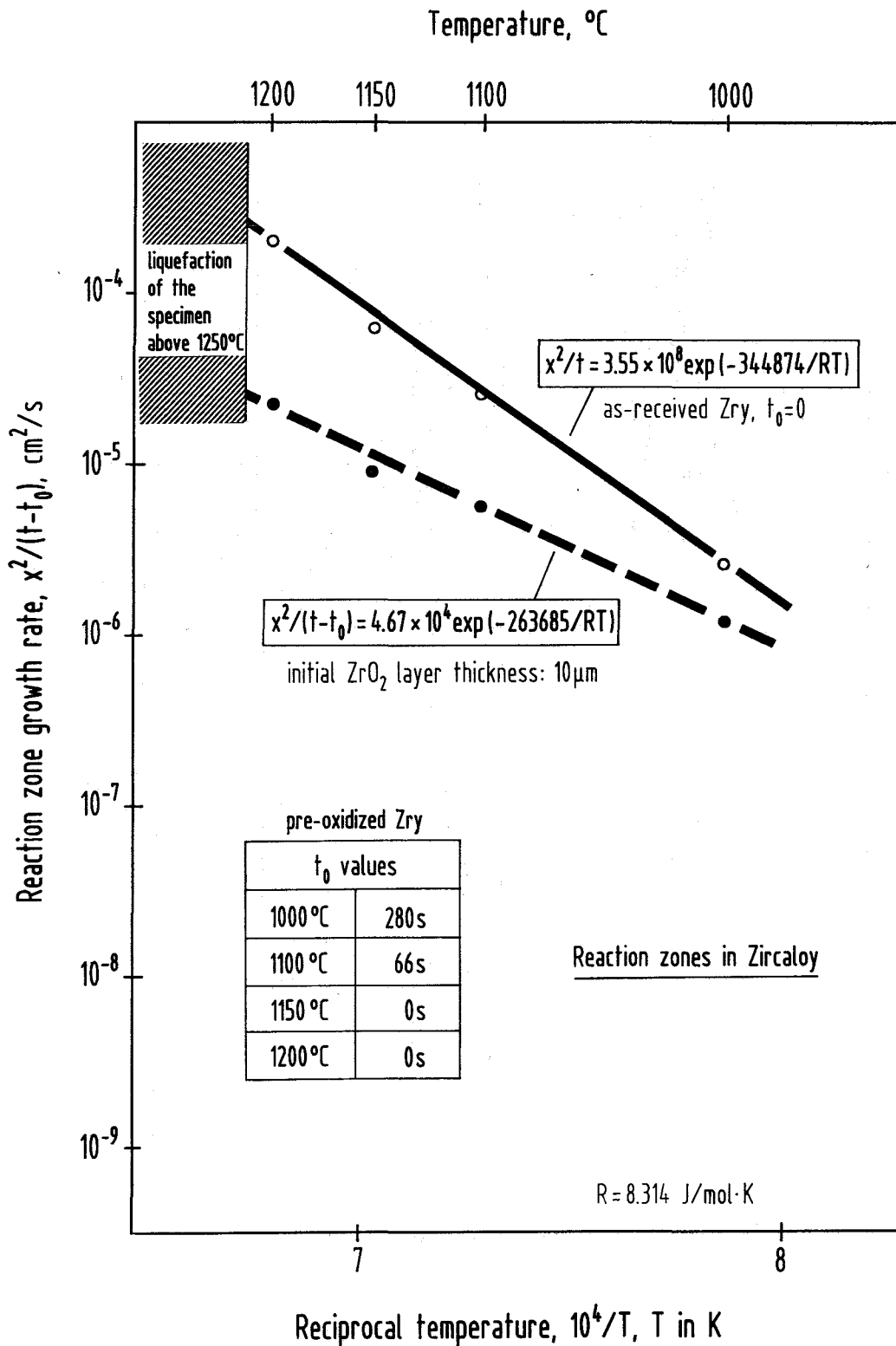
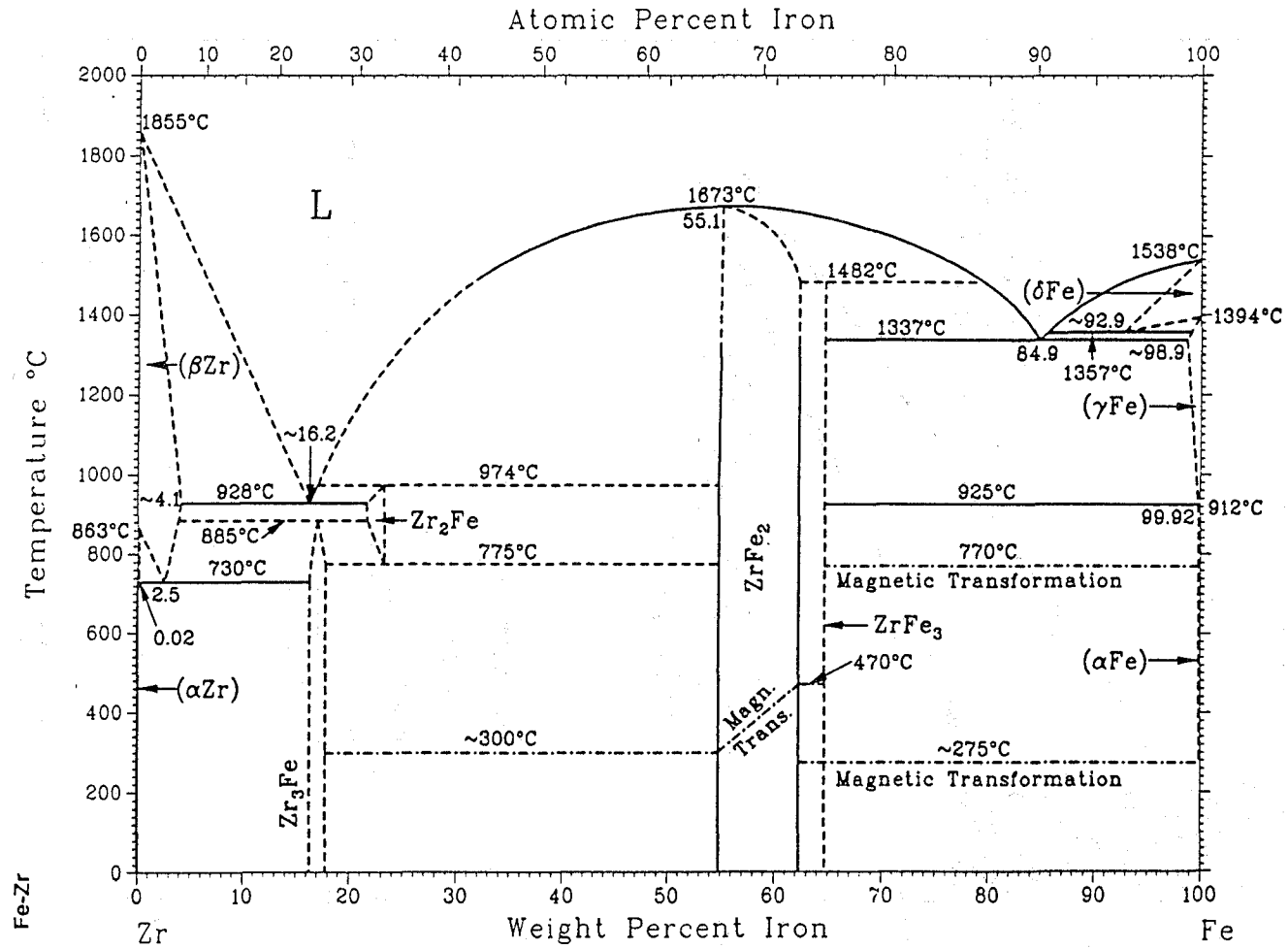


Fig. 23: Reaction zone growth rates for the reaction system (Ag,In,Cd) alloy/pre-oxidized Zircaloy-4; initial ZrO_2 layer thickness: $10\mu\text{m}$ (table 4).

Fig. 24: Binary alloy phase diagram of the system Fe-Zr [7,8].



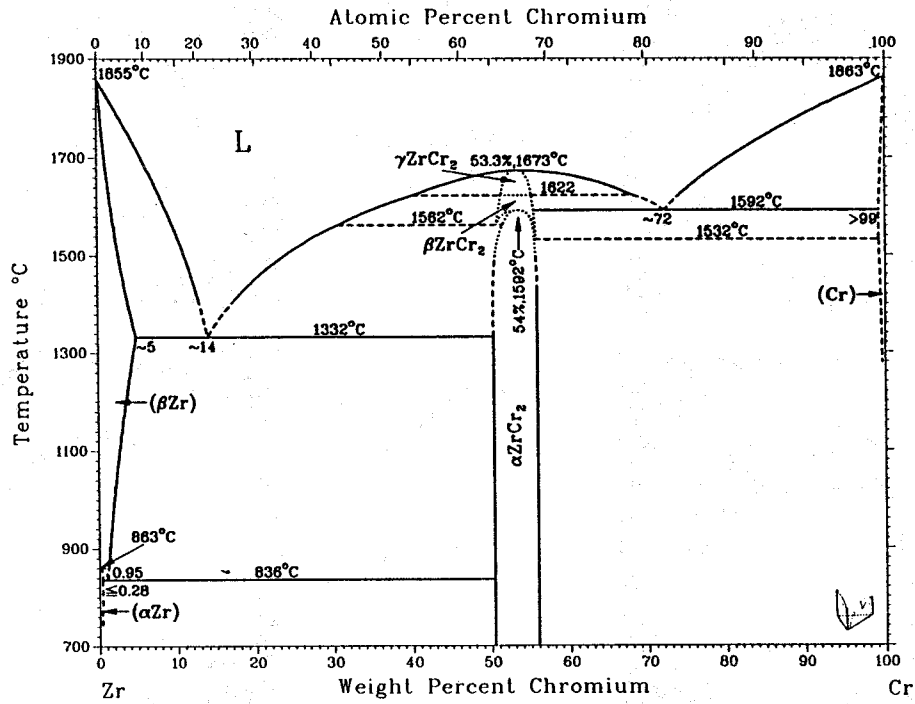
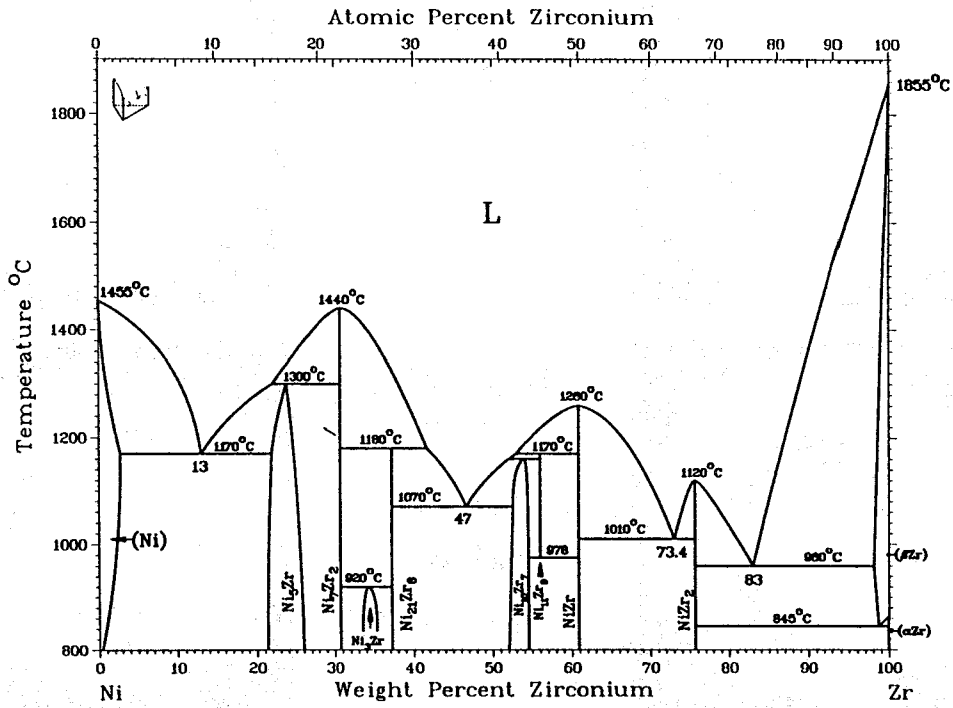


Fig. 25: Binary alloy phase diagrams of the systems Ni-Zr and Cr-Zr [7].

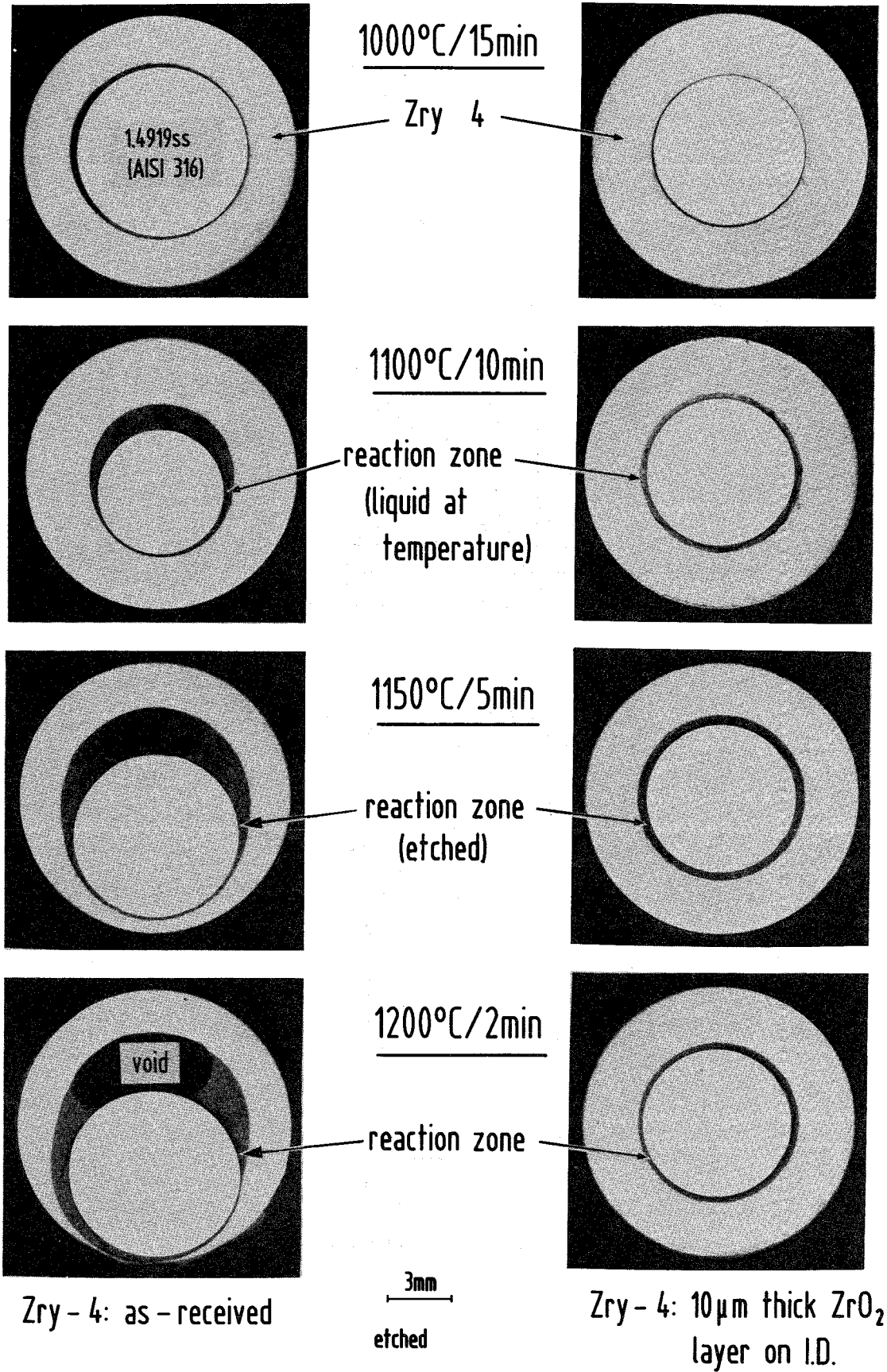


Fig. 26: Chemical interactions between Zircaloy-4 and stainless steel 1.4919 (AISI 316) at different temperatures; influence of a thin ZrO₂ layer on the reaction behavior (right row of pictures).

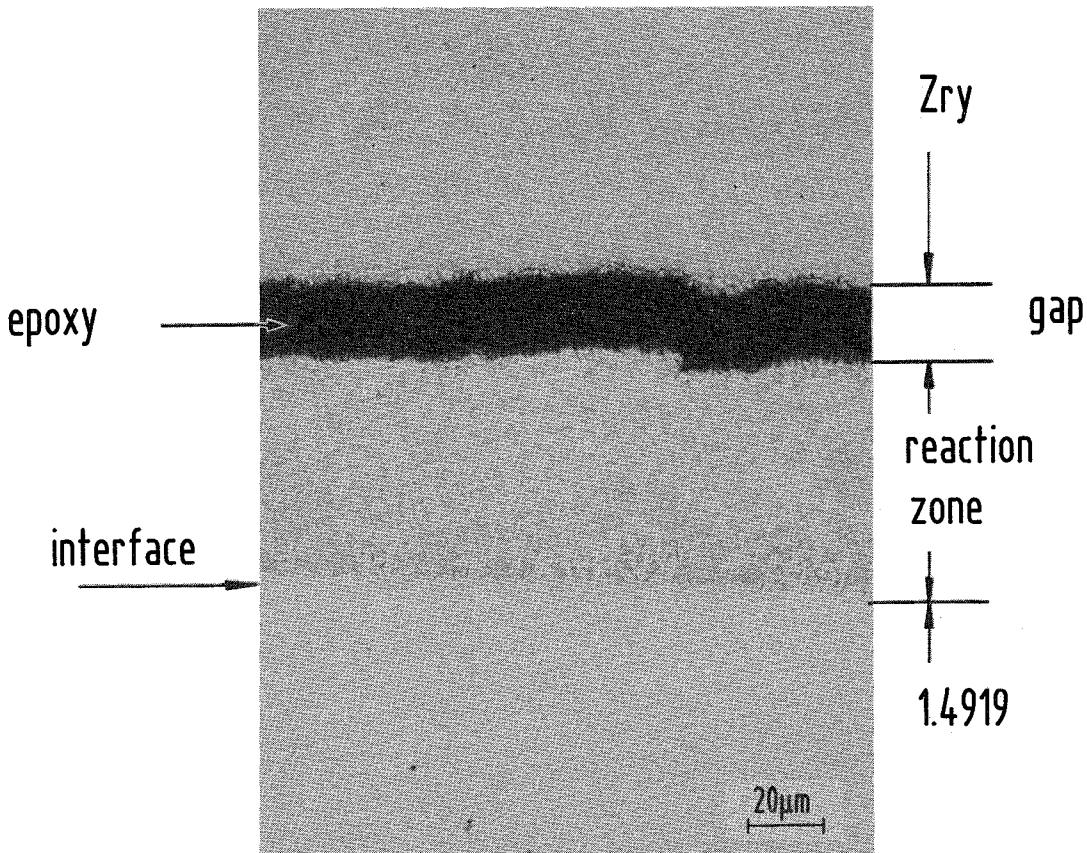
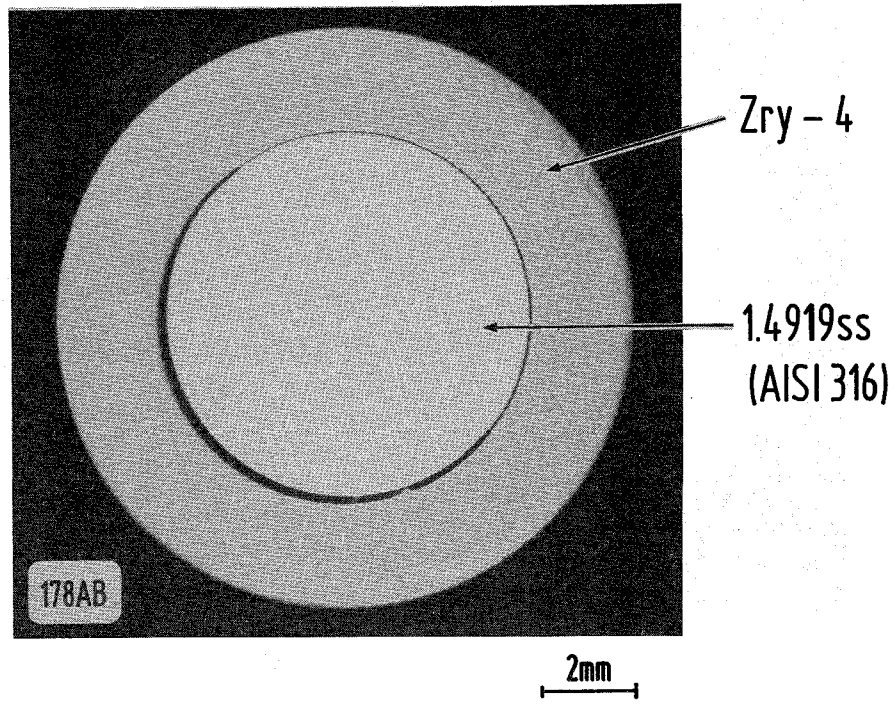


Fig. 27: Chemical interactions between Zircaloy-4 and stainless steel 1.4919 (AISI 316); 1000 °C/5 min.

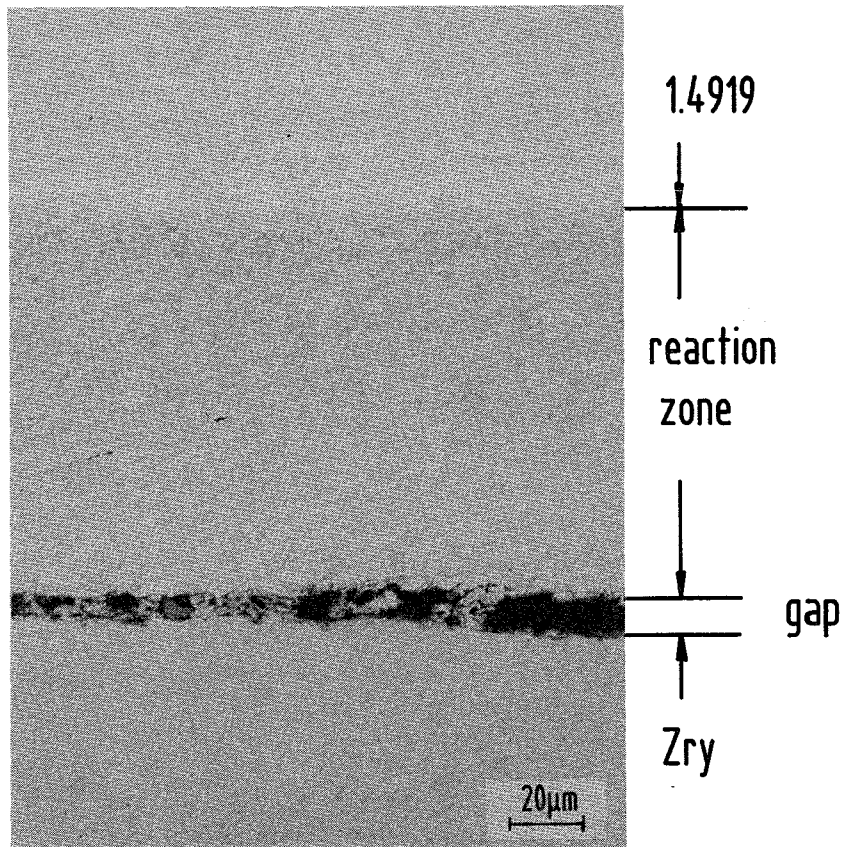
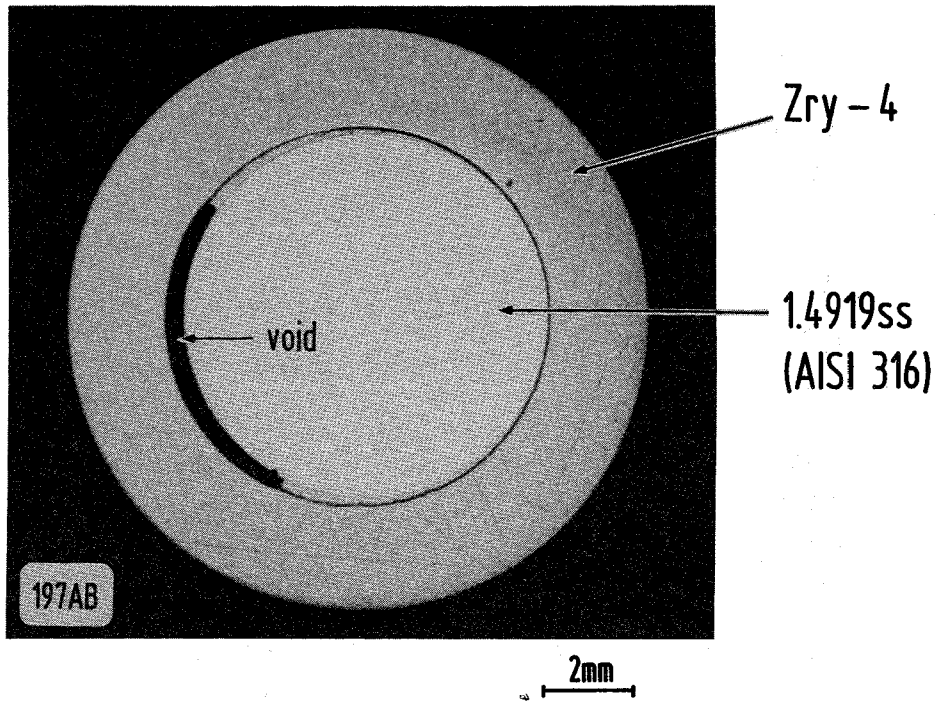


Fig. 28: Chemical interactions between Zircaloy-4 and stainless steel 1.4919 (AISI 316); 1000 °C/15 min.

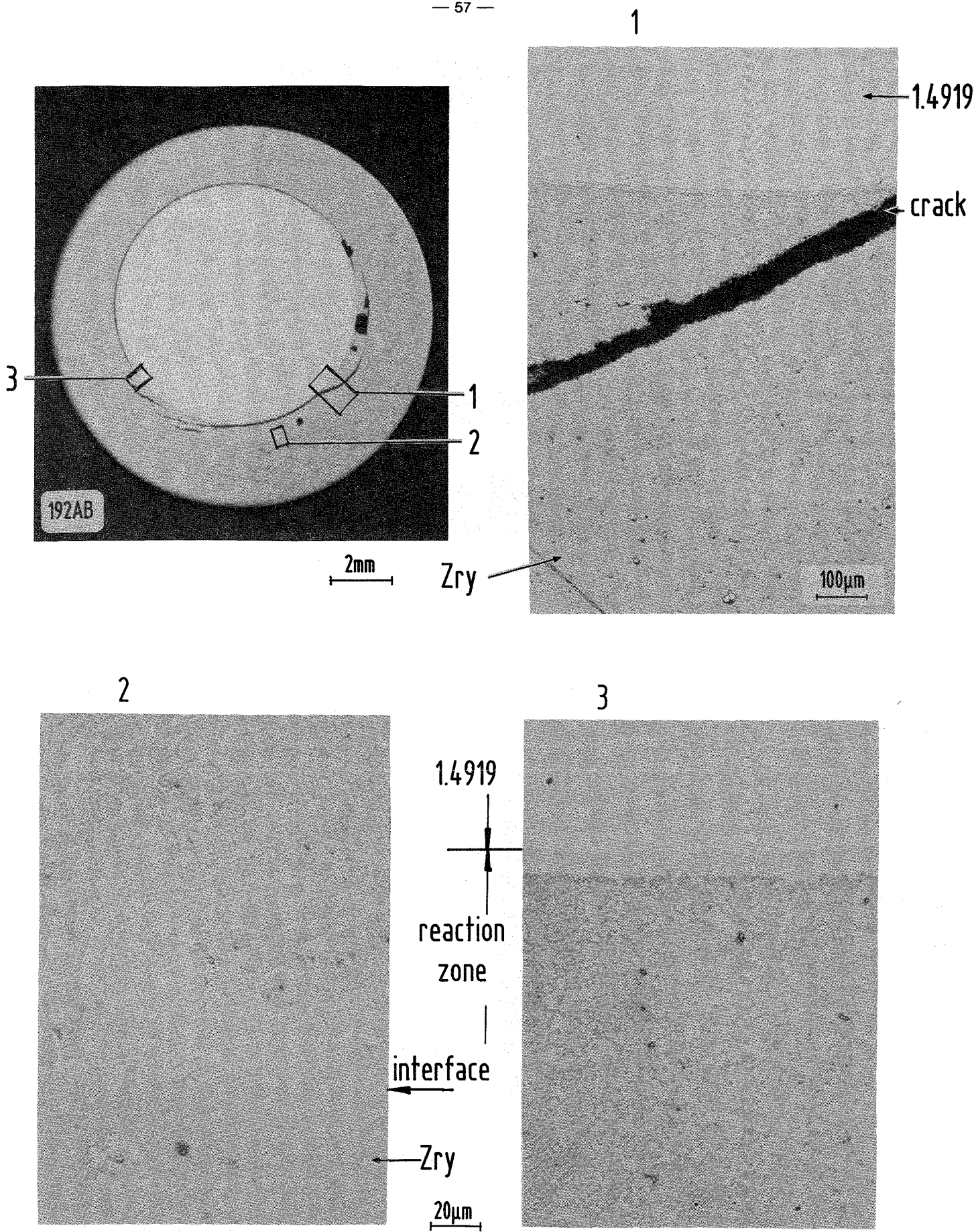


Fig. 29: Chemical interactions between Zircaloy-4 and stainless steel 1.4919 (AISI 316); 1100 °C/2 min.

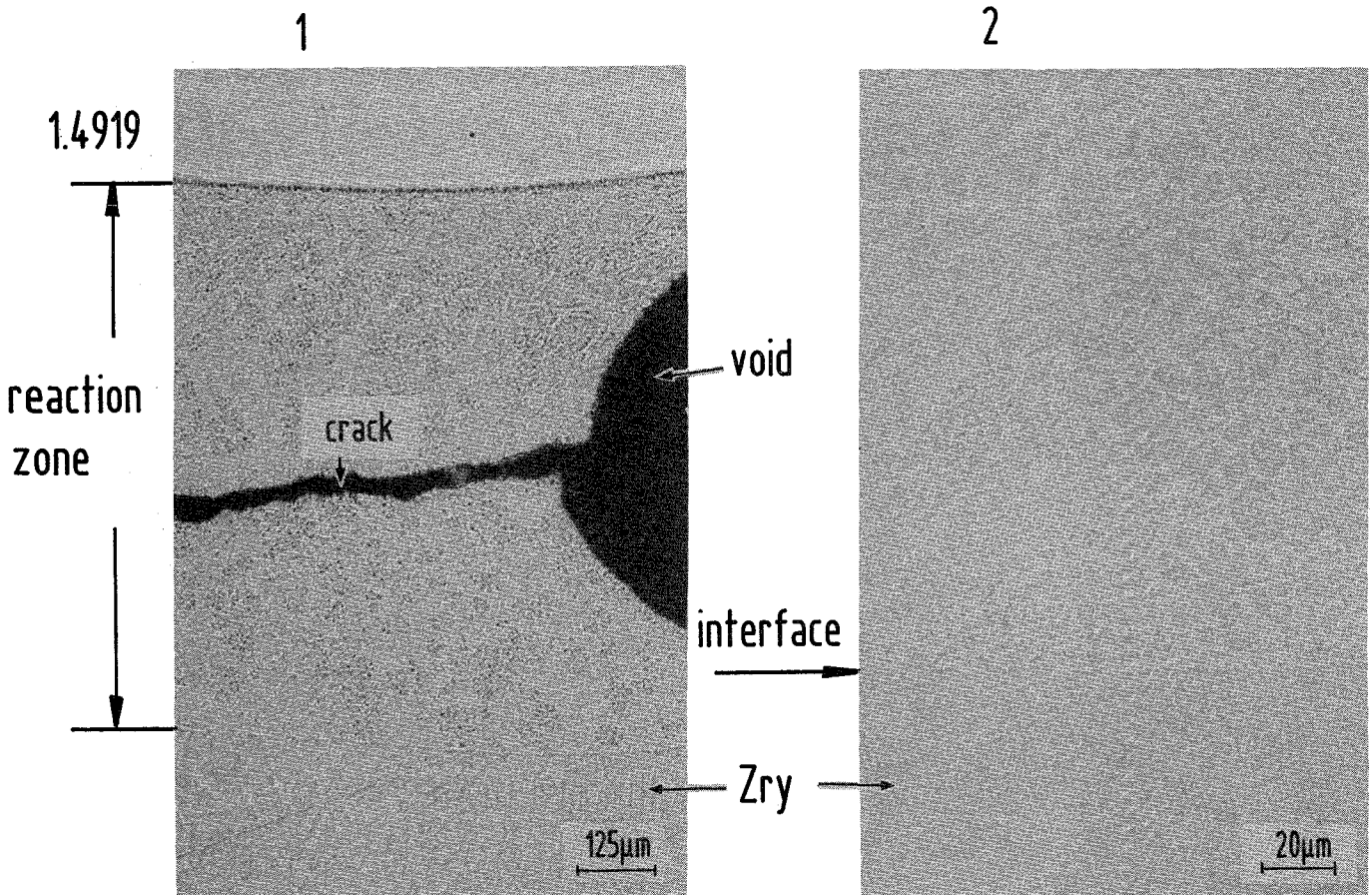
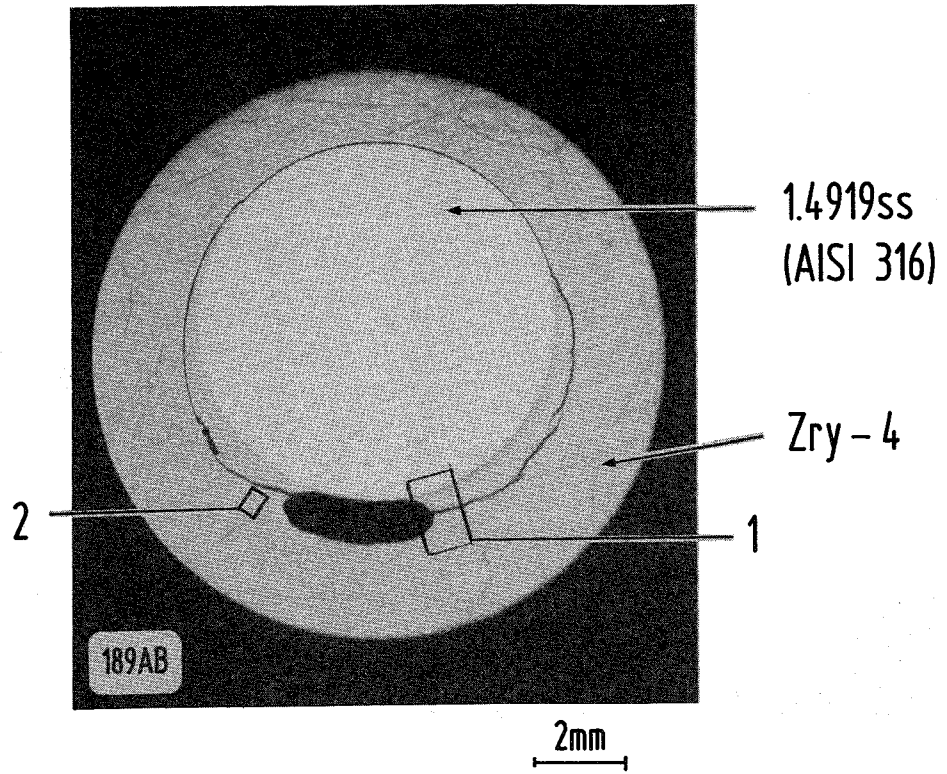


Fig. 30: Chemical interactions between Zircaloy-4 and stainless steel 1.4919 (AISI 316); 1100 °C/ 5 min.

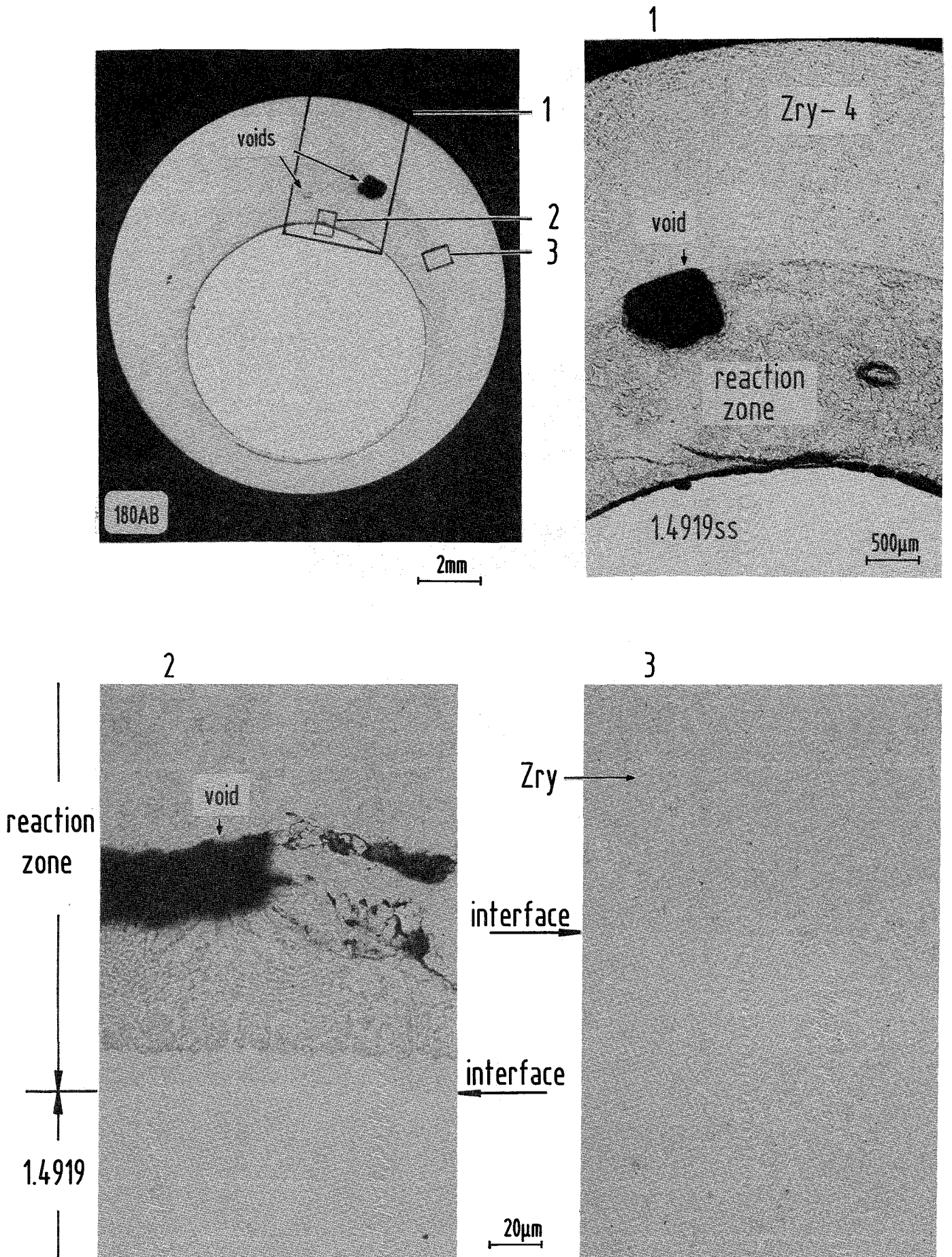


Fig. 31: Chemical interactions between Zircaloy-4 and stainless steel 1.4919 (AISI 316); 1100 °C/15 min.

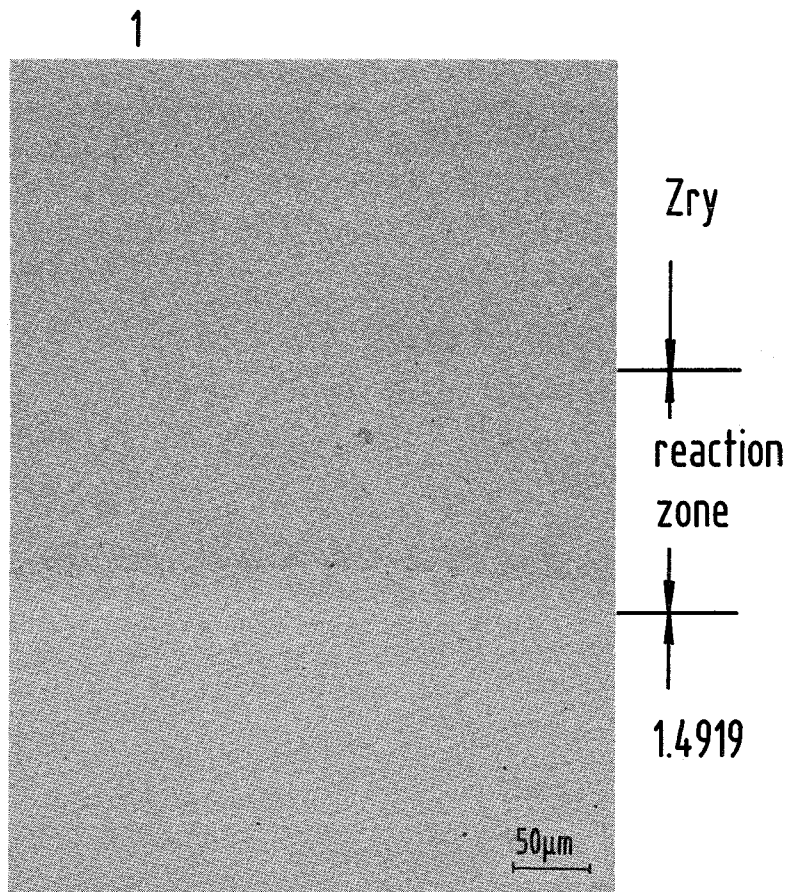
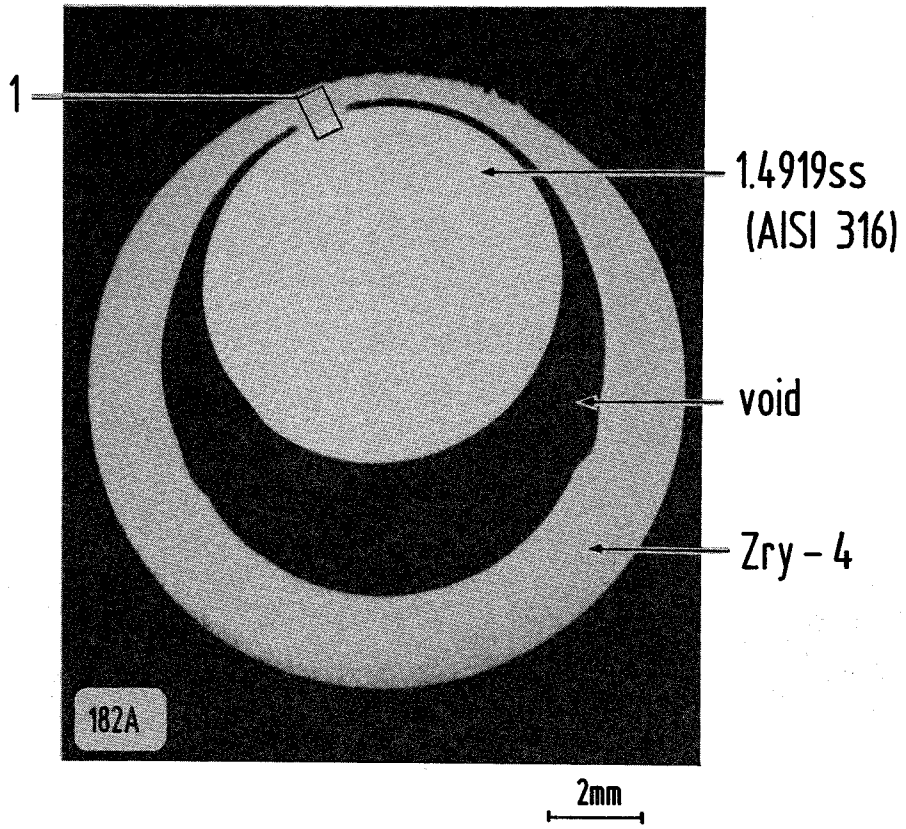


Fig. 32: Chemical interactions between Zircaloy-4 and stainless steel 1.4919 (AISI 316); 1100 °C/30 min.

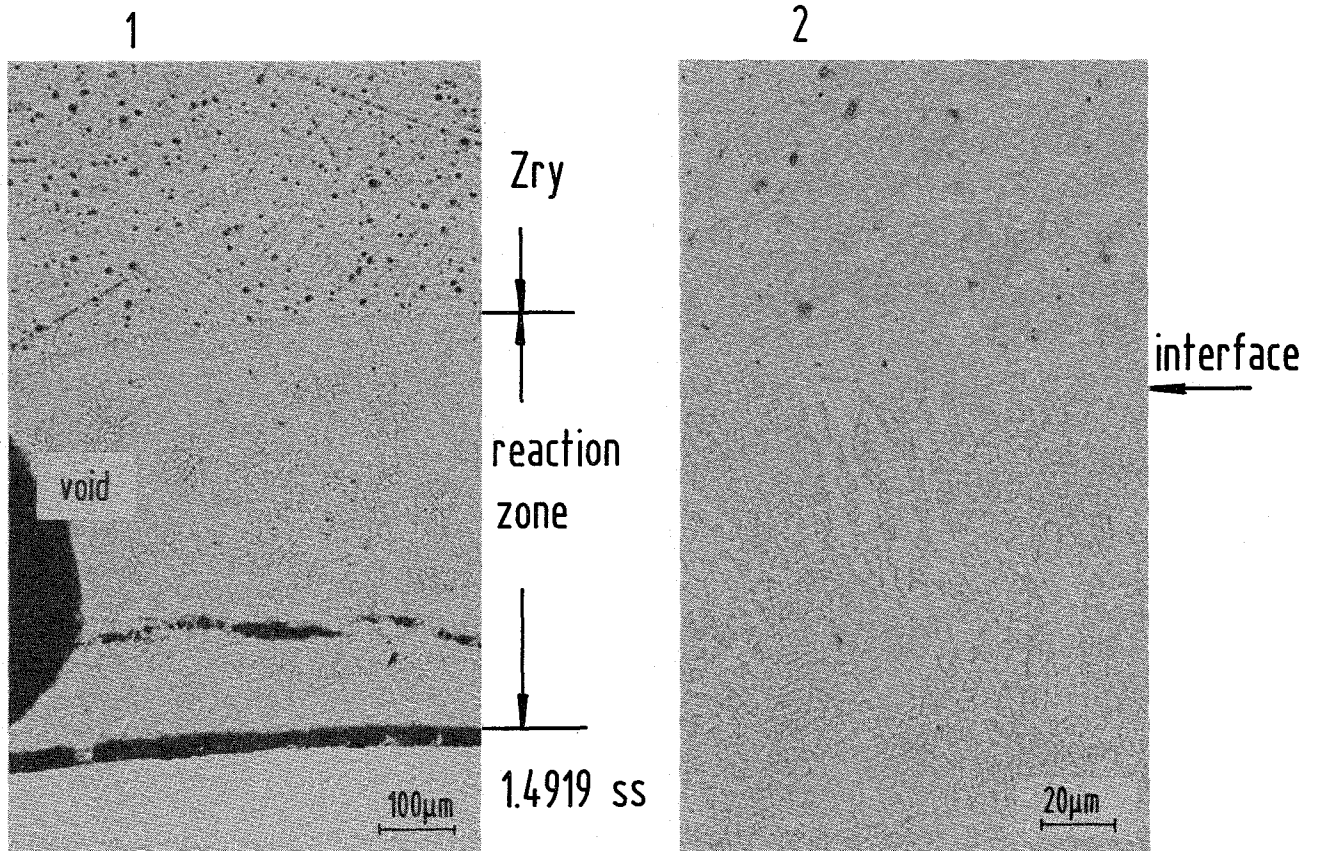
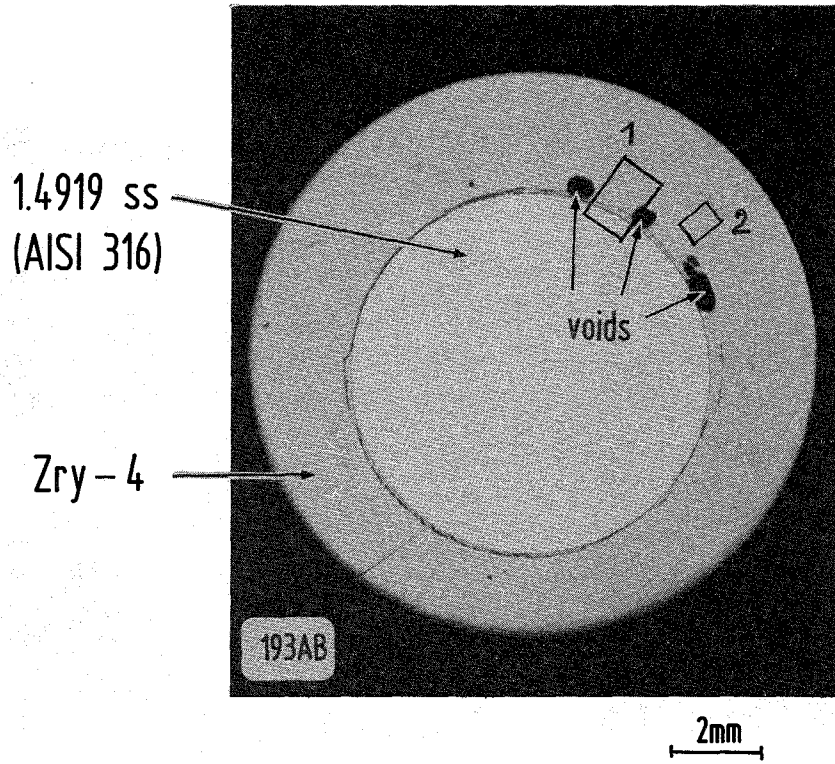
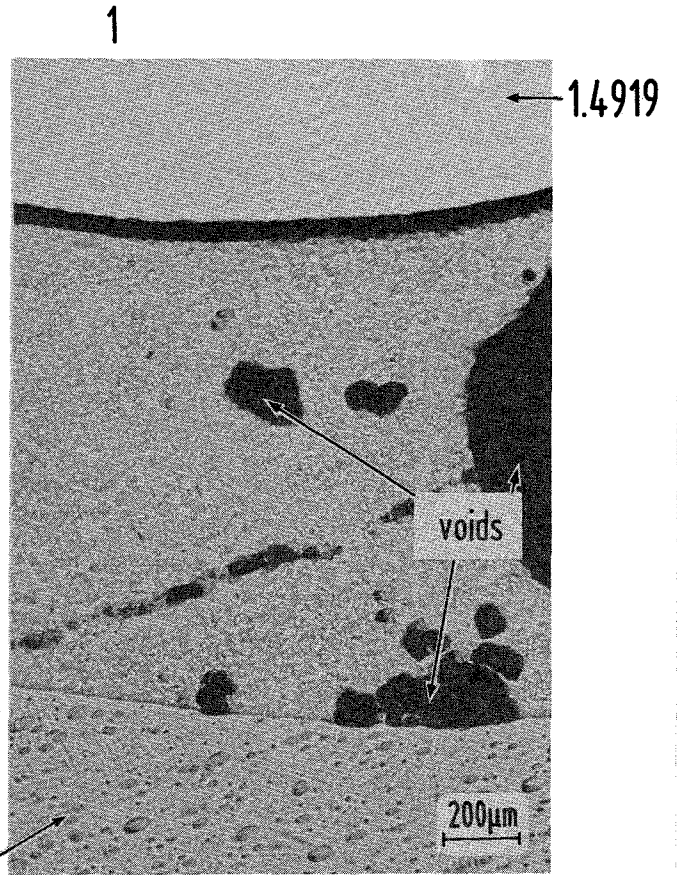
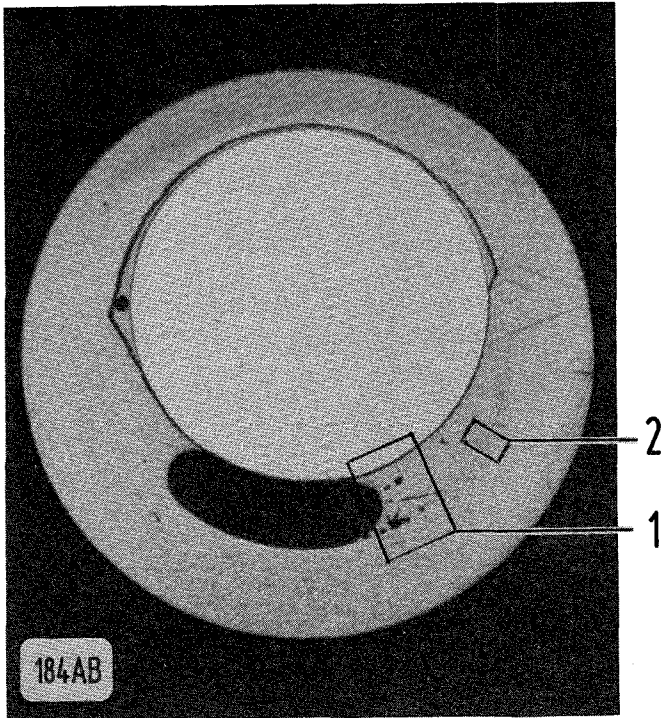
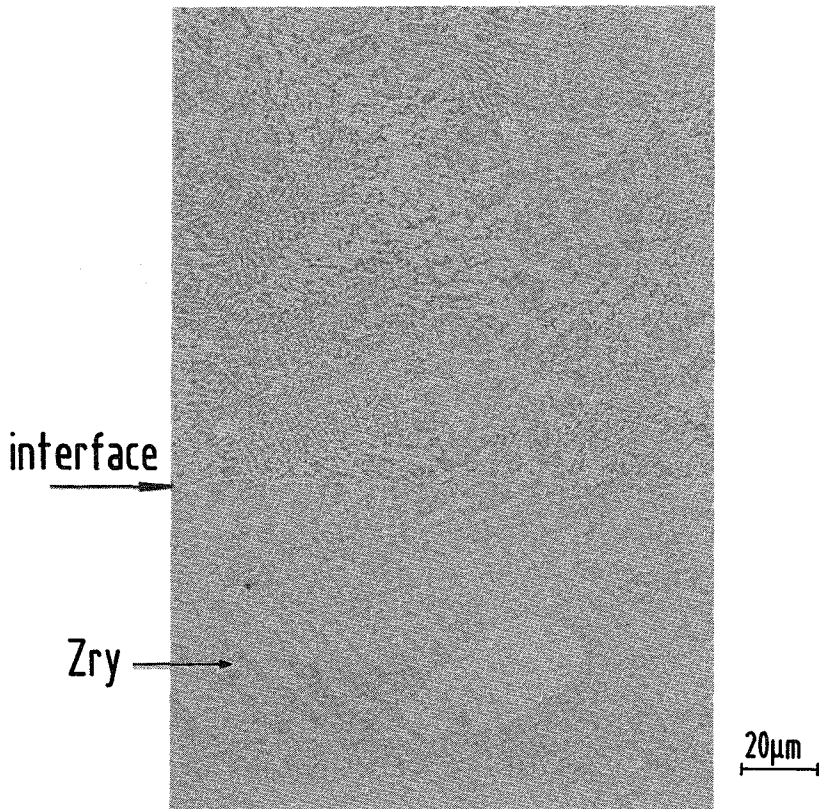


Fig. 33: Chemical interactions between Zircaloy-4 and stainless steel 1.4919 (AISI 316); 1150 °C/1 min.



2



interference picture

Fig. 34: Chemical interactions between Zircaloy-4 and stainless steel 1.4919 (AISI 316); 1150 °C/2 min.

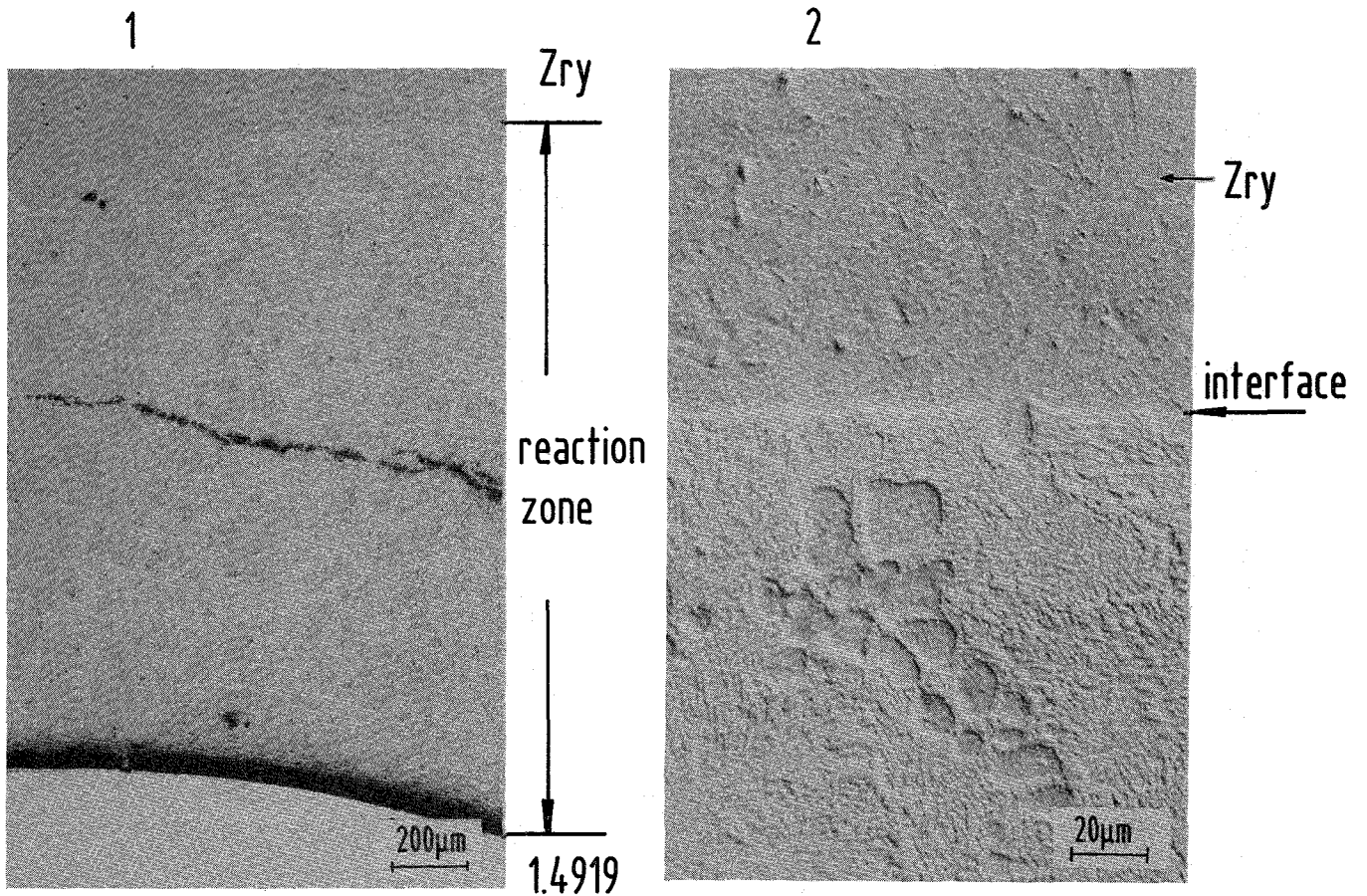
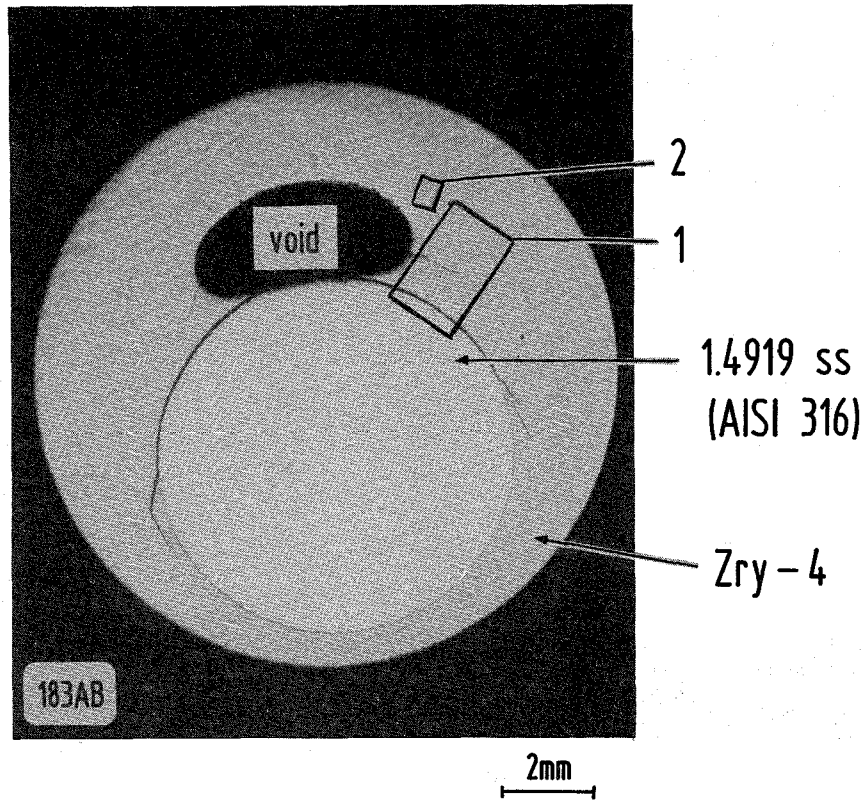


Fig. 35: Chemical interactions between Zircaloy-4 and stainless steel 1.4919 (AISI 316); 1150 °C/5 min.

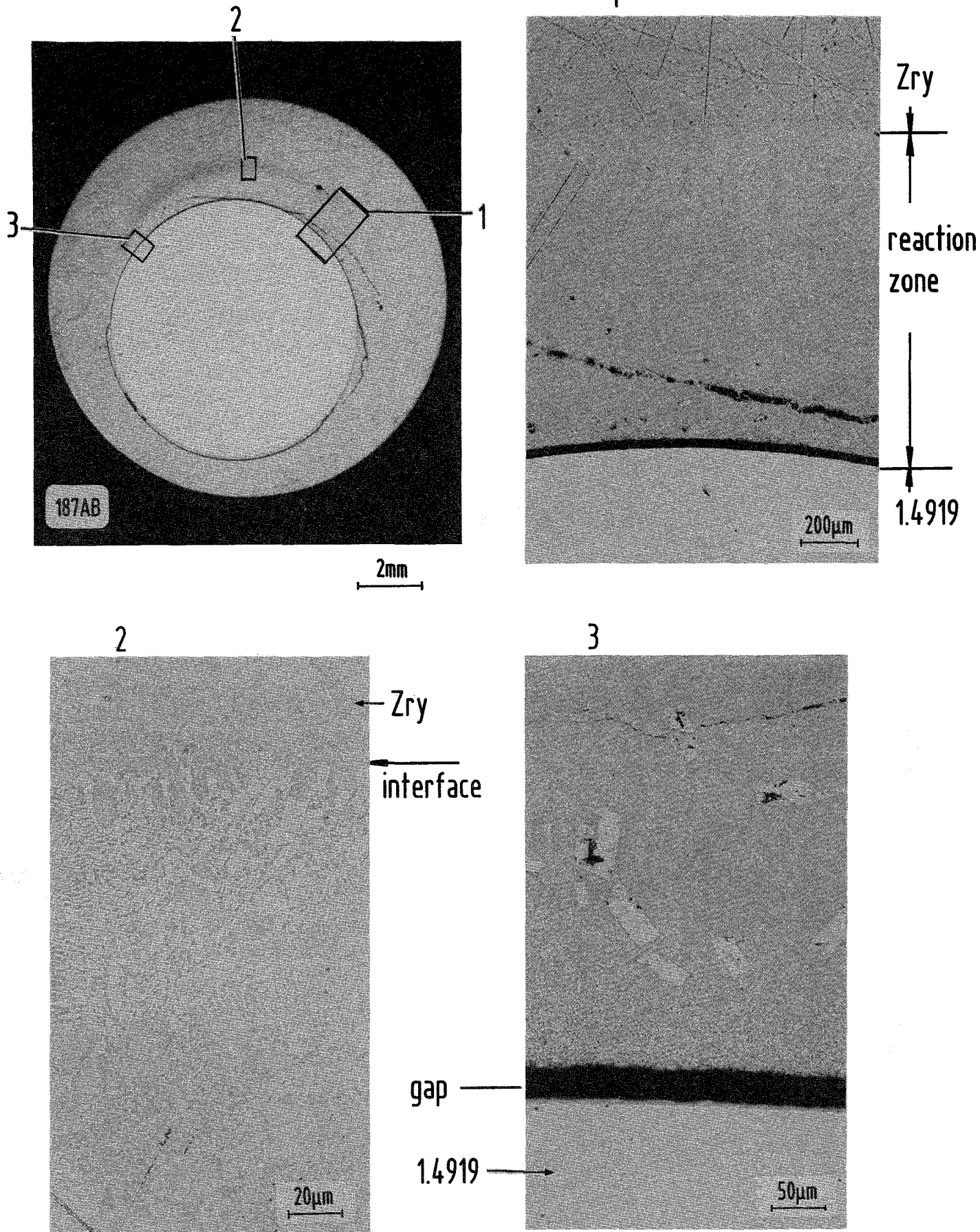


Fig. 36: Chemical interactions between Zircaloy-4 and stainless steel 1.4919 (AISI 316) ; 1200 °C/1 min.

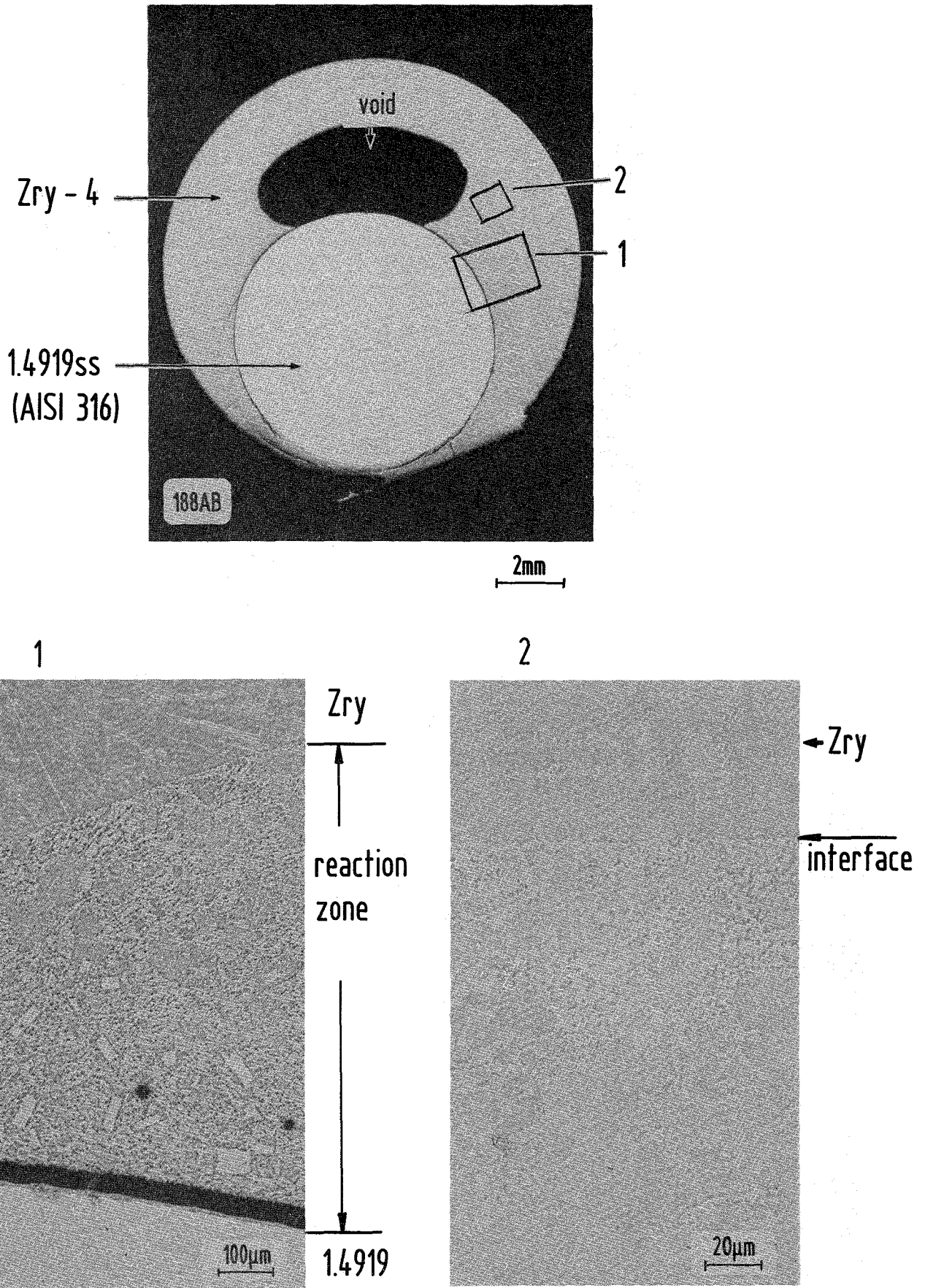


Fig. 37: Chemical interactions between Zircaloy-4 and stainless steel 1.4919 (AISI 316); 1200 °C/2 min.

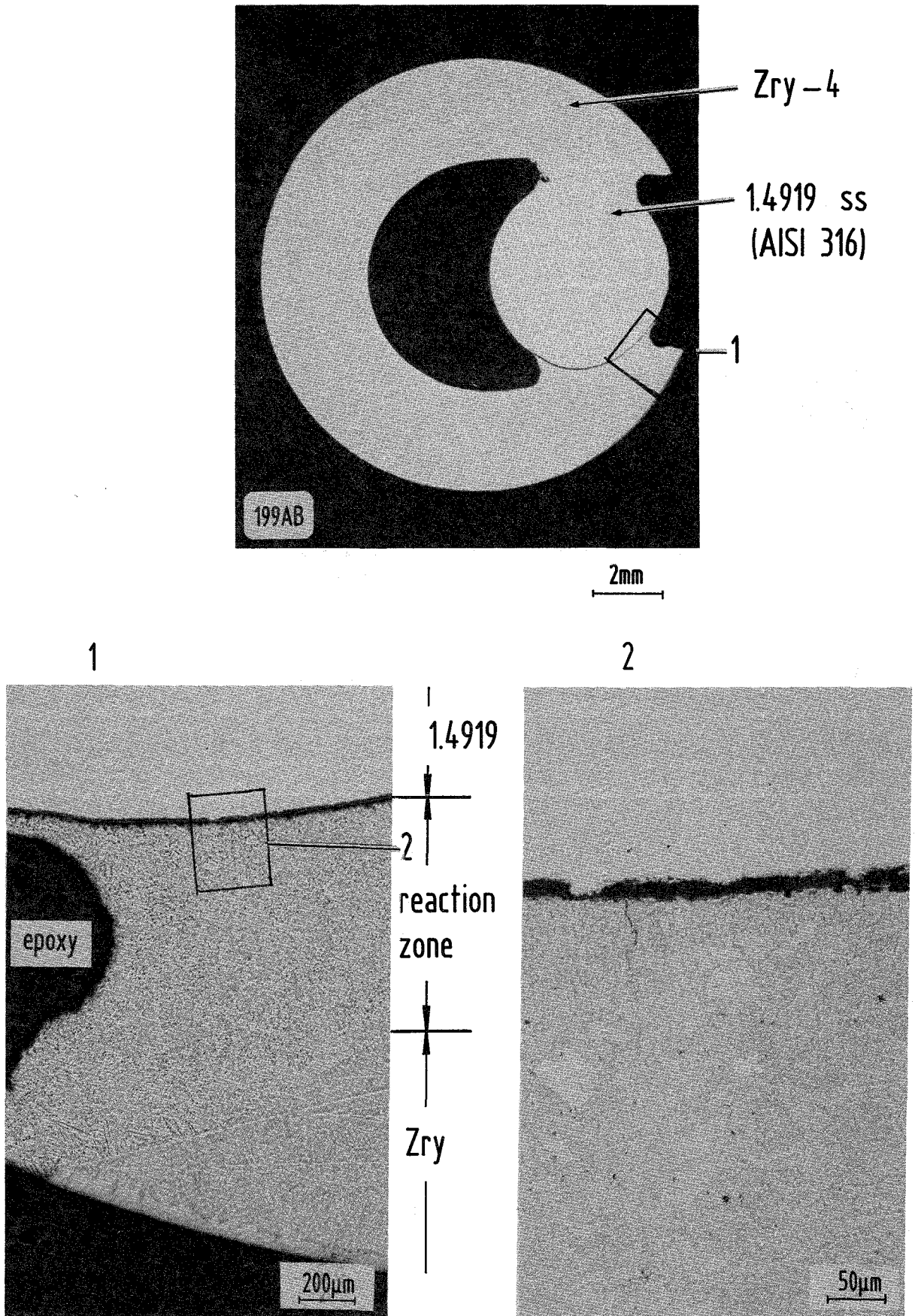


Fig. 38: Chemical interactions between Zircaloy-4 and stainless steel 1.4919 (AISI 316); 1200 °C/4.5 min.

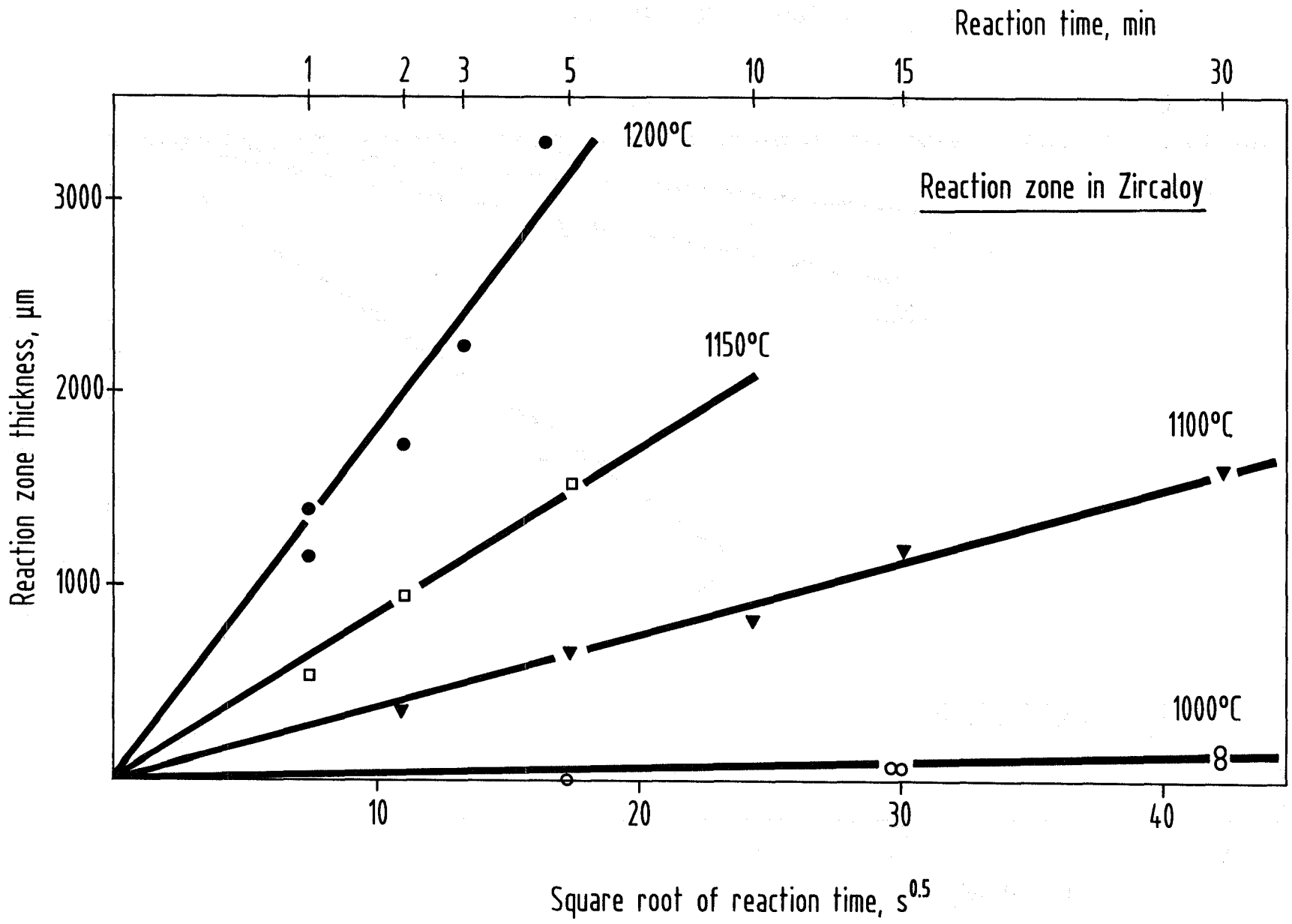


Fig. 39: Maximum reaction zone thicknesses in Zircaloy for the system Zircaloy-4/stainless steel 1.4919 (AISI 316) versus the square root of time between 1000 and 1200°C (table 5).

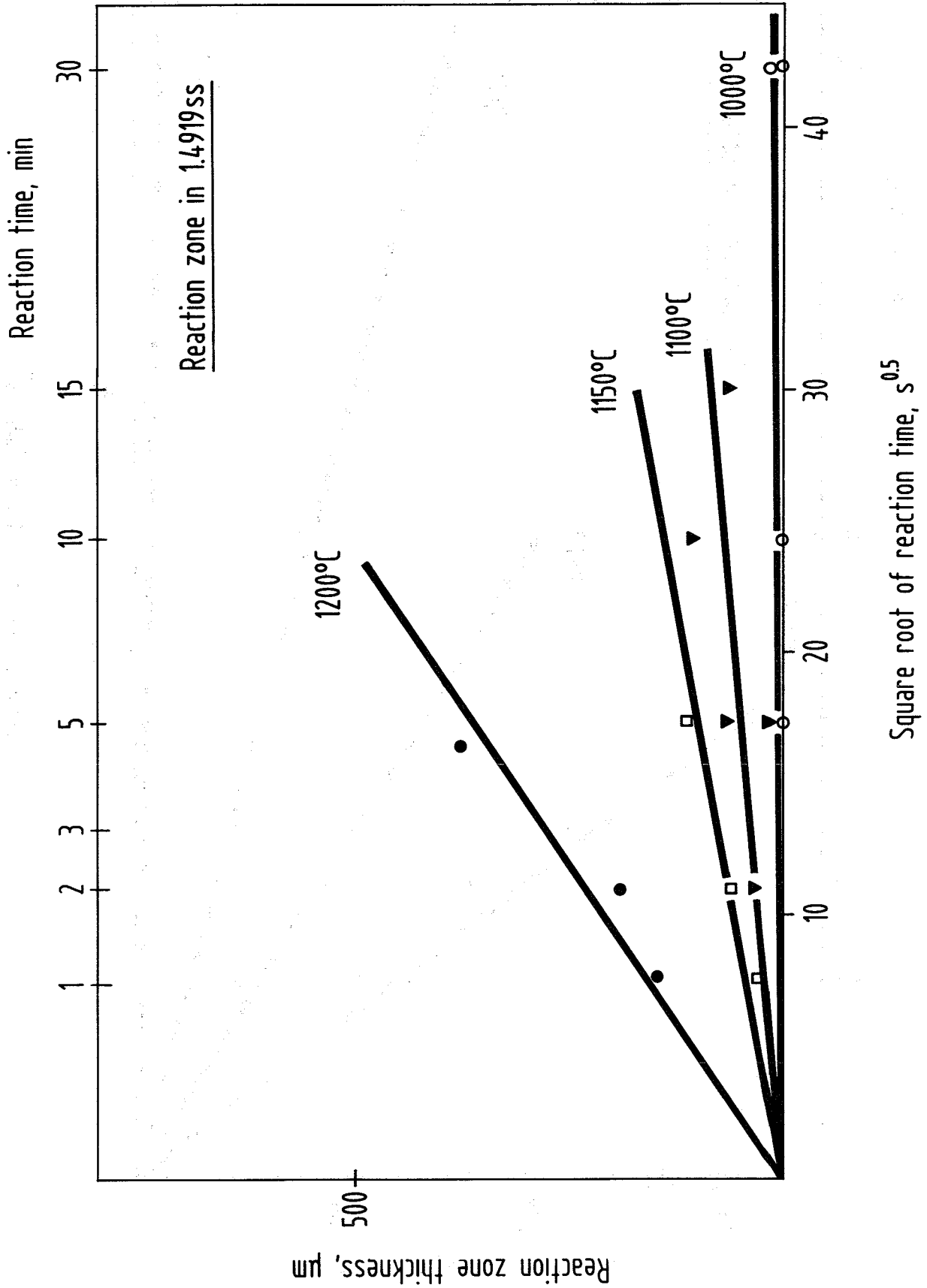


Fig. 40: Maximum reaction zone thicknesses in stainless steel for the system Zircaloy-4/stainless steel 1.4919 (AISI 316) versus the square root of time between 1000 and 1200 $^{\circ}\text{C}$ (table 6).

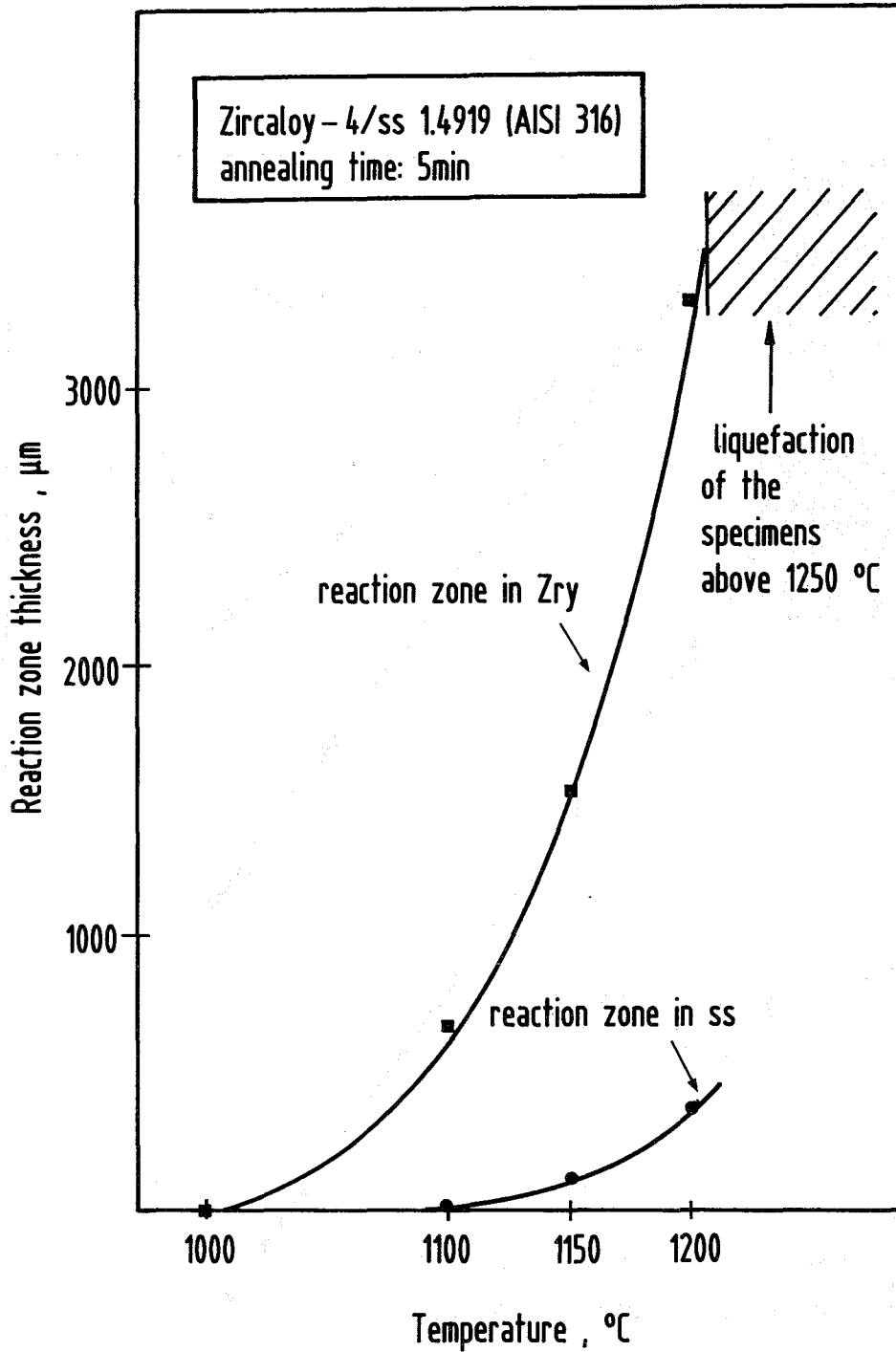


Fig. 41: Comparison of the reaction zone thicknesses in Zircaloy and stainless steel for the system Zircaloy-4/stainless steel 1.4919 (AISI 316) versus temperature; annealing time: 5 min.

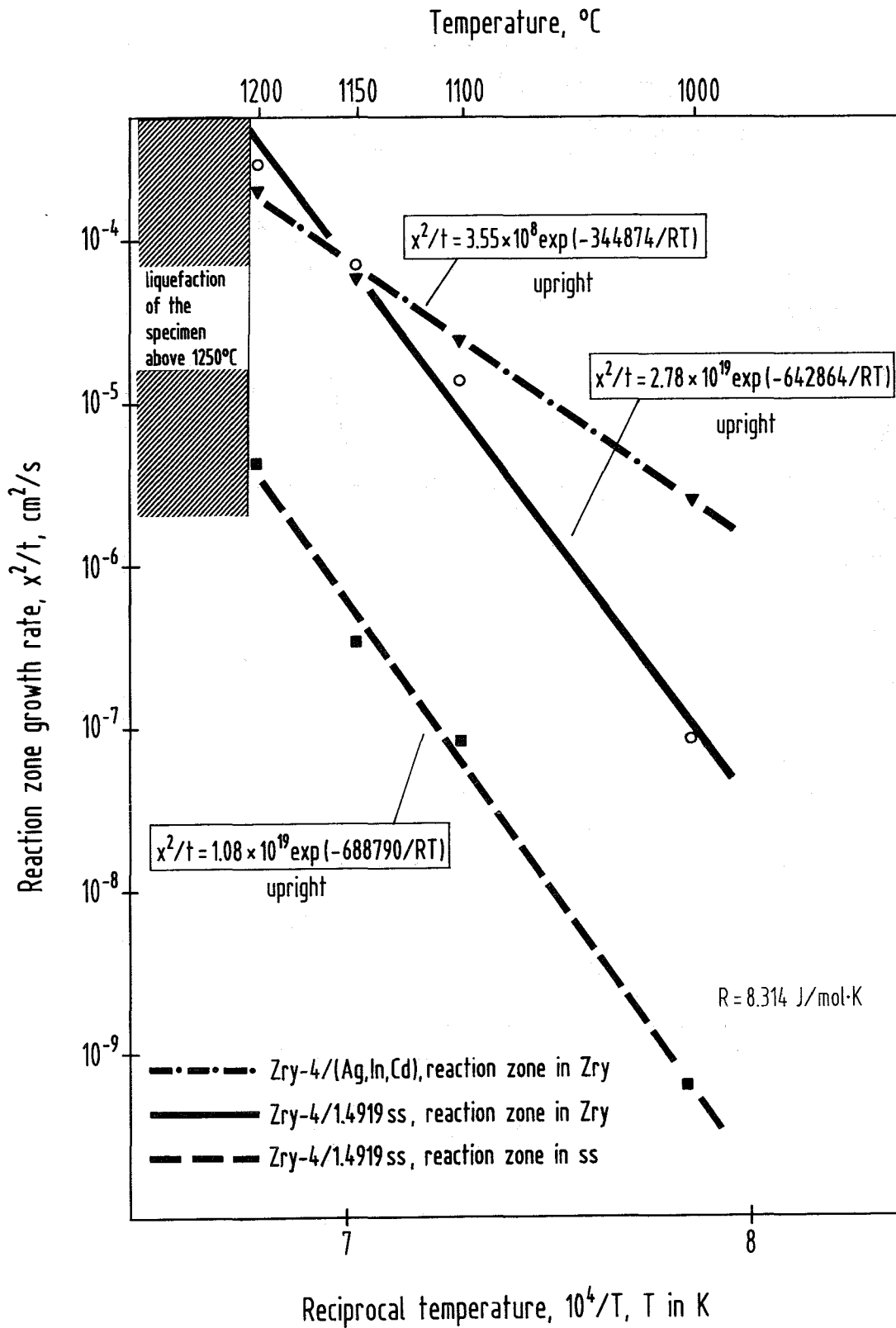


Fig. 42: Reaction zone growth rates for the reaction system Zircaloy-4/stainless steel 1.4919 (AISI 316) (table 7).

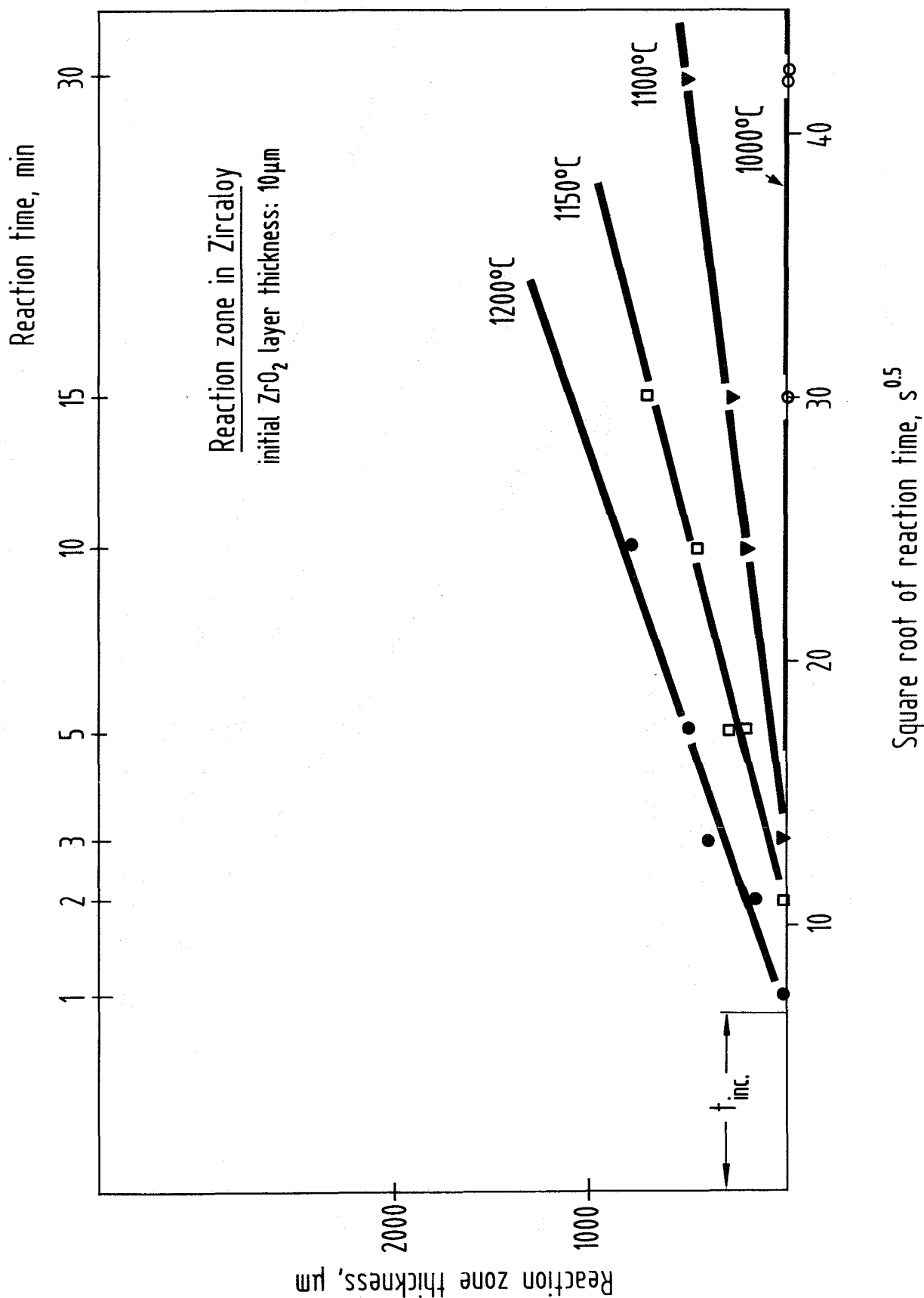


Fig. 43: Maximum reaction zone thicknesses in Zircaloy for the system pre-oxidized Zircaloy-4/stainless steel 1.4919 (AISI 316) versus the square root of time; initial ZrO₂ layer thickness: 10 µm. The interactions start first after the incubation time t_0 has been passed (table 8).

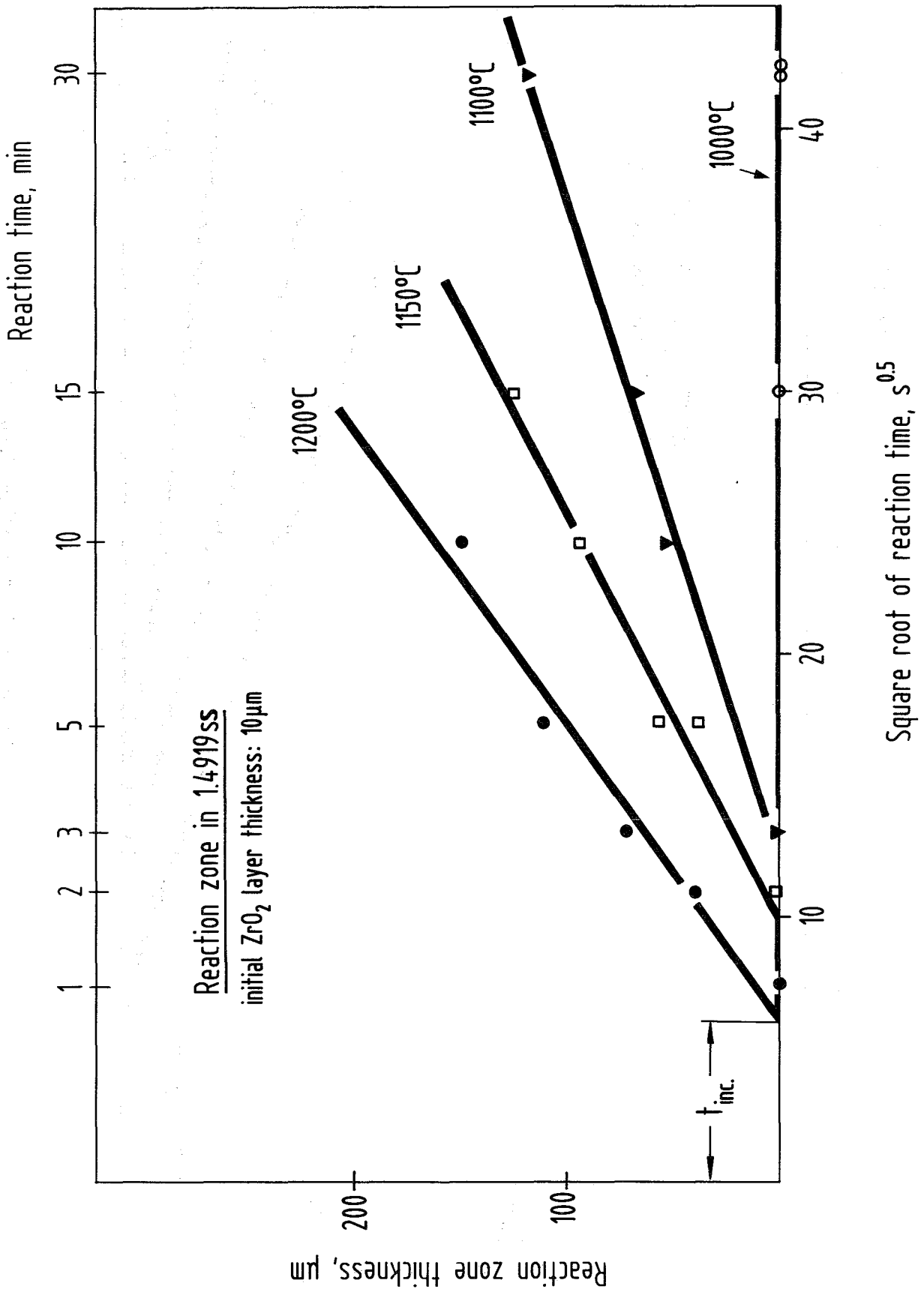


Fig. 44: Maximum reaction zone thicknesses in stainless steel for the system pre-oxidized Zircaloy-4/stainless steel 1.4919 (AISI 316) versus the square root of time; initial ZrO₂ layer thickness: 10 μm. The interactions start first after the incubation time t_0 has been passed (table 8).

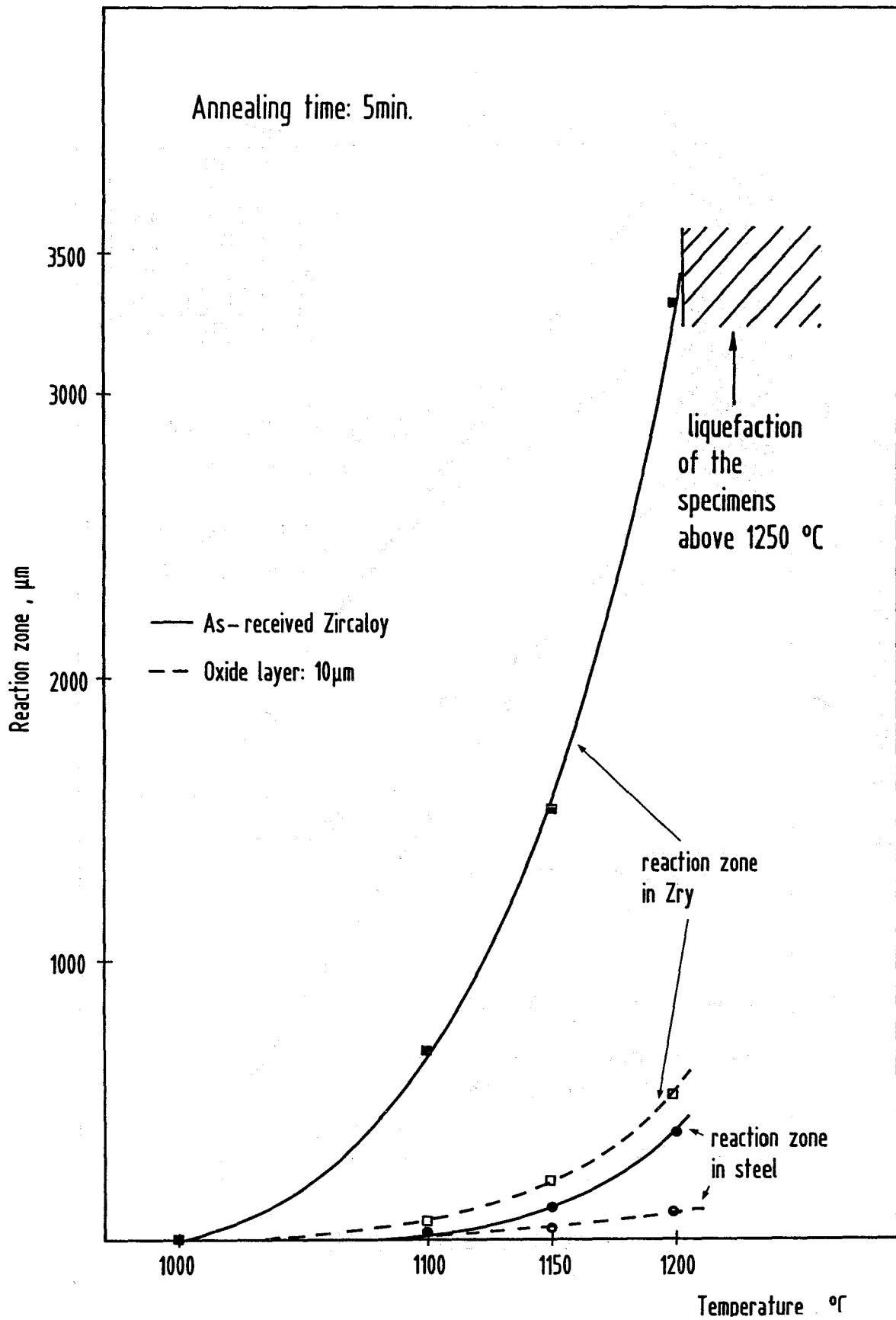
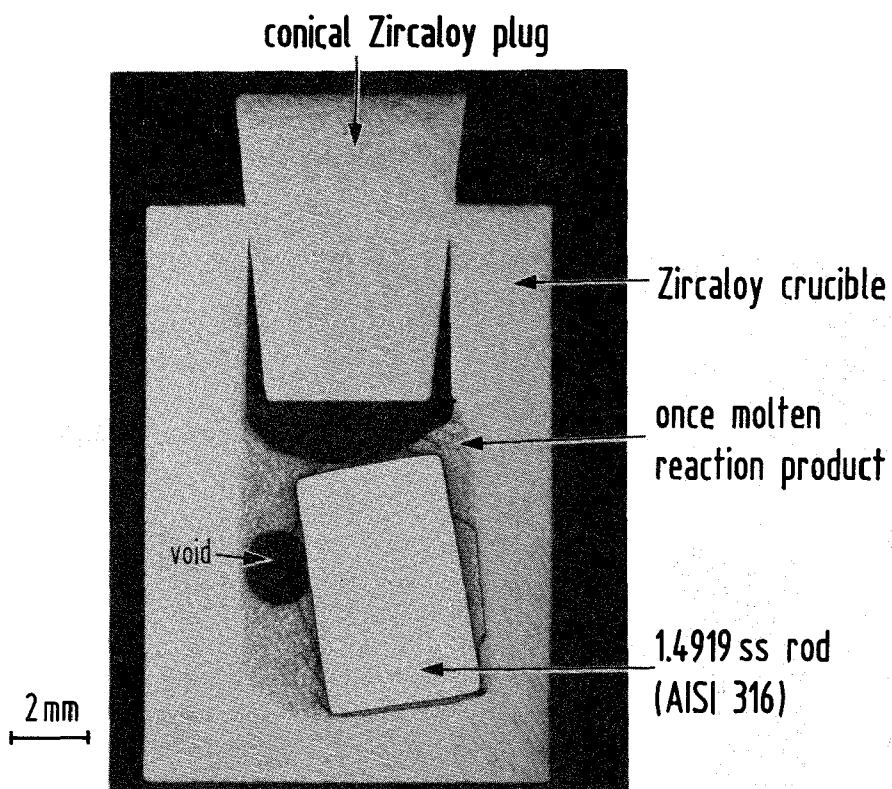
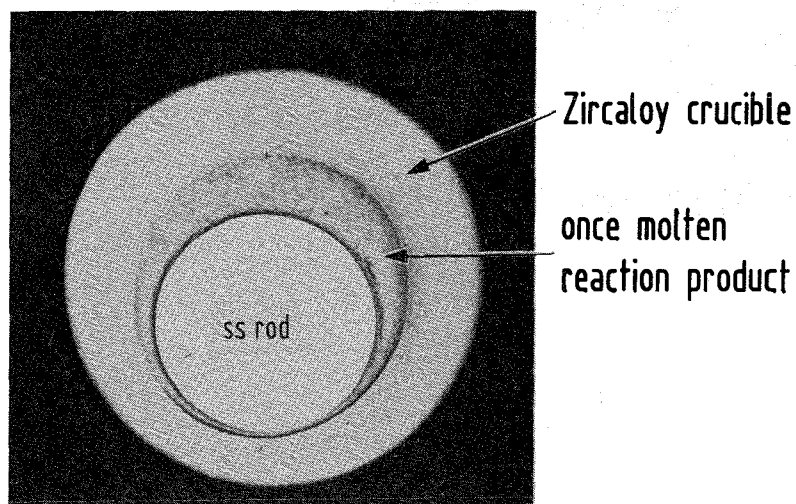


Fig. 45: Comparison of the reaction zone thicknesses in Zircaloy and stainless steel for as-received and pre-oxidized Zircaloy-4 (initial ZrO_2 layer thickness: $10\mu\text{m}$). versus temperature; annealing time 5 min.



specimen annealed in upright position



specimen annealed in horizontal position

1100°C/15min

Fig. 47: Extent of chemical interactions between Zircaloy and stainless steel in dependence on annealing conditions (upright or horizontal).

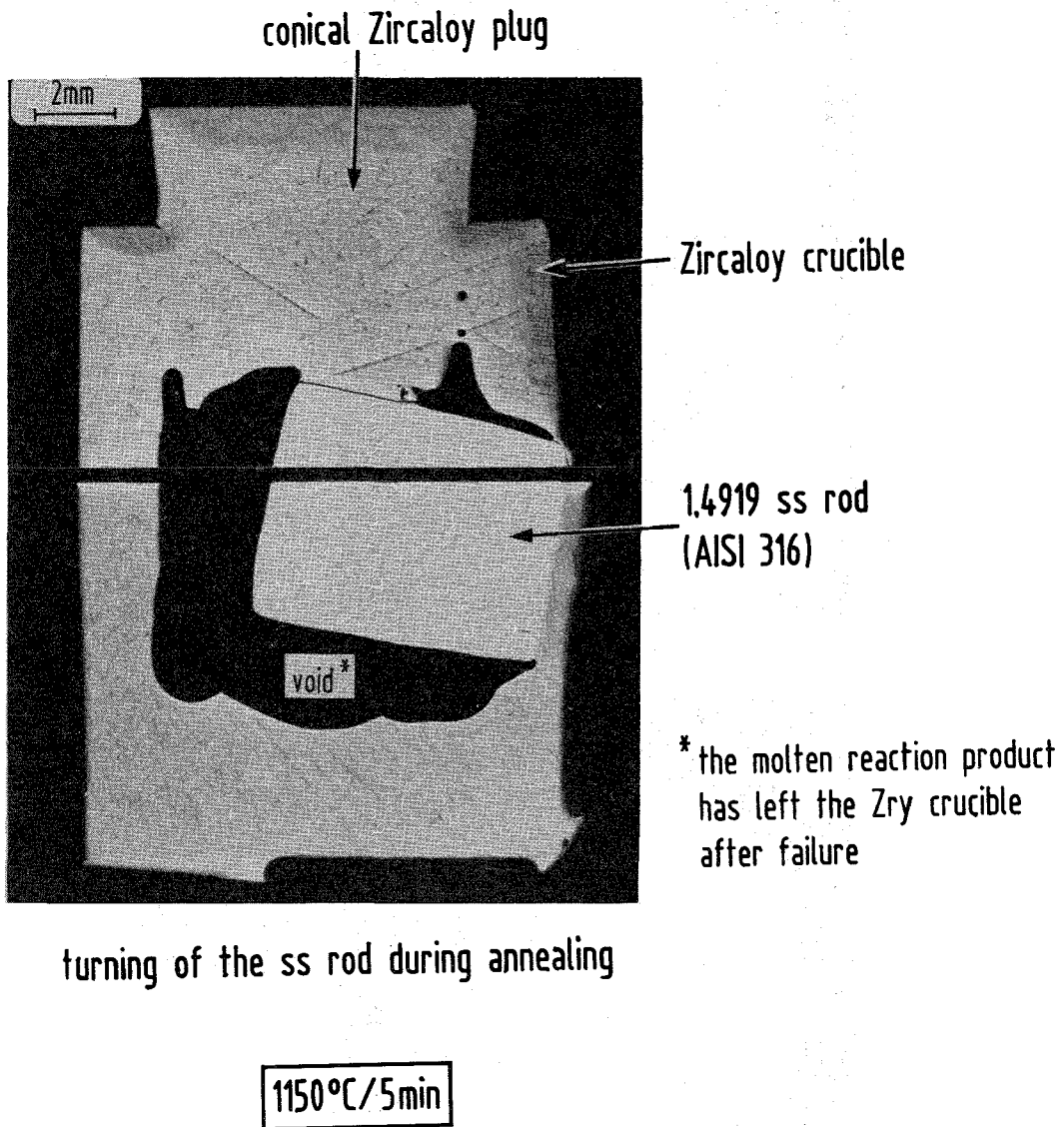


Fig. 48: Turning of the stainless steel rod within the Zircaloy crucible as a results of liquid phase formation. The relocated melt form a large void.

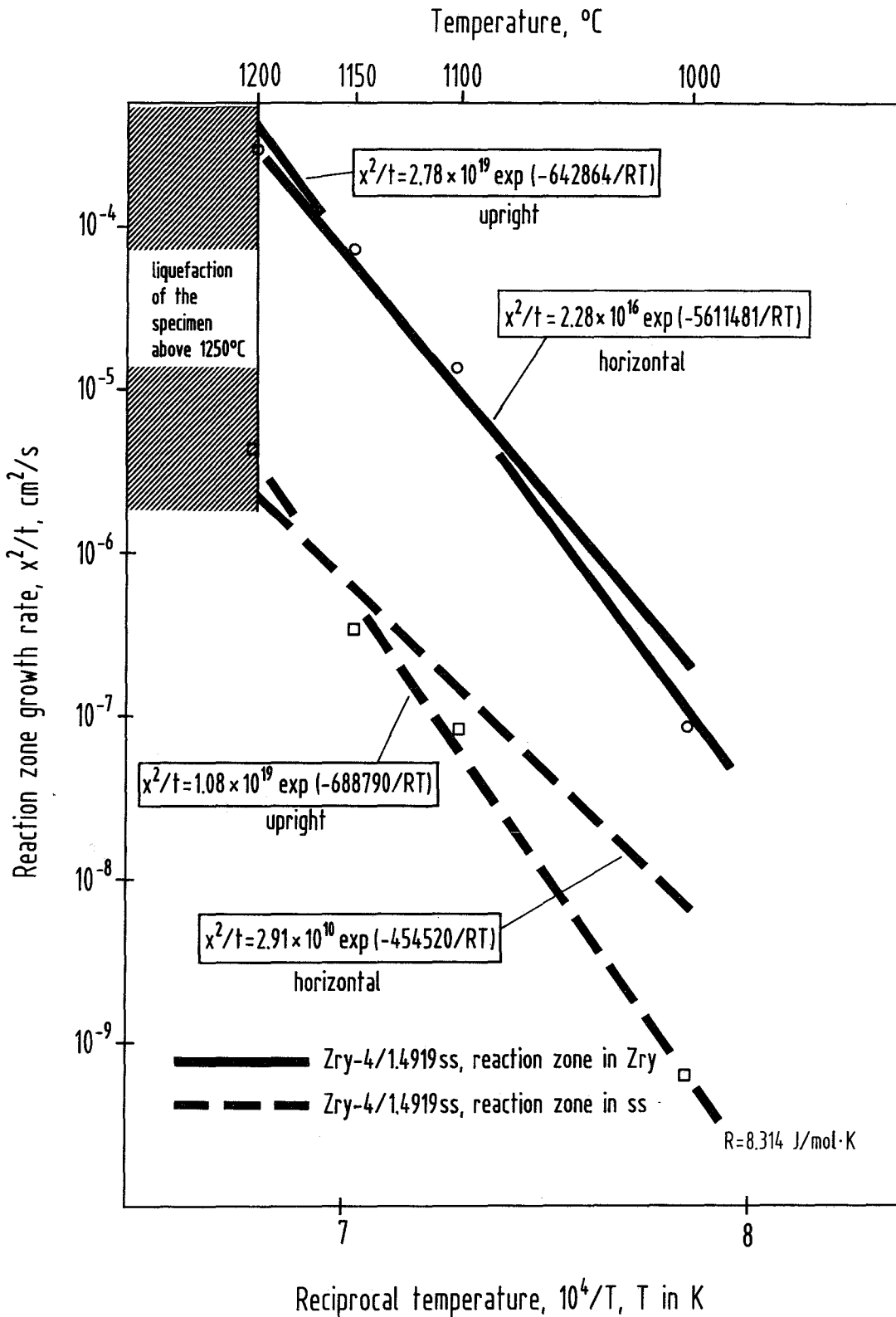


Fig. 49: Reaction zone growth rates for the reaction system Zircaloy/stainless steel 1.4919 (AISI 316) for two modes of annealing conditions (upright or horizontal).